The Philosophical Magazine

FIRST PUBLISHED IN 1798

A Journal of Theoretical Experimental and Applied Physics

Vol. 4 December 1959 No. 48
Eighth Series

25s. 0d., plus postage
Annual Subscription £13 10s. 0d., payable in advance

Printed and Published by
TAYLOR & FRANCIS LTD
RED LION COURT, FLEET STREET, LONDON E.C.4

THE PHILOSOPHICAL MAGAZINE

Authors wishing to submit papers for publication in the Journal should send manuscripts directly to the Publishers.

Manuscripts should be typed in *double* spacing on one side of quarto (8 × 10 in.) paper, and authors are urged to aim at absolute clarity of meaning and an attractive presentation of their texts.

References should be listed at the end in alphabetical order of authors and should be cited in the text in terms of author's name and date. Diagrams should normally be in Indian ink on white card, with lettering in soft pencil, the captions being typed on a separate sheet.

A leaflet giving detailed instructions to authors on the preparation of papers is available on request from the Publishers.

Authors are entitled to receive 25 offprints of a paper in the Journal free of charge, and additional offprints can be obtained from the Publishers.

The *Philosophical Magazine* and its companion journal, *Advances in Physics*, will accept papers for publication in experimental and theoretical physics. The *Philosophical Magazine* publishes contributions describing new results, letters to the editor and book reviews. *Advances in Physics* publishes articles surveying the present state of knowledge in any branch of the science in which recent progress has been made. The editors welcome contributions from overseas as well as from the United Kingdom, and papers may be published in English, French and German.

Fatigue Deformation in the Interior of Aged Ternary Aluminium–Magnesium–Zinc Alloys†

By I. J. Polmear and I. F. Bainbridge
Australian Defence Scientific Service (Aeronautical Research Laboratories), Melbourne

[Received June 20, 1959]

Abstract

Metallographic observations have been made of deformation associated with the fatigue process in the interior of several aged ternary aluminium–zinc–magnesium alloys. It has been found that the deformation occurring in these relatively complex alloys differs from that observed in pure metals.

With alloys which had a high zinc content the fatigue process was essentially a grain boundary phenomenon and cracking was intercrystalline. As the magnesium: zinc ratio was increased deformation occurred within the grains but was concentrated in certain slip bands along which cracking could occur. Cavities have been observed in these slip bands and appeared to precede the formation of an actual crack. Zones which were depleted of precipitate were found adjacent to slip bands in heavily deformed regions and these zones are considered to form by a process of re-solution of the precipitate. As the magnesium: zinc ratio was increased still further the fatigue process was accompanied by little visible evidence of deformation. This structural stability is attributed to the relatively high magnesium content and these alloys had the best fatigue properties.

§ 1. Introduction

Metallographic observations of the fatigue process in a number of metals and alloys have shown that much of the associated deformation is not homogeneous and tends to be concentrated in localized regions in the material. Current theories of fatigue in age-hardened aluminium alloys suggest that this characteristic behaviour is particularly undesirable in these materials as the dispersed precipitate in these regions may become unstable (Orowan 1939, Hanstock 1954, Forsyth and Stubbington 1955, 1957, Broom and Whittaker 1956, Forsyth 1957a, 1957b, Broom *et al.* 1957). This causes the regions to become softer than the surrounding matrix and a further concentration of deformation may result so that the whole process becomes catastrophic. The mechanism by which softening occurs is uncertain but it is thought to be associated with dislocation movements in the highly stressed regions.

The mobility of dislocations may be reduced by interaction with solute atoms (strain-ageing). Such interactions are thought to occur in binary aluminium–magnesium alloys (Phillips *et al.* 1953, Phillips 1953) and these

† Communicated by the Authors.

alloys display good fatigue properties. However, as the alloys show only slight age hardening, they do not develop high static strength properties. A high response to age hardening is obtained in many alloys based on the aluminium–magnesium–zinc system but these materials have in common a relatively low fatigue strength.

In view of these remarks the results of a study by Polmear (1958) of age-hardening phenomena in a number of high purity ternary aluminium–magnesium–zinc alloys may be significant. This work suggested that, when the ratio of magnesium : zinc exceeds a certain value, excess magnesium atoms are available which are not required in the ageing process. It thus seemed possible that a composition range may exist in which the processes of age-hardening and strain-ageing may both play an important rôle. These alloys might then show the desirable combination of high static strength and high fatigue strength.

In order to test this hypothesis, partial fatigue (S–N) curves were determined for a series of six alloys which had different magnesium : zinc ratios but for which the same heat treatment cycle gave approximately the same value of ultimate tensile strength. This provided a basis for comparing the fatigue properties and the initial results have been reported (Polmear 1959). Details of the compositions and tensile properties of the alloys are included in the table (alloy Nos. B to G) and the S–N curves are shown in fig. 1. Results for two additional alloys are also given. Alloy A had a high zinc content whereas alloy J is of interest because the zinc and magnesium contents are similar to those of several commercial high strength materials.

Alloy Compositions and Tensile Properties

Alloy	Magnesium (Mg) wt %	Zinc (Zn) wt %	Mg : Zn	0·1% proof stress (P.S.) p.s.i.	Ultimate tensile strength (U.T.S.) p.s.i.	0·1% P.S. U.T.S.	Elong. %
A	0·90	10·4	0·09	N.D.	N.D.	N.D.	N.D.
B	1·05	8·3	0·13	44,000	55,200	0·80	14·4
C	2·0	5·8	0·35	47,600	58,300	0·80	15·5
D	3·0	5·1	0·59	44,900	59,000	0·76	17·7
E	4·0	4·5	0·89	31,000	54,300	0·57	30·0
F	5·0	4·1	1·22	31,800	53,200	0·60	27·7
G	6·0	3·7	1·62	47,000	56,000	0·84	15·5
J	2·5	5·5	0·45	53,000	67,200	0·79	13·5

The results showed a considerable variation in fatigue properties and one alloy was notably better than the others. The reasons for the variation in properties are now being sought and this paper gives details of a metallographic study which has been made of the fatigue process in each alloy.

Many workers have made similar studies of a number of metals and alloys but so far observations have been mostly confined to surface regions.

In the present work changes occurring in the interior of the alloys have been observed by preparing sections through the fatigue specimens. Although this provided only limited information with regard to the initiation of cracks it did enable a detailed comparison to be made of crack propagation which is thought to occupy the greater part of the life of a specimen.

§ 2. Experimental Details

The alloys were water-chill cast and hot forged to $\frac{5}{8}$ in. square bar. The bars were solution treated for $1\frac{1}{2}$ hours at 460°C, cold water quenched, and aged for 16 hours at 125°C.

Fig. 1

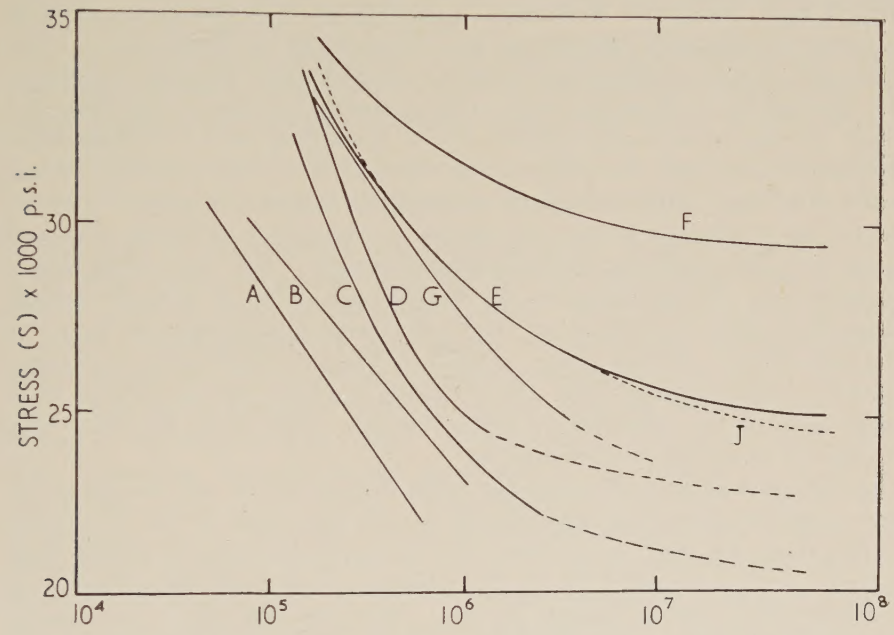

Partial fatigue (S–N) curves for the alloys.

Rotating cantilever fatigue specimens of 0·300 in. test diameter were prepared from these bars. Standard machining techniques were used and the final surfaces of the test sections were prepared with a tungsten carbide-tipped tool. To check the possible effects of machining on subsequent fatigue deformation the test sections of specimens of two alloys were polished with successively finer abrasives starting with 320 grit emery paper and finishing with 15 μ grade aloxite powder. Most specimens were tested to failure or to 10^8 cycles in rotating cantilever machines operating at 12 000 c.p.m. Stress levels within the range $\pm$ 20 000 p.s.i. to $\pm$ 35 000 p.s.i. were used.

After testing, appropriate fatigue specimens were carefully centre-sectioned in a longitudinal direction using a slitting wheel flooded with coolant. Most of the specimens had completely fractured and care was

taken to section through that area of the fracture surface which had failed by fatigue. The specimens were then mounted in a cold setting, non-shrinking resin so that the edges could be preserved during polishing. All specimens were hand polished using, progressively, emery papers, diamond pastes, and a magnesium oxide slurry contained in a silk velvet pad. The specimens were examined in the as-polished condition and then given a standard etch with Modified Keller's reagent (87·5% H_2O, 10% HNO_3, 1·5 HCl, 1% HF).

Before discussing the metallographic observations the following points should be noted:

1. The S–N curves shown in fig. 1 are typical of most metals and alloys in that they fall sharply towards the N axis as the applied stress is decreased from a high value, and then tend to parallelism with this axis. Studies of torsional fatigue in pure copper and alpha–brass by Wood (1956, 1958, 1959) and Wood and Segall (1957) have suggested that, for these materials, the form of the S–N curves is due to two distinct modes of deformation. High stresses caused appreciable strain hardening and metallographic evidence showed that the deformation was similar to that occurring during static stressing. Slip took place in relatively coarse steps which caused heavy disorientation within the grains. Subsequent cracking occurred along irregular and non-crystallographic paths. On the other hand, lower stresses corresponding to the flatter part of the S–N curve caused much less strain hardening so that very large plastic strains may be accommodated. Deformation occurred by fine slip which became concentrated in bands or striations and ultimate cracking was attributed to a breakdown of the structure in these regions. This latter sequence was thought to characterize true fatigue.

In the present work most of the observations which will be described were made on specimens which failed within the range 10^5 to 10^6 cycles. In this range the S–N curves were still sloping towards the N axis so that it might be expected that the deformation would be more characteristic of a static rather than a fatigue process. However, the alloys were fairly complex materials and it will be shown that the mode of deformation may be controlled more by the alloy structure than by the magnitude of the applied stress.

2. Complete recrystallization occurred during solution treatment of each alloy so that the grains were equi-axed. The grain size of each alloy was fairly similar and varied from 60 to 100 grains/mm^2.

3. The characteristics of rotating beam fatigue testing are such that the stress is greatest at the surface of the specimen and decreases to zero at the centre. With single point rotating cantilever testing the stress in a longitudinal direction varies from a maximum value close to the minimum cross section to lower values on either side of this section. Therefore, by examining the specimen at varying distances normal to the surface, or in a longitudinal direction away from the minimum cross section, some indication may be obtained of deformation at different stages of the life.

4. It is sometimes difficult to distinguish between deformation truly characteristic of the fatigue process in a particular alloy and that which is associated with the intense stress concentrations occurring during the final tensile fracture. This complication has been taken into account when assessing the deformation characteristics of each alloy.

5. An additional unavoidable complication is that quenching stresses arising during heat treatment cause some slip to occur within the grains before fatigue testing. The slip bands are shown up on etching due to the preferential formation of the precipitate in these regions during ageing. It is also necessary to take this factor into account when assessing the deformation truly associated with the fatigue process. However this was not difficult as the structure in the test section could be compared with that in an unstressed end of the specimen.

6. A comparison of specimens of the same alloy, the surfaces of which had been prepared by the two methods described above, showed that the metallographic changes accompanying fatigue were similar in each case.

§ 3. Characteristics of Fatigue Cracking

The type of deformation associated with the fatigue process in each alloy was found to depend upon the ratio of magnesium : zinc and the alloys could be classified into three groups. With alloys A and B which had high zinc contents the fatigue process was essentially a grain boundary phenomenon and cracking was completely intercrystalline (fig. 2, Pl. 156). There was also evidence of grain boundary weakness or brittleness in the region of the main fatigue crack. Forsyth and Stubbington (1955, 1957) have observed intercrystalline cracking during fatigue of a binary aluminium–10% zinc alloy. Furthermore, it is well known that aluminium–zinc or aluminium–magnesium–zinc alloys in which either the zinc content is high or in which the sum of the magnesium and zinc contents exceeds about 10%, are susceptible to grain boundary weakness even in the absence of an applied stress (Perryman and Blade 1950, Herenguel and Chaudron 1941, 1943). This behaviour is usually attributed to localized depletion of solute atoms in the region of the grain boundaries. In the present work grain boundary depletion was not observed, which indicates that the regions are very narrow or that some other mechanism must be operative. In view of this, the proposal by Gobin and Montuelle (1958) may be a more likely explanation. These workers suggested that the loss of cohesion at the grain boundaries is due to the aggregation there of vacant lattice sites to form stable cavities which ultimately join to produce an intercrystalline crack.

In both the above alloys some deformation and cracking occurred along crystallographic planes within the grains but this was of minor importance in relation to the overall mode of failure. However, as the magnesium : zinc ratio was increased, deformation became more and more concentrated in these regions. Thus in alloys, C, D and J fatigue failure occurred primarily

by the propagation of cracks along crystallographic slip planes. A complicated crack path may result and an example of this is shown in fig. 3 (Pl. 156). The importance of slip planes in surface grains in providing a path for the progress of fatigue cracks is evident from fig. 4. (Pl. 156). Because of this it is usual in the highly stressed specimens to find several small cracks in addition to the main crack which has resulted in failure.

The concentration of fatigue deformation in certain slip planes caused several interesting modifications to the alloy structure and these will be described in the next section. It may be noted that these effects and the crystallographic nature of the crack paths became less evident as the applied stress was reduced.

The remaining alloys E, F and G had high ratios of magnesium : zinc and in each case the fatigue crack path was completely transcrystalline and non-crystallographic (fig. 5, Pl. 157). The path of the fatigue crack was always close to perpendicular to the specimen axis and in no case were any smaller side cracks detected. Intense slip markings were infrequent and were associated only with the fatigue crack where excessive deformation may have occurred. The appearance of the markings differed from those in the other alloys and, as shown in fig. 6 (Pl. 157), they are present as short, wavy lines, which is due to the fact that slip has occurred on many planes. The virtual absence of evidence of deformation in these alloys is perhaps surprising when it is considered that the alloys were in the age-hardened condition and that, with alloys E and F, some fatigue tests were made at a stress which exceeded the 0·1% proof stress of the material.

Alloys E and F had low values of the ratio of 0·1% proof stress : ultimate tensile strength and it might be suggested that the absence of visible evidence of deformation is due to the fact that these alloys can more readily accommodate heavy plastic strains. However, alloy G has similar tensile properties to the remaining alloys and again very little evidence of deformation was found. As all three alloys had in common high ratios of magnesium : zinc it would seem that the desirable property of structural stability during fatigue stressing is associated primarily with a relatively high magnesium content.

§ 4. Structural Changes Associated with Slip Band Deformation

4.1. *Slip striations and Cavity Formation*

The concentration of deformation in certain slip planes caused these planes to be preferentially attacked by the etching reagent. They appear as intense lines (fig. 3, Pl. 156) and occasionally as wider striations (fig. 7, Pl. 157). The incidence of these slip lines and slip striations decreased as the applied stress was reduced. This observation is interesting as Wood (1956, 1958, 1959) and Kemsley (1956) have found that, in copper and alpha-brass, slip striations tend to become more prominent as the applied stress is reduced. The different results are thought to have their origin in the different materials being studied.

The intense slip lines and slip striations frequently contained small cavities or larger diamond-shaped (cubic) etch pits (fig. 7, Pl. 157, and fig. 8 (*a*), Pl. 158). The cavities and etch pits were found in slip bands and slip striations associated with actual cracks, and occasionally in grains, apparently remote from cracks in the interior of a specimen to a depth of 0·5 mm from the surface. It was shown that the cavities were not related to the precipitated phase. The cavities and the tendency to form etch pits appeared to precede the formation of a crack in the slip band or slip striation. Although it was not possible to follow the sequence of events in any one slip plane in the interior of an alloy there is some indirect evidence to support this conclusion. In fig. 8 (*a*) (Pl. 158) slip has occurred in two parallel planes a short distance apart. In one plane cubic etch pits are evident whereas an actual crack has formed in the adjacent plane. It is suggested that this represents an early stage in the formation of a crack system similar to that shown in fig. 8 (*b*) (Pl. 158). It is also commonly observed that a line of discrete cavities may be present ahead of an advancing crack again suggesting that crack growth occurs by joining of the cavities.

If this conclusion concerning the relationship of cavities and crack formation is correct, then it appears that the 'embryonic' stage of crack formation may occur in the interior of those alloys in which deformation is concentrated in certain slip planes. However, no internal cracks were observed which could not be related to cracks which had been initiated at the surface.

Because of their possible significance in relation to crack propagation the cavities and etch pits were studied in more detail. The section of alloy J containing the slip striation shown in fig. 7 (Pl. 157) was repolished and examined in the unetched condition. Some small cavities were present but the slip striation was not evident (fig. 9, Pl. 158). On re-etching cubic pits formed at the sites of the cavities and the slip striation reappeared. The alloy was then heated in vacuo for 1 hour at 450 °C, cooled, and polished to remove the surface layers. Cavities were again present in the unetched condition. However, this time etching had no effect on the size or shape of the cavities and the slip striation did not reappear.

The sequence of polishing and observing the appearance of the cavities was repeated several times. It was found that the sites of the cavities changed in a random manner with successive polishes and that the cavities were not elongated in any particular direction. The size of the cavities varied up to a maximum of approximately 2 μ (0·002 mm).

The same series of experiments was repeated with a fatigue specimen of alloy D. Similar results were obtained.

The appearance of the striations on etching, together with the fact that relatively large etch pits are developed at the sites of the cavities, suggests that these areas are appreciably cold worked. It has been shown that the cold work can be removed by heat treatment but the cavities remain as permanent damage resulting from the fatigue process.

Cavities have also been observed in slip bands in pure aluminium, a dilute aluminium–magnesium alloy, and in an age hardened alloy of aluminium–7·5% zinc–2·5% magnesium tested in fatigue (Harries and Smith 1956, Forsyth 1957 a, 1957 b, Smith 1957). These workers also suggested an association between the presence of cavities and subsequent fatigue cracking. However, it was concluded that the cavities take the form of conical or cylindrical tubes which may be regularly spaced in a slip band. Furthermore, in areas remote from cracks, the cavities have been observed only in slip bands in surface grains to a depth of a few microns from the surface.

No explanation can be offered for the apparent difference in the shape of the cavities observed in the present investigation and those reported by other workers. The presence of intense slip bands, slip striations, and cavities to a much greater depth from the surface in the present work may be a characteristic of the method of fatigue testing. However, it is more likely that it is dependent upon the material being studied as the effects were most common in alloys C, D and J which are very susceptible to structural changes during fatigue stressing.

The origin of the cavities is uncertain. Broom *et al.* (1956) proposed that a large number of vacant lattice sites are generated in slip bands and slip striations and that cavities may form by the condensation of some of these vacant lattice sites. Recent work by McCammon and Rosenberg (1957) and Hull (1958) has shown that fatigue fracture in slip bands in several metals can occur at temperatures as low as 4°K where these point defects are not mobile. Accordingly, attention has been directed at mechanisms by which cavities may form in the absence of mobile vacant sites. Fujita (1954) had proposed that a minute crack may be formed by the interaction of two edge dislocations of opposite sign moving on adjacent slip planes less than 10 A.U. apart. This crack or cavity would grow by the adsorption of other edge dislocations moving on the same planes. Mott (1958) has suggested a similar geometric process by which a void may be generated in a slip band or slip striation by cross slip between closely spaced slip bands.

4.2. *Depletion of Precipitate in Slip Band Regions*

Another important consequence of the concentration of fatigue deformation in certain slip bands is the effect on the dispersion of precipitate in age-hardened alloys. Forsyth and Stubbington (1957) have observed regions, depleted of precipitate, associated with slip bands in an aluminium–4% copper alloy fatigue tested at 250°C. Evidence of similar depletion in an aluminium–5·9% zinc–3·0% magnesium–0·8% copper alloy, tested at room temperature, was revealed by electron microscopy (Broom *et al.* 1957). In the present work depleted bands were not common but some examples were found in those alloys in which deformation was concentrated in slip planes. These depleted bands were observed either in association with cracks in slip bands, as in fig. 10 (Pl. 159), or in surface

grains and in grains in the interior of the alloy but close to the fracture surface. An example of this latter effect is shown in fig. 11 (Pl. 159) and closer examination revealed that, adjacent to the depleted bands, were wider zones in which the particles of precipitate appeared to be smaller and less numerous than in the general matrix (fig. 12, Pl. 159). Micro-hardness tests showed that the depleted regions were softer than the surrounding matrix.

The fact that relatively wide depleted bands were observed in some alloys tested at room temperature, whereas the bands were only evident in an aluminium copper alloy tested at an elevated temperature, suggests that the dispersion of precipitate is less stable in the present alloys. However, the usual association of the depleted bands with regions of heavy deformation suggests that their origin may be due, in part, to a static component of the stress. In this regard it may be recalled that Polmear and Bainbridge (1958) have observed depleted bands in the interior of a tensile specimen of one alloy (D) the structure of which appeared to be particularly susceptible to structural changes under stress.

Several mechanisms have been suggested to account for the formation of these depleted regions and these have been summarized by Broom *et al.* (1957).

1. The creation of vacant lattice sites by moving dislocations, with the consequent increase in diffusion rate, causes localized overageing comparable with that occurring at a high temperature (Broom *et al.* 1956).

2. An increase in the diffusion rate is brought about by multiplication of dislocations with the consequent greater chances of 'short-circuit' diffusion paths (Turnbull 1954).

3. The interaction of mobile dislocations with other dislocations which form the boundaries of coherent precipitates may cause these precipitates to become incoherent, thereby reducing local elastic strains (Averbach 1954).

4. Hardy (1955) has suggested that the nucleation of stable precipitates may occur in these regions.

5. Freudenthal and Weiner (1956) have proposed that sufficiently high temperatures may be generated in slip bands by moving dislocations for normal thermal ageing to take place, leading to softening and cracking.

6. Depletion may occur by the re-solution of precipitates. Wilson (1957) has proposed that there is a partition of solute atoms between dislocations and precipitates. The multiplication of dislocations may necessitate the transfer of solute atoms from precipitates.

These mechanisms fall into two categories: (1)–(5) all involve some form of over-ageing in the region of the slip bands, whereas (6) is the reverse process of re-solution of the precipitate which was present initially. Suggestion (5) may be eliminated as Eshelby and Pratt (1956) have shown that the actual temperature rise will be, at the most, only a few degrees. The mechanism outlined in (3) would involve little or no change in the

appearance of the precipitate. Over-ageing by the other mechanisms (1), (2) or (4) should involve some change in the appearance of the affected regions. A smaller number of precipitate particles would be expected but their size should be increased. This would follow because increased diffusion rates, or the nucleation of stable precipitates, would cause the preferential growth of some precipitate particles at the expense of other adjacent particles. Forsyth (1957*a*) has shown experimentally that the diffusion rate is higher in slip bands but the appearance of the precipitate in depleted regions in the present work does not conform with any of the above predictions. Relatively wide regions which appeared to contain no precipitate particles at all were found associated with slip bands. This suggests that re-solution of the precipitate rather than over-ageing is the mechanism of softening in these regions. This conclusion is supported by the observations made on alloy C (figs. 11, 12, Pl. 159). The presence of zones, adjacent to depleted regions, in which the precipitate particles are smaller and less numerous than the general matrix suggests a stage of partial re-solution of the precipitate.

In this regard a further observation is relevant. It was found that, in low stress, long-life specimens of some alloys, the fine slip markings due to quenching stresses were less evident in the test section than in the unstressed ends of the specimens. In other words, the slip markings in the test sections had 'disappeared' during the fatigue test and this apparent change in microstructure was accompanied by a small decrease in hardness. It might be proposed that fatigue stressing has induced further ageing in the test section so that the general level of precipitation within the matrix has been increased to that present in the slip bands. This explanation is unlikely however as such a mechanism would increase the rate of etching of the alloy in that region. This behaviour was not observed. Instead it is suggested that the increased dislocation density accompanying fatigue stressing has caused the precipitate in the slip bands to re-dissolve. It is possible that the process is on such a fine scale that the resistance of the alloys to fatigue cracking is little affected.

If softening in slip bands is due to re-solution of the precipitate then it is necessary to explain both the process of re-solution and to account for the location of the solute atoms which had previously formed the precipitate. Where depleted regions were observed, the precipitate particles in the adjacent matrix appeared to be similar to the precipitate in the remainder of the grain. This suggests that most of the solute atoms must remain in the depleted zone as transport of these atoms to neighbouring regions would result in growth of the precipitate there. In view of the observation that these regions are softer than the surrounding matrix, the solute atoms must be dispersed so that they cause less hardening than when they were present as a precipitate.

The mechanism for re-solution of the precipitate in the highly stressed regions may be that proposed by Wilson (1957). Another suggestion is that the relative disorder and increased diffusion rates in these regions may

cause re-solution of the precipitate in the same way that the precipitate would be dissolved if the alloy was heated to a sufficiently high temperature below the solidus line.

It may be noted that the reverse effect to the formation of depleted regions namely, the formation of bands of heavy precipitation, has been observed by Hanstock (1954) in his study of torsional fatigue of the commercial alloy DTD 683. This effect was not detected in the present work or in a similar study of fatigue deformation in quaternary aluminium zinc–magnesium–copper alloys by Broom *et al.* (1957), Hanstock showed that cracks may be associated with these bands of precipitate and, in view of the high frequency of the tests (1000 c.p.s), it has been suggested that most of the effects may have their origin in normal high temperature precipitation around energy dissipating cracks (Hanstock 1955, Broom *et al.* 1957). This proposal is supported by the observation of Polmear and Bainbridge (1958) that heavy precipitation has occurred at the tip of an internal crack in a tensile specimen of an age-hardened aluminium–zinc–magnesium alloy.

§ 5. Conclusions

1. It has been found that the deformation associated with different parts of the S–N curves of fairly complex age hardened aluminium-zinc–magnesium alloys differs from that observed in pure metals and alpha-brass. Furthermore, the type of deformation showed a considerable variation within the range of these alloys which were studied. In the case of alloys with a high zinc content the fatigue process was essentially a grain boundary phenomenon and cracking was intercrystalline. As the magnesium : zinc ratio was increased deformation occurred within the grains but was concentrated in certain slip bands along which fatigue cracks were readily propagated. Deformation became more homogeneous as the above ratio was increased still further and the fatigue process was accompanied by little visible evidence of any concentration of stress. This desirable property of structural stability has been attributed to the relatively high magnesium content and these alloys showed the best fatigue properties.

2. The concentration of fatigue deformation in certain slip bands in some alloys caused interesting modifications to the alloy structure.

(*a*) Intense slip bands and slip striations were found in the region of cracks and to a depth of 0·5 mm from the surface of specimens. These slip bands and slip striations frequently contained a random dispersion of small cavities which were found to constitute permanent fatigue damage. It is considered that major fatigue cracks are formed by means of a network of smaller cracks linking the cavities. In this way the presence of the cavities greatly assists in crack propagation.

The fact that cavities were observed in slip bands and slip striations in grains in the interior of several alloys suggests the possibility that cracks may be initiated at these sites. However, no internal cracks were detected which could not be related to cracks already initiated at the surface.

(*b*) Regions which were depleted of precipitate were found in heavily deformed zones. The formation of these depleted regions is considered to take place by re-solution of the precipitate rather than by an over-ageing mechanism. It is proposed that the solute atoms remain in the depleted regions but are so dispersed that they cause less hardening.

Acknowledgments

This paper is published with the permission of the Chief Scientist, Australian Defence Scientific Service, Department of Supply, Melbourne. The authors' thanks are also due to Mr. J. B. Dance for his encouragement, to Messrs. J. Y. Mann and J. M. Finney who carried out the fatigue tests and to Mr. L. Wilson who made the chemical analyses of the alloys.

References

Averbach, D. L., 1954, *Trans. Amer. Soc. Metals*, **41,** 262.
Broom, T., Molineux, J. H., and Whittaker, V. N., 1956, *J. Inst. Met.*, **84,** 357.
Broom, T., and Whittaker, V. N., 1956, *Nature, Lond.*, **177,** 486.
Broom, T., Mazza, J. A., and Whittaker, V. N., 1957, *J. Inst. Met.*, **86,** 17.
Eshelby, J. D., and Pratt, P. L., 1956, *Acta. Met.*, **4,** 560.
Forsyth, P. J. E., 1957 a, *Proc. roy. Soc.* A, **242,** 198; 1957 b, *Phil. Mag.*, **2,** 437.
Forsyth, P. J. E., and Stubbington, C. A., 1955, *J. Inst. Met.*, **83,** 395; 1957, *Ibid.*, **85,** 339.
Freudenthal, A. M., and Weiner, J. H., 1956, *J. appl. Phys.*, **27,** 44.
Fujita, F. E., 1954, *Sci. Rep. Res. Insts Tôhoku Univ.* A, **6,** 564.
Gobin, P., and Montuelle, J., 1958, *Comp. rend.*, **246,** 1853.
Hanstock, R. F., 1954, *J. Inst. Met.*, **83,** 11; 1955, *Ibid.*, **83,** 532.
Hardy, H. K., 1955, *J. Inst. Met.*, **83,** 529.
Harries, D. R., and Smith, G. C., 1956, *Colloquium in Fatigue* (Berlin : Springer-Verlag), p. 89.
Herenguel, J., and Chaudron, G., 1941, *Métaux, Corrosion, Usure*, **16,** 33 and 49; 1943, *Ibid.*, **18,** 30 and 37.
Hull, D., 1958, *J. Inst. Met.*, **86,** 425.
Kemsley, D. S., 1956, *J. Inst. Met.*, **85,** 153.
McCammon, R. D., and Rosenburg, H. M., 1957, *Proc. roy. Soc.* A, **242,** 203.
Mott, N. F., 1958, *Acta Met.*, **6,** 195.
Orowan, E., 1939, *Proc. roy. Soc.* A, **171,** 79.
Perryman, E. C. W., and Blade, J. C., 1950, *J. Inst. Met.*, **77,** 263.
Phillips, V. A., Swain, A. J., and Eborall, R., 1953, *J. Inst. Met.*, **81,** 625.
Phillips, V. A., 1953, *J. Inst. Met.*, **81,** 649.
Polmear, I. J., 1958, *J. Inst. Met.*, **87,** 24; 1959, *Nature, Lond.*, **183,** 1388.
Polmear, I. J., and Bainbridge, I. F., 1958, *Phil. Mag*, **3,** 655.
Smith, G. C., 1957, *Proc. roy. Soc.* A, **242,** 198.
Turnbull, D., 1954, *Rep. Conf. on Defects in Cryst. Solids* (American Society Metals), p. 95.
Wilson, D. V., 1957, *Acta. Met.*, **5,** 293.
Wood, W. A., 1956, *Fatigue of Aircraft Structures* (New York: Academic Press), p. 1; 1958, *Phil. Mag.*, **3,** 692; 1959, Conference on Fracture, Swampscott Massachusetts, U.S.A., Chapter 16.
Wood, W. A., and Segall, R. L., 1957, *Proc. roy. Soc.* A, **242,** 180.

The Effect of Viscosity on the Stability of Incompressible Magnetohydrodynamic Systems†

By A. Hare
University College of North Wales, Bangor

[Received July 16, 1959]

Abstract

A variational principle is derived, which may be used to discuss the stability of incompressible magnetohydrodynamic systems in the absence of viscosity, and its application is briefly described. The effect of viscosity is then discussed and comparison with the non-viscous case shows that conditions for stability derived in its absence are still valid.

§ 1. Introduction

The stability of equilibrium of magnetohydrodynamic systems has recently been discussed by several workers. In particular, Tayler (1957 a, b) has investigated the stability of the pinched discharge, by a normal mode analysis, and Bernstein *et al.* (1958) have considered the stability of more general configurations, by means of an energy principle. Similar problems have also been discussed by Kruskal and Tuck (1958), and by Hain *et al.* (1957), though the effect of viscosity on stability does not seem to have been considered.

It will be shown that for the incompressible case, conditions for stability derived in the absence of viscosity, are unchanged when the effect of viscosity is included.

We begin by deriving a variational principle, which can be used to discuss stability in the absence of viscosity and which is to a large extent equivalent to the energy principle of Bernstein *et al.*, and then proceed to investigate the modifications necessary to include the effect of viscosity.

§ 2. The Equilibrium State

The initial equilibrium state will be supposed to be constituted by a finite volume τ^i, of ideally conducting, incompressible fluid, of arbitrary shape, surrounded by a volume τ^0 of non-conducting material, extending to infinity (superscripts i and 0 are used throughout to distinguish, where ambiguity arises, between quantities relating to the conducting and non-conducting regions respectively). The theory may also be applied to a two-dimensional system in which τ^i is an infinite cylindrical volume with a finite cross section. The conducting fluid carries a volume current density

† Communicated by the Author.

$\mathbf{I}$, and we shall allow its surface S to carry a sheet current. It will however be assumed that the normal component of the magnetic field at S vanishes, i.e. the magnetic lines of force do not link the separate regions.

If P and $\mathbf{H}$ denote the equilibrium pressure and magnetic field (in e.m.u.), we have

$$\nabla P^i = \mathbf{I} \wedge \mathbf{H}^i = (1/4\pi)(\mathrm{curl}\,\mathbf{H}^i) \wedge \mathbf{H}^i, \quad . \quad . \quad . \quad . \quad . \quad (1)$$

$$P^0 = \text{constant}. \quad . \quad . \quad . \quad . \quad . \quad . \quad . \quad . \quad . \quad (2)$$

Due to the possibility of a sheet current at S, the pressure and tangential components of the magnetic field need not be continuous across S; however, the 'total pressure' $P + (1/8\pi)H^2$ will be continuous there.

In order to discuss the stability of the equilibrium configuration, we shall suppose it to be subjected to a small perturbation depending on time through a factor $e^{\sigma t}$, linearize in the usual way, and obtain a variational principle for the determination of σ^2.

§ 3. Boundary Conditions

If the material velocity in a perturbation is $\mathbf{v}$, $\boldsymbol{\xi}$ is the displacement of the boundary S, and p, $\mathbf{h}$, and $\mathbf{e}$ denote the perturbations in pressure, magnetic and electric fields respectively, then the boundary conditions to be imposed at S are:

$$4\pi(p^i - p^0) = \mathbf{H}^0 . \mathbf{h}^0 - \mathbf{H}^i . \mathbf{h}^i + 4\pi\xi_n \mathbf{n} . [\nabla(P + (1/8\pi)H^2)] \quad . \quad . \quad (3)$$

where square brackets indicate the discontinuity in a quantity in crossing S in the direction of the unit normal vector $\mathbf{n}$ (directed into τ^0).

$$\mathbf{n} \wedge \mathbf{e}^0 = v_n \mathbf{H}^0, \quad . \quad . \quad . \quad . \quad . \quad . \quad . \quad . \quad . \quad (4)$$

$$v_n{}^i = v_n{}^0. \quad . \quad . \quad . \quad . \quad . \quad . \quad . \quad . \quad . \quad . \quad (5)$$

These equations express respectively the conditions of continuity of the total pressure, the tangential component of the total electric field and the normal component of the material velocity, at the boundary.

§ 4. The Variational Principle

The magnetohydrodynamic equation of motion and the equation of field change, give for the region τ^i, to a first order in the perturbations, (ρ being the density):

$$\rho^i \sigma \mathbf{v}^i = -\nabla p^i + (1/4\pi)\{(\mathbf{H}^i . \nabla)\mathbf{h}^i + (\mathbf{h}^i . \nabla)\mathbf{H}^i - \nabla(\mathbf{H}^i . \mathbf{h}^i)\}, \quad . \quad . \quad (6)$$

$$\sigma \mathbf{h}^i = \mathrm{curl}(\mathbf{v}^i \wedge \mathbf{H}^i) \quad . \quad . \quad . \quad . \quad . \quad . \quad . \quad . \quad . \quad . \quad . \quad (7)$$

the corresponding equations for τ^0 are:

$$\rho^0 \sigma \mathbf{v}^0 = -\nabla p^0, \quad . \quad . \quad . \quad . \quad . \quad . \quad . \quad . \quad . \quad (8)$$

$$\mathrm{curl}\,\mathbf{h}^0 = 0. \quad . \quad . \quad . \quad . \quad . \quad . \quad . \quad . \quad . \quad . \quad (9)$$

Also, since the fluid is assumed to be incompressible, for both regions

$$\mathrm{div}\,\mathbf{v} = 0. \quad . \quad . \quad . \quad . \quad . \quad . \quad . \quad . \quad . \quad (10)$$

Now multiply (6) and (8) by $4\pi\sigma\mathbf{v}^* d\tau^i$ and $4\pi\sigma\mathbf{v}^* d\tau^0$ respectively (a star denoting the complex conjugate), integrate over the appropriate regions

and add. If $d\tau$ denotes an element of the composite volume $\tau^i+\tau^0$, this gives, on using Green's theorem and eqn. (10),

$$4\pi\sigma^2\int\rho\mathbf{v}\,.\,\mathbf{v}^*\,d\tau=-4\pi\sigma\int v_n{}^*(p^i-p^0)\,dS-\sigma\int v_n{}^*(\mathbf{H}\,.\,\mathbf{h}^i)\,dS$$
$$+\sigma\int\mathbf{v}^*\,.\{(\mathbf{H}\,.\,\nabla)\mathbf{h}+(\mathbf{h}\,.\,\nabla)\mathbf{H}\}\,d\tau^i. \quad . \quad . \quad . \quad (11)$$

The surface integrals on the right-hand side of (11) may, by virtue of (3), be replaced by

$$-\sigma\int v_n{}^*(\mathbf{H}\,.\,\mathbf{h}^0)\,dS-4\pi\int v_nv_n{}^*\mathbf{n}\,.\,[\nabla(P+(1/8\pi)H^2)]\,dS. \qquad (12)$$

Using (4), we may write the first integral of (12) in the form

$$-\sigma\int\mathbf{n}\,.\,(\mathbf{e}^{0*}\wedge\mathbf{h}^0)\,dS$$
$$=\sigma\int\nabla\,.\,(\mathbf{e}^*\wedge\mathbf{h})\,d\tau^0$$
$$=\sigma\int\mathbf{h}\,.\,\mathrm{curl}\,\mathbf{e}^*\,d\tau^0$$
$$=-\sigma\sigma^*\int\mathbf{h}\,.\,\mathbf{h}^*\,d\tau^0.$$

Thus the surface integrals of (11) may be written

$$-\sigma\sigma^*\int\mathbf{h}\,.\,\mathbf{h}^*\,d\tau^0-4\pi\int v_nv_n{}^*\mathbf{n}\,.\,[\nabla(P+(1/8\pi)H^2)]\,dS. \qquad (13)$$

The remaining volume integral on the right-hand side of (11) may, after some transformation with the help of (7), be written

$$-\int\{|\mathbf{H}\,.\,\nabla\mathbf{v}\,|^2+\mathbf{v}^*\mathbf{v}:\nabla\nabla\Psi'\}\,d\tau^i\,\dagger$$

where

$$\Psi'=\tfrac{1}{2}H^2+4\pi P.$$

Thus, (11) becomes

$$4\pi\sigma^2\int\rho\mathbf{v}\,.\,\mathbf{v}^*\,d\tau+\sigma\sigma^*\int\mathbf{h}\,.\,\mathbf{h}^*\,d\tau^0=-\int\{|\mathbf{H}\,.\,\nabla\mathbf{v}\,|^2+\mathbf{v}^*\mathbf{v}:\nabla\nabla\Psi'\}\,d\tau^i$$
$$-4\pi\int v_nv_n{}^*\mathbf{n}\,.\,[\nabla(P+(1/8\pi)H^2)]\,dS. \qquad (14)$$

---

† Note on the tensor notation :—

The double product $\boldsymbol{w}:\boldsymbol{w}'$ of the two tensors $\boldsymbol{w}$ and $\boldsymbol{w}'$ is defined to be $\sum_i\sum_j w_{ij}w_{ji}'$.

The unit tensor $\boldsymbol{U}$, introduced in § 5, is the tensor whose components in any Cartesian coordinate system are given by $U_{xx}=U_{yy}=U_{zz}=1$; the non-diagonal components, U_{xy}, U_{xz}, etc., all vanish.

The tensor conjugate to $\boldsymbol{w}$ is denoted by $\widetilde{\boldsymbol{w}}$, thus the (i,j)th component of $\widetilde{\nabla\mathbf{v}}$ is $\partial v_i/\partial x_j$.

This equation is the form of the variational principle appropriate to the incompressible case.

A somewhat more convenient form, involving $\mathbf{h}$ and the displacement $\boldsymbol{\xi}$ may be obtained, since to a first order, $\mathbf{v} = \sigma\boldsymbol{\xi}$ enabling the equation of field change to be written

$$\mathbf{h} = \operatorname{curl}(\boldsymbol{\xi} \wedge \mathbf{H}).$$

Accordingly, in terms of these variables, the variational principle becomes

$$4\pi\sigma^2 \int \rho\boldsymbol{\xi} \,.\, \boldsymbol{\xi}^* \, d\tau = -\int \mathbf{h} \,.\, \mathbf{h}^* \, d\tau^0 - \int \{|\mathbf{H} \,.\, \nabla\boldsymbol{\xi}|^2 + \boldsymbol{\xi}^*\boldsymbol{\xi} : \nabla\nabla\Psi\} \, d\tau^i$$
$$- 4\pi \int \xi_n \xi_n^* \mathbf{n} \,.\, [\nabla(P + (1/8\pi)H^2)] \, dS. \quad . \quad . \quad (15)$$

It can be shown (though the proof will not be given here) that the value of σ^2 given by the ratio of the right-hand side of (15) to $4\pi \int \rho\boldsymbol{\xi} \,.\, \boldsymbol{\xi}^* \, d\tau$ is stationary to variations $\boldsymbol{\delta\xi}$ and $\boldsymbol{\delta h}$ in $\boldsymbol{\xi}$ and $\mathbf{h}$, which are solenoidal and satisfy the equation of field change, the equation curl $\boldsymbol{\delta h}^0 = 0$ and certain boundary conditions on S. Moreover, the largest eigenvalue σ_1^2, is in fact a maximum, so that to establish instability it is sufficient to find arbitrary trial functions $\boldsymbol{\xi}$, $\mathbf{h}$ which, substituted into (15) yield a positive value for σ^2. To establish stability by the same method, it would be necessary to use a complete set of trial functions. In certain cases, however, it is possible to find sufficient conditions on $\mathbf{H}$ which make the right-hand side of (15) negative whatever the form of $\boldsymbol{\xi}$ and $\mathbf{h}$. This approach has been applied to the stability of a cylindrical plasma carrying an axial volume current; the results obtained being in agreement with those given by Tayler (1957 a, b).

§ 5. The Viscous Case

Our purpose here is to discuss the effect of viscosity on stability and accordingly we now consider the necessary modifications of (14) or (15).

Firstly, the scalar pressure must be replaced by a stress tensor $\boldsymbol{p}$, thus (6) and (8) are replaced by

$$\rho^i \sigma \mathbf{v}^i = \nabla \,.\, \boldsymbol{p}^i + (1/4\pi)\{(\mathbf{H}^i \,.\, \nabla)\mathbf{h}^i + (\mathbf{h}^i \,.\, \nabla)\mathbf{H}^i + \nabla(\mathbf{H}^i \,.\, \mathbf{h}^i)\}, \quad . \quad (16)$$

$$\rho^0 \sigma \mathbf{v}^0 = \nabla \,.\, \boldsymbol{p}^0. \quad . \quad . \quad . \quad . \quad . \quad . \quad . \quad . \quad . \quad . \quad . \quad . \quad (17)$$

The initial stress tensor $\boldsymbol{p}$ in the equilibrium state is given by $-P\boldsymbol{U}$ where $\boldsymbol{U}$ is the unit tensor. The boundary condition (3) is also modified and the appropriate form is

$$4\pi\mathbf{n} \,.\, (\boldsymbol{p}^i - \boldsymbol{p}^0) = (\mathbf{H} \,.\, \mathbf{h}^i - \mathbf{H} \,.\, \mathbf{h}^0)\mathbf{n} - 4\pi\mathbf{n}\xi_n \mathbf{n} \,.\, [\nabla(P + (1/8\pi)H^2)]. \quad (18)$$

To find the viscous counterpart to (14), we proceed as before, to multiply the equations of motion, (16) and (17) by $4\pi\sigma\mathbf{v}^* \, d\tau^i$ and $4\pi\sigma\mathbf{v}^* \, d\tau^0$ respectively, integrate over the appropriate regions and add.

Consider first the contribution from the right-hand sides due to the terms involving the stress tensors; this is

$$4\pi\sigma \int \mathbf{v}^* \,.\, (\nabla \,.\, \boldsymbol{p}^i) \, d\tau^i + 4\pi\sigma \int \mathbf{v}^* \,.\, (\nabla \,.\, \boldsymbol{p}^0) \, d\tau^0. \quad . \quad . \quad . \quad (19)$$

On transforming the first term, we have

$$4\pi\sigma\int \mathbf{v}^*\,.\,(\nabla\,.\,\boldsymbol{p}^i)\,d\tau^i = 4\pi\sigma\int (\boldsymbol{p}^i\,.\,\mathbf{v}^*)\,.\,\mathbf{n}\,dS - 4\pi\sigma\int \boldsymbol{p}^i : \tilde{\nabla}\mathbf{v}^*\,d\tau^i$$
$$= 4\pi\sigma\int \mathbf{v}^*(\mathbf{n}\,.\,\boldsymbol{p}^i)\,dS - 4\pi\sigma\int \boldsymbol{p}^i : \tilde{\nabla}\mathbf{v}^*\,d\tau^i.$$

The second term of (19) may be similarly transformed. Thus the counterpart of (11) is

$$4\pi\sigma^2\int \rho\mathbf{v}\,.\,\mathbf{v}^*\,d\tau = 4\pi\sigma\int \mathbf{v}^*\,.\,\{\mathbf{n}\,.\,(\boldsymbol{p}^i-\boldsymbol{p}^0)\}\,dS - 4\pi\sigma\int \boldsymbol{p}:\tilde{\nabla}\mathbf{v}^*\,d\tau$$
$$+\sigma\int \mathbf{v}^*\{(\mathbf{H}\,.\,\nabla)\mathbf{h}+(\mathbf{h}\,.\,\nabla)\mathbf{H}\}\,d\tau^i - \sigma\int v_n{}^*(\mathbf{H}\,.\,\mathbf{h}^i)\,dS. \quad (20)$$

The new boundary condition (18), enables all the surface integrals on the right-hand side of (20) to be replaced by (12) which, as before, may be transformed into the integrals (13).

Thus the previous result is changed only to the extent of the inclusion of the volume integral

$$-4\pi\sigma\int \boldsymbol{p}:\tilde{\nabla}\mathbf{v}^*\,d\tau \quad . \quad . \quad . \quad . \quad . \quad . \quad . \quad (21)$$

on the right-hand side of (11) and hence (14). We now show that this is an essentially negative multiple of σ.

If μ is the coefficient of viscosity, the stress tensor in the incompressible case is given by

$$\boldsymbol{p} = -p\boldsymbol{U}+\mu(\nabla\mathbf{v}+\tilde{\nabla}\mathbf{v}). \quad . \quad . \quad . \quad . \quad . \quad . \quad (22)$$

On substituting into (21) we find

$$-4\pi\sigma\int \boldsymbol{p}:\tilde{\nabla}\mathbf{v}^*\,d\tau = 4\pi\sigma\int p\boldsymbol{U}:\tilde{\nabla}\mathbf{v}^*\,d\tau - 4\pi\sigma\int \mu(\nabla\mathbf{v}+\tilde{\nabla}\mathbf{v}):\tilde{\nabla}\mathbf{v}^*\,d\tau.$$

But the first integral on the right-hand side vanishes since

$$\boldsymbol{U}:\tilde{\nabla}\mathbf{v}^* = \nabla\,.\,\mathbf{v}^* = 0$$

and the integrand of the second is essentially negative. In fact, in terms of Cartesian components

$$\mu(\nabla\mathbf{v}+\tilde{\nabla}\mathbf{v}):\tilde{\nabla}\mathbf{v}^* = \mu\left\{2\left|\frac{\partial v_x}{\partial x}\right|^2+2\left|\frac{\partial v_y}{\partial y}\right|^2+2\left|\frac{\partial v_z}{\partial z}\right|^2\right.$$
$$\left.+\left|\frac{\partial v_z}{\partial y}+\frac{\partial v_y}{\partial z}\right|^2+\left|\frac{\partial v_x}{\partial z}+\frac{\partial v_z}{\partial x}\right|^2+\left|\frac{\partial v_y}{\partial x}+\frac{\partial v_x}{\partial y}\right|^2\right\}.$$

This is the usual expression for the rate of dissipation of energy per unit volume due to viscosity. The effect of the additional terms in (14) and (15) may now be seen.

Initially (15) is of the form

$$\sigma^2 = J_1$$

and the configuration is stable if $J_1 < 0$. The above argument indicates that in the viscous case the form of (15) is modified so as to become

$$\sigma^2 + 2J_2\sigma = J_1 \quad (J_2 > 0),$$

thus

$$\sigma = -J_2 \pm \sqrt{(J_2{}^2 + J_1)}.$$

Hence the condition for stability is unchanged, i.e. J_1 must still be negative. If a particular perturbation gives rise to instability in the non-viscous case, it will also give rise to instability in the viscous case, and conversely, a stable perturbation in the non-viscous case will also be stable in the viscous case. The character of the stability will be changed however. There are three distinct cases:

(i)	$J_1 < -J_2{}^2$	damped oscillations,
(ii)	$-J_2{}^2 < J_1 < 0$	exponential decay,
(iii)	$0 < J_1$	instability.

It may be shown that, in the presence of viscosity, the stationary property exists only for cases (ii) and (iii) i.e. when σ is purely real.

§ 6. Concluding Remarks

It might be supposed that the methods used here to consider the effect of viscosity may equally well be applied to the case of ohmic dissipation when the conductivity is not assumed to be infinite, and that an equation like (20) may exist for this case also. With finite conductivity however, eqn. (7) takes the form

$$\sigma \mathbf{h}^i = \mathrm{curl}(\mathbf{v}^i \wedge \mathbf{H}^i) + (1/4\pi\kappa)\nabla^2 \mathbf{h}^i$$

(where κ is the electrical conductivity) and does not now allow $\mathbf{h}$ to be determined simply in terms of $\mathbf{v}$. The effect of ohmic dissipation thus enters into the problem rather differently, than does viscous dissipation, and it would seem that the argument in its present form cannot be simply modified to take account of finite conductivity.

Acknowledgments

The work described above was undertaken under contract with the Atomic Energy Research Establishment at Harwell, and I wish to thank the Director for his permission for its publication. I also wish to express my thanks to Professor T. G. Cowling, F.R.S., who read this paper in draft, for helpful suggestions and criticisms.

References

Bernstein, I. B., Frieman, E. A., Kruskal, M. D., and Kulsrud, R. M., 1958, *Proc. roy. Soc.*, A, **244,** 17.

Hain, K., Lüst, R., and Schlüter, A., 1957, *Z. Naturf.*, A, **12,** 833.

Kruskal, M. D., and Tuck, J. L., 1958, *Proc. roy. Soc.* A, **245**, 222.

Tayler, R. J., 1957 a, *Proc. phys. Soc. Lond.*, B, **70,** 31 ; 1957 b, *Ibid.*, B, **70,** 1049.

The Change of Volume Produced by Martensitic Transformation in Lithium and Sodium†

By Z. S. Basinski and L. Verdini‡
Division of Pure Physics, National Research Council, Ottawa, Canada

[Received September 22, 1959]

Abstract

The volume change produced by the martensitic transformation in lithium and sodium has been measured. The h.c.p. phase has in lithium a smaller volume, and in sodium a larger volume, than the cubic phase. The values are $\Delta V/V \simeq -7\times10^{-4}$ and $\Delta V/V \simeq +3\times10^{-3}$ for lithium and sodium respectively.

§ 1. Introduction

The martensitic transformation in lithium and sodium has been studied extensively in recent years. No reliable estimate, however, is available of the volume change accompanying the change of structure. Such data would be of interest especially in view of the study of the pressure effects in these transitions. The x-ray method cannot give sufficient accuracy in measurements of the lattice parameters to evaluate the small *changes* of volume involved (Barrett 1956). Some work on this problem was done previously by measuring the change of linear dimensions of the specimen (Verdini 1959a, Gindin *et al.* 1958). These measurements however do not provide a reliable means of evaluating the volume change in view of the large shear taking place during the transformation. Indeed, Gindin *et al.* (1958) obtained a totally unreasonable value for the volume change: -15% in lithium and -8% in sodium.

We have directly measured the volume change in lithium by a liquid displacement method. Unfortunately the transition in sodium occurs at temperatures for which no suitable liquid is available. The volume change in this case was obtained from the measurement of the change of pressure of helium gas enclosed between the container and the sodium specimen.

§ 2. Lithium

A lithium specimen§ in the form of a solid cylinder having a volume of about 35 cm^3 at room temperature, was enclosed in a brass container (see figure) which could be sealed at the operating temperature by a needle

† Communicated by D. K. C. MacDonald.

‡ National Research Council Postdoctorate Fellow 1957–59, on leave from Istituto ' O. M. Corbino ', Consiglio Nazionale Delle Ricerche, Roma, Italy.

§ Lithium Corporation of America, $\rho_{4\cdot2°K}/\rho_{300°K} = 2\times10^{-3}$.

valve. The dead space between the container and the specimen was measured several times with the untransformed and the transformed specimen at 86°K.

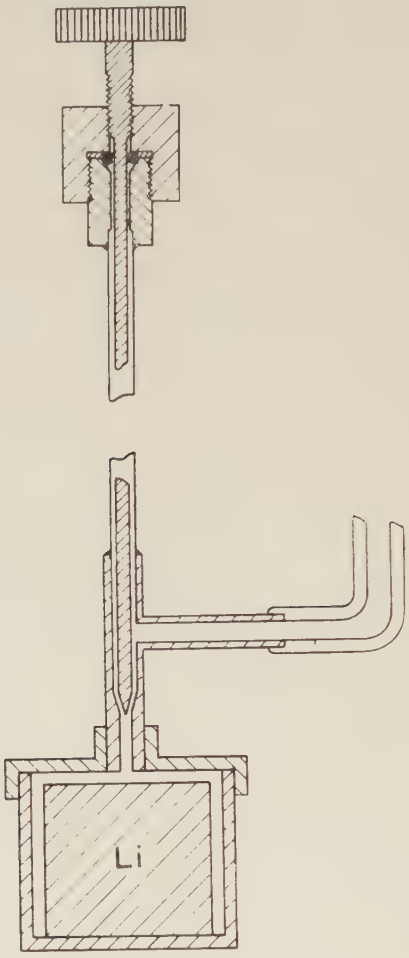

Apparatus for determining volume change in Li.

In each case the specimen was cooled by immersion in a mixture of liquid oxygen and liquid nitrogen. Purified argon was then condensed in the dead space until the level of liquid in the glass tube leading to the container was about 5 cm above the needle valve. The temperature was determined by measuring the vapour pressure of argon and was adjusted at the desired value by changing the composition of the bath. To make certain that no bubbles were present in the liquid surrounding the specimen, the bath was lowered until the level of liquid argon was 5 cm higher than that of the refrigerant. This produced an increase of about 10 cm Hg in the pressure of the liquid, the needle valve was then closed. All the argon

above the needle valve was pumped off, and the argon from the dead space introduced into a calibrated volume. The quantity of gas contained in the dead space was determined by measuring the pressure in the calibrated volume with the specimen at room temperature.

The process was repeated after the specimen had been cooled to 4·2°K and warmed up to 86°K. It is known from other experiments (Verdini 1959 b, Martin 1958) that the reverse transition does not take place until lithium is warmed up to at least 90°K. The dead volume with the untransformed specimen was 2·639 cm³ reproducible to within 0·02% (the density of liquid argon was taken as 1·408 g/cm³ at 86°K and that of the gas at N.T.P. as $1{\cdot}784 \times 10^{-3}$ g/cm³). After the transformation the dead volume was observed to increase by $(11 \pm 1) \times 10^{-3}$ cm³ which gives for the fractional volume change in lithium $-(3{\cdot}3 \pm 0{\cdot}3) \times 10^{-4}$. If we assume that about 50% of lithium is transformed on cooling to 4·2°K (Basinski, unpublished work) this gives

$$\frac{V_{\text{h.c.p.}} - V_{\text{b.c.c.}}}{V_{\text{b.c.c.}}} \simeq -7 \times 10^{-4}.$$

§ 3. Sodium

The same method could not be applied to determine the volume change occurring during the martensitic transformation in sodium. This takes place on cooling the specimen to about 35°K; at this temperature no suitable liquid is available. Instead we have measured the change of pressure of helium gas to determine the volume change of the dead space produced by the transformation. A cylindrical specimen of sodium having a volume of about 50 cm³ at the reference temperature of 43°K was sealed in a copper container leaving a dead space of $(2{\cdot}9 \pm 0{\cdot}1)$ cm³. The container was connected by a 0·5 mm I.D. capillary to one arm of a differential oil manometer; the other arm was connected by a similar capillary to a copper bulb having a volume approximately equal to that of the dead space. A cryostat of standard design in this laboratory (Dauphinee and Woods 1955) which could maintain a preset specimen temperature to within $\pm 10^{-3}$°K was used, and the temperature was measured with a calibrated platinum resistance thermometer.

Both bulbs were filled with helium gas at 43°K to a pressure of 226 mm Hg corresponding to a pressure of 2925 mm of oil. The temperature was held constant for about two hours until equilibrium was attained. The temperature was then lowered to 4·2°K. The specimen was next slowly warmed up to 43°K and kept there for another hour. The volume change produced by the transformation resulted in an increase of pressure of about (72 ± 1) mm of oil in the first cycle. However, the second cycle after reheating to 67°K and then cooling to 4·2°K gave a pressure change of only 35 mm of oil. The difference was presumably due to the smaller amount of h.c.p. phase formed in the second cycle. This effect is commonly observed

in sodium during the second conversion cycle without an intermediate room temperature annealing. (Gugan and Dugdale 1958, Martin 1958). After reheating to 67°K the original pressures were obtained at 43°K.

Unlike lithium, sodium shows an *expansion* when transformed into a close-packed structure. The values of the fractional volume change of the specimen obtained from the first and the second experiment are $1{\cdot}45\times10^{-3}$ and $0{\cdot}7\times10^{-3}$ respectively. If we assume that in the very coarse grained specimen about 45% of the metal transformed on the first run (Hull and Rosenberg 1959) we get for the fractional difference of volume of the two phases:

$$\frac{V_{\text{h.c.p.}}-V_{\text{b.c.c.}}}{V_{\text{b.c.c.}}}\simeq 3\times10^{-3}.$$

§ 4. Conclusion

The main uncertainty in our determination of the volume difference of the two phases arises from our ignorance of the fraction of the specimen which transforms; the quoted values should therefore be regarded only as approximate. Nevertheless, the small magnitude of the volume change indicated by the x-ray work (Barrett 1956) is confirmed.

Gindin *et al.* (1958) claimed to have found a volume contraction of about 15% in lithium and about 8% in sodium. They have compressed the specimens plastically at 1·4°K and measured the change of length of the specimens during the subsequent warming. It is very probable that the observed changes resulted from a macroscopic shear during the reverse transformation rather than from a true volume change. In fact plastic compression would be expected to favour the formation of those martensitic plates whose orientation would relieve the applied stress. The shear angle of about 9° expected here (Mackenzie 1959, private communication) is sufficiently large to explain the magnitude of the observed effect.

Gugan and Dugdale (1958) have measured the influence of pressure on the transition temperature in lithium. They have found an increase of about 0·5°K in the transition temperature using pressures of about 2000 atmospheres. If we assume that the compressibility of the two phases is not much different, and that the M_s temperature changes with pressure by approximately the same amount as the equilibrium temperature then the Clausius-Clapeyron eqaution gives for the temperature change resulting from the increase in pressure of 2000 atmospheres

$$\Delta T=\frac{T\Delta V\Delta p}{\Delta H}\approx 2^{\circ}\text{K}$$

where $\Delta H\simeq 20$ cal/mole (Martin 1958). The scatter in the observed M_s temperatures suggests that the difference between the temperature change observed by Gugan and Dugdale, and that calculated from the volume change is not significant.

Acknowledgments

We are much indebted to Dr. S. B. Woods for the use of a cryostat. We are grateful to Drs. J. S. Dugdale, D. Gugan and D. Martin for their helpful discussions.

References

Barrett, C. S., 1956, *Acta cryst.*, **9,** 671.
Dauphinee, T. M., and Woods, S. B., 1955, *Rev. sci. Instrum.*, **26,** 693.
Gindin, I. A., Lazarev, B. G., Starudubov, D., and Khotkevich, V. I., 1958, *J. exp. theor. Phys.*, **35,** 802; 1959, *Soviet Physics JETP*, **35,** 556.
Gugan, D., and Dugdale, J. S., 1958, *Canad. J. Phys.*, **38,** 1248.
Hull, D., and Rosenberg, H. M., 1959, *Phys. Rev. Letters*, **2,** 205.
Martin, D. S., 1958, *Phys. Rev. Letters*, **1,** 4.
Verdini, L., 1959 a, *Ric. sci.*, **9,** 3; 1959 b, *Nuovo Cim.* (to be published).

The Ductile–Brittle Transition in Ionic Solids†

By T. L. Johnston, R. J. Stokes and C. H. Li
Minneapolis-Honeywell Research Center,
Hopkins, Minnesota, U.S.A.

[Received July 9, 1959]

Abstract

Polished monocrystals of silver chloride, sodium chloride, lithium fluoride and magnesium oxide have been shown to exhibit ductility transitions when loaded by impact bending. The behaviour of silver chloride stood apart from that of the other solids in that the temperature below which it cleaved without macroscopic deformation was less than 0·1 T_m (where T_m is the melting point in degrees Kelvin) whereas the corresponding temperatures for sodium chloride, lithium fluoride and magnesium oxide were in the range 0·6–0·7 T_m. Notched monocrystals of silver chloride exhibited a change in fracture mode from cleavage to shear at a temperature of the order of 0·4 T_m.

It is emphasized that the ductility of ionic solids is extremely sensitive to strain rate and the presence of a notch.

§ 1. Introduction

In general, high purity ionic crystals having the rock-salt structure are regarded as brittle materials which can be cleaved readily over (100) planes. The silver halides are an exception in that they are very ductile and it is commonly thought that they cannot be cleaved. However, as Mitchell (1957) has observed, it is possible to obtain cleavage in thin sheets of silver chloride at liquid air temperature. In addition, we have found recently that under certain conditions large single crystals and polycrystalline specimens can also be cleaved at low temperatures. When these conditions are made more severe they become brittle even at room temperature. It appears then that the ability to cleave is a characteristic feature common to all the rock-salt ionic solids.

It is well known that metals which possess a cleavage mode of fracture also have a well defined ductile–brittle transition. It is the purpose of this paper to direct specific attention to the ductile–brittle transition in ionic solids and to consider some of its consequences.

In the case of metals the transition is manifested in two ways, either in terms of ductility or of fracture mode. The ductility transition refers to a fairly rapid decrease in the ability of a metal to deform without fracture with a decrease in temperature. The fracture mode transition makes reference to the fact that at low temperatures cracks propagate by cleavage whereas

† Communicated by the Authors.

above the transition temperature they tend to propagate in a ductile or shear mode. With these aspects of the transition in metals to serve as an experimental guide we have investigated the behaviour of silver chloride, sodium chloride, lithium fluoride and magnesium oxide monocrystals.

Although it is already clear that the rock-salt ionic solids have a ductility transition (both sodium chloride and potassium chloride become more ductile at elevated temperatures (Schmid and Boas 1935)) very little is known about the form that it takes or how sensitive it is to certain parameters. In particular it is important to determine how it may be affected by strain rate and the presence of a notch, both of which are known to be sensitive factors in the case of metals. One aspect of the effect of a notch is that it provides a ready means of localizing plastic flow and thereby increases the probability of forming a ductile crack.

§ 2. Experimental Procedure

2.1. *Material Used*

Optically pure single crystals of silver chloride, sodium chloride and lithium fluoride were purchased from the Harshaw Chemical Company (Cleveland, Ohio). In the case of silver chloride, great care was taken by the manufacturer to eliminate carbonates, nitrates and phosphates. Spectrographic analysis showed that no cationic impurities were present in excess of a few parts in 10^6. In sodium chloride, the only detectable cationic impurities were a few parts in 10^5 of silver and a few parts in 10^6 of copper. The lithium fluoride was slightly less pure and contained a few parts in 10^5 of magnesium and silver and a few parts in 10^6 of copper, sodium and iron.

Magnesium oxide crystals, nominally 99·5% pure, were purchased from the Norton Company (Worcester, Massachusetts). The concentrations of the principal impurities iron and silica varied from one crystal to another.

2.2. *Specimen Preparation*

Oversize sodium chloride, lithium fluoride and magnesium oxide prisms were prepared by cleavage and reduced to final dimensions with a chemical polish. This polish also served to eliminate any severe surface damage. Specimens were $1\frac{1}{4}$ in. long and had a final square section of 0·2 in × 0·2 in.

The greatest care in preparation was given to the sodium chloride prisms which were water polished by hand on wet silk supported on a glass plate. At least 0·030 in. were removed from each surface. Lithium fluoride and magnesium oxide crystals were polished by immersion for five minutes in boiling 85% orthophosphoric acid.

Since silver chloride could not be cleaved in the conventional manner, prisms of prescribed orientation were carefully sawn from a parent crystal. They were mechanically polished with a fine wet emery paper and finally chemically polished in hot ammonia. Orientations were determined most conveniently by examination of the cleavage markings on specimens

fractured at liquid nitrogen temperature (see later), although these determinations were also checked by x-ray diffraction.

It was most convenient to assess the effect of a 'V' notch on the transition of silver chloride since it was more readily machined than the other solids. A 90° notch (0·025 in. deep) was introduced into the mid-section of the prism with a razor blade guided by a profile jig.

2.3. *Experimental Method*

We chose to determine the ductility transition of the various solids by measurement of the energy absorbed in the deformation and fracture of specimens impact loaded in air at different temperatures. Specimens were held in a horizontal position by supports ($1\frac{1}{16}$ in. apart) at each end and subjected to an impact bending load at the mid-span with a swinging pendulum pivoted above the specimen. This arrangement was similar to that of the Charpy impact test. At the moment of impact the pendulum striker had a velocity of 55 in./sec and an energy of 10 in.-pounds; the corresponding maximum strain rate in the outer fibres of unnotched specimens was estimated to be approximately 40/sec.

The following temperature baths were used to heat or cool the specimens prior to testing. Iso-pentane cooled with liquid nitrogen was used for sub-zero temperatures, while a heated bath of mineral oil reached temperatures between 20 and 175°C. Above 175°C, specimens were raised to the test temperature while in position in the machine with a small removable resistance furnace. In all cases at least five minutes was allowed for specimens to reach thermal equilibrium.

It proved necessary to test magnesium oxide at temperatures of the order of 2000°C. To do this, specimens were heated on carbon beam supports in a carbon resistance furnace and then subjected *in situ*, to an impact bending load provided by a molybdenum drop weight. The height and weight of the latter was adjusted to give the same striking velocity and input energy as those involved in the impact bending of the other solids. Although it was not possible to measure the energy absorbed during impact under these conditions, the transition temperature range could be readily recognized by visual examination of the loaded specimens.

§ 3. The Ductility Transition

3.1. *Unnotched Single Crystals*

Each solid tested, namely silver chloride (of cubic orientation), sodium chloride, lithium fluoride and magnesium oxide exhibited a ductility transition. In fig. 1 the energy versus the temperature of impact is plotted for all the crystals tested except magnesium oxide. The temperature has been expressed as a fraction of the melting point in degrees Kelvin to permit convenient comparison of the respective transitions. The point on each curve at which an increase in energy could just be detected will be defined here as the nil-ductility temperature. This also coincided with the temperature below which no plastic bending could be measured when the

two fractured halves were butted together. Figure 2 (Pl. 160) shows a series of sodium chloride and magnesium oxide crystals fractured over the transition range of temperature. From the photograph it may be deduced that the nil-ductility temperature of sodium chloride lies between 350 and 380°c (energy absorption measurements indicate 370°c) and that the corresponding temperature for magnesium oxide lies between 1860°c and 1960°c. The estimated position of the magnesium oxide curve in fig. 1 was based upon the appearance of the crystals in fig. 2.

One should not attach any significance to the temperature at which specimens absorbed the impact energy without fracture since it depended upon (*a*) the rate at which the striker decelerated, which in turn was a function of the initial flow stress and the strain hardening rate of the specimen, (*b*) the form that the specimens adopted as they wrapped around the striker and were carried between the specimen supports and thus on the geometry of the system. In contrast, the nil-ductility temperature had better experimental identity in that the above factors were absent.

Fig. 1

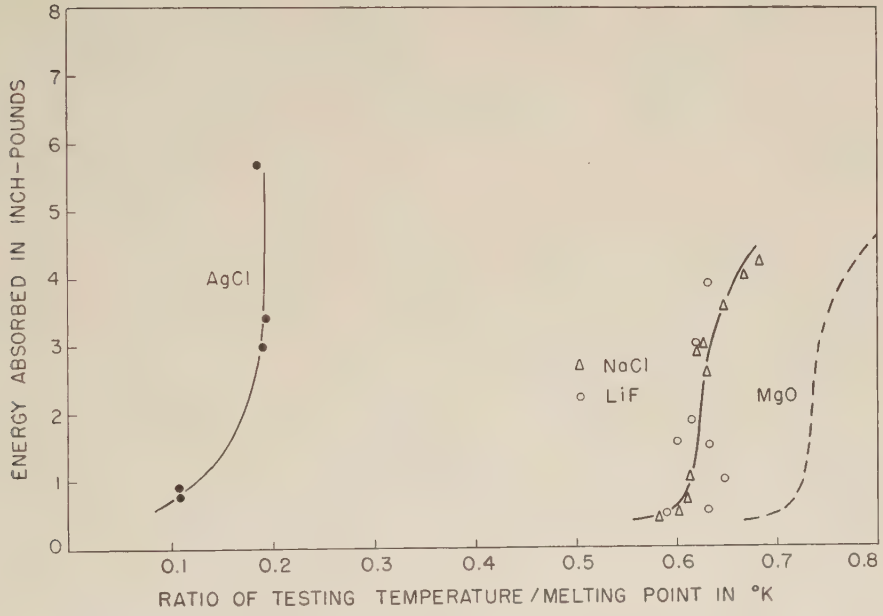

Impact data for single crystals of AgCl (cubic orientation), NaCl, LiF and MgO. The position of the curve for MgO was estimated from fig. 2.

In fig. 1 it will be noted that the energy absorption figures for lithium fluoride crystals do not lie on a curve as smooth as that for the sodium chloride crystals. This is now believed to be the result of an inadequate removal of the surface damage (introduced during cleavage) when the crystals were chemically polished. It was difficult to preserve the shape of lithium fluoride specimens during prolonged immersion in orthophosphoric acid.

A number of carefully polished sodium chloride crystals were impacted while still dissolving in distilled water at room temperature. They were also found to be brittle. The enhancement of ductility normally associated with such a treatment at a low strain rate does not appear to apply under these conditions.

It is important to note from fig. 1 that, with the above factors in mind, the behaviour of silver chloride stands apart from the other solids in that its nil-ductility temperature is less than $0{\cdot}1\ T_m$ whereas for both sodium chloride and lithium fluoride the nil-ductility temperature is approximately $0{\cdot}6\ T_m$ and for magnesium oxide approximately $0{\cdot}7\ T_m$. Silver chloride monocrystals tend to become brittle when loaded at a high strain rate at a low temperature.

3.2. *Notched Silver Chloride Crystals*

In fig. 3 it can be seen that for silver chloride crystals having approximately the cubic orientation (i.e. orientation number 1) the nil-ductility

Fig. 3

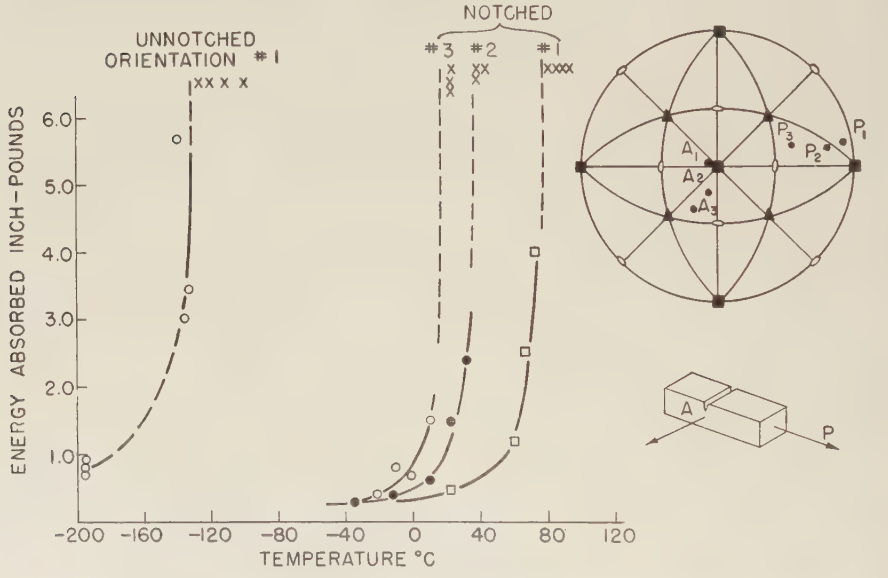

Impact data for notched AgCl single crystals having the orientations specified in the stereogram. The points marked " x " refer to specimens which absorbed impact without fracture.

temperature was increased from the unnotched value of less than $0{\cdot}1\ T_m$ to $0{\cdot}4\ T_m$ in the presence of a notch (i.e. from < -200°C to approximately 10°C). In addition, fig. 3 shows that the transition range of notched crystals depended upon the orientation of the specimens. The more the orientation deviated from that of the cubic, so the transition was shifted to lower temperatures.

§ 4. Fracture Mode

4.1. *Unnotched Specimens*

Even though there was a big difference between the homologous nil-ductility temperatures of unnotched silver chloride and the other solids tested, the fracture mode was identical in all cases. Fracture occurred by cleavage over (100) planes and the origin was invariably located at a point near or at the tension surface opposite to the point of impact. This mode persisted throughout the respective ductility transition ranges right up to the temperature at which specimens were driven between the supports without fracture. It is important to note that specimens never fractured at the load points, indeed small plastic indentations were produced at the two supports and especially beneath the striker even at temperatures below the nil-ductility temperature. Figure 4 (Pl. 160) is a photomacrograph of a silver chloride cleavage obtained at liquid nitrogen temperature. As the crack spread across the original neutral axis the cleavage lines tended to follow [100] directions, this, together with the cleavage plane, provided a convenient means of checking crystal orientation visually as mentioned earlier.

In view of the fact all specimens fractured by cleavage in the ductility transition range, it must be assumed that the increase in the absorbed energy measured in fig. 1 stemmed primarily from the increasing deformation which preceded fracture (shown in fig. 2).

4.2. *Notched Silver Chloride Crystals*

Below the nil-ductility temperature notched silver chloride crystals fractured by the characteristic (100) cleavage for each of the orientations shown in fig. 3. Above the nil-ductility temperature, however, the fracture appearance depended both upon temperature and crystal orientation. For orientations 1 and 3 it was found that small regions developed at the base of the notch wherein fracture appeared to have propagated by a ductile mode. In particular, for crystals of the cubic orientation (number 1) the ductile cracks assumed a lenticular shape before cleavage nucleated from some point along their periphery. The size of the ductile crack and the corresponding degree of lateral contraction across the base of the notch increased with temperature through the transition range. Figure 5 (Pl. 161) is a photomacrograph of the fracture surface of the specimen fractured at 65°C (note the transition curve in fig. 3). This photograph clearly shows that a fracture mode transition can exist in a single crystals.

By contrast, crystals having orientation number 2 did not display ductile areas on the fracture surfaces of specimens impacted in the transition range of temperature. Instead, the notch widened by plastic deformation along the whole of its length before cleavage nucleated from some point in this worked surface.

Figure 6 (Pl. 161) illustrates the microscopic features of the boundary between the two fracture modes in a specimen of orientation 1 impacted at

room temperature. The surface of the ductile crack was characterized by ripples or corrugations. One set of corrugations tended to be parallel and regularly spaced and possibily represented successive positions of the ductile crack front. The other set radiated from the region of the origin of fracture at the base of the notch. The latter surface markings developed along the line where more than one ductile crack joined up. As the testing temperature was increased the surface markings became more complex and the corrugations occurred on a much finer scale. In addition, wavy slip traces were superposed on this background. Figure 7 (Pl. 162) shows the surface of a ductile crack formed at 65°c in a specimen having the cubic orientation.

It is important, therefore, to remember that the energy absorbed by notched silver chloride specimens in the transition range was a reflection not only of the energy required to bend the specimens but also the energy required to propagate a ductile crack.

§ 5. Discussion

The ability of an ionic solid to accommodate plastic flow at a given temperature without fracture depends to a marked degree upon the imposed plastic strain rate. This statement is re-emphasized by the present work when it is remembered that magnesium oxide crystals may be bent to a surface plastic strain of 15% when tested at room temperature at a strain rate of 10^{-5}/sec (Stokes *et al.* 1959a). The nil-ductility temperature is therefore less than $0{\cdot}1\,T_m$ at this strain rate. On the other hand, we have shown here that at a strain rate of 40/sec it is necessary to raise the temperature to 2000°c to accommodate similar deformation. Likewise, Joffe *et al.* (1924) found that the fracture strength of sodium chloride remained constant within the temperature range of -190°c to $+600$°c providing the strain rate was increased so as to prevent macroscopic deformation prior to fracture. In effect, the nil-ductility temperature was raised approximately 800°c by this treatment. The marked effect of a notch on the nil-ductility temperature of silver chloride as described in this paper is further evidence of the exteme sensitivity to the strain rate.

The magnitude of the strain rate effect in ionic solids is very much greater than that characteristic of the b.c.c. and h.c.p. metals. Magnussen and Baldwin (1957) showed that an approximate 10^6-fold increase in strain rate from 8×10^{-4}/sec to 300/sec increased the ductility transition of tungsten only 250°c, i.e. from $0{\cdot}1\,T_m$ to $0{\cdot}17\,T_m$. For polycrystalline zinc, a similar increase in strain rate raised the transition 50°c, i.e. from $0{\cdot}4\,T_m$ to $0{\cdot}48\,T_m$.

Impurities currently play an essential rôle in the theortical analysis of the ductile brittle transition in b.c.c. metals. They are considered to act in two ways, first by locking the dislocation sources thereby causing a strong temperature dependence of the yield stress to initiate plastic flow, and second, by their influence on the lattice friction stress resisting dislocation motion. In covalent solids, on the other hand, impurities probably play a less responsible rôle in the ductility transition. This class of materials is

one in which the yield stress is controlled primarily by the inherent lattice resistance to dislocation motion (Orowan 1954)†.

It is important to consider the relative importance of dislocation locking by impurities and lattice resistance in the brittleness of the ionic solids. Dislocation behaviour in lithium fluoride and magnesium oxide suggests that the promotion of plastic flow in these solids depends more strongly upon the fractional resistance of the lattice than the activation of pinned sources (Johnston and Gilman 1959, Stokes *et al.* 1959 b). The stress to overcome this frictional force has been measured directly in lithium fluoride and is found to decrease exponentially with an increase in temperature, and to increase with the velocity of the dislocation across the slip plane (Johnston and Gilman 1959).

On this basis the present authors are inclined to believe that the ductility transition of ionic solids is a consequence of the strongly temperature-dependent lattice friction stress. It is further believed that if impurities influence the transition temperature, then they will do so primarily through a corresponding change in lattice resistance rather than through the locking of dislocation sources.

Of course, one cannot account for a ductility transition in terms of the stress to overcome lattice resistance alone. Consideration must be given also to the crack nucleation mechanism upon which this stress acts. It is already known that cracks are formed at the intersection of slip bands in magnesium oxide deformed at a low temperature and at a slow strain rate. (Stokes *et al.* 1959 a. Washburn *et al.* 1959). However, it remains to be determined what effects a change in temperature and strain rate will have upon the fracture mechanism in magnesium oxide and other ionic solids, before mechanistic details of the ductility transition can be clarified.

Regardless of the interpretation of the ductile–brittle transition the interesting fact remains that silver chloride is quite ductile at low homologous temperatures when compared with the other ionic solids. It could be that the ability of silver chloride to slip readily on so many slip systems at low temperatures modifies the manner in which cracks form, which for that observed on magnesium oxide at least, depends upon the consequences of simple conjugate slip (Stokes *et al.* 1959 a). If this should prove to be the case, then it is very important to know the fundamental factors responsible for the difference in slip behaviour.

Acknowledgments

The authors are especially grateful to D. J. Landis for experimental assistance throughout this investigation. They wish to express their appreciation to Dr. J. J. Harwood and to Dr. F. J. Larsen, Director of Research, Honeywell Research Center for their continued interest and permission to publish this work which was partially supported by the O.N.R.

† It is interesting to note that carefully polished zone-refined germanium (having an impurity concentration of only one part in 3×10^{10}) tends to fracture without macroscopic deformation at temperatures up to 0·5 T_m, even for extremely slow strain rates.

References

Joffe, A., Kirpitschewa, M. W., and Lewitsky, M. A., 1924, *Z. Phys.*, **22**, 286.

Johnston, W. G., and Gilman, J. J., 1959, *J. appl. Phys.*, **30**, 129.

Magnussen, A. W., and Baldwin, W. M., 1957, *J. Mech. Phys. Solids*, **5**, 172.

Mitchell, J. W., 1957, *Dislocations and Mechanical Properties of Crystals* (New York : John Wiley), p. 72.

Orowan, E., 1954, *Dislocations in Metals* (A.I.M.M.E.), p. 127.

Schmid, E., and Boas, W., 1935, *Plasticity of Crystals* (English translation) (F. A. Hughes Co., Ltd.), p. 227.

Stokes, R. J., Johnston, T. L., and Li, C. H., 1959 a, *Phil. Mag.*, **4**, 920 ; 1959 b, *Trans. Amer. Inst. min. (metall.) Engrs*, **215**, 437.

Washburn, J., Gorum, A. E., and Parker, E. R., 1959, *Trans. Amer. Inst. min. (metall.) Engrs*, **215**, 230.

Scattering of Thermal Neutrons in Aluminium†

By L. S. Kothari
Atomic Energy Establishment, Trombay,
Apollo Pier Road, Bombay, India

[Received June 25, 1959; and in revised form August 10, 1959]

Abstract

In order to investigate theoretically the scattering of thermal and cold neutrons by crystals, one normally uses the Debye spectrum for the lattice vibrations and assumes the velocity of sound in the medium to be constant. Taking a more realistic model (suggested by the Born von Karman theory) for the dispersion relation and the frequency distribution function, we have here calculated the inelastic scattering cross section for cold neutrons and have shown, in the particular case of aluminium, that the results conform better with experiment. The scattering surface for long wavelength neutrons has also been obtained and it agrees well with the highly detailed calculations of Squires (1956).

§ 1. Introduction

The specific heat of metals at low temperatures and also the scattering cross section of thermal neutrons for polycrystalline materials is normally calculated assuming (i) the Debye spectrum for the lattice vibrations and (ii) that the velocity of sound waves in the medium is independent of the wavelength, i.e. there is no dispersion. The agreement between theory and experiment is very good for most of the materials that have been investigated. This is mainly due to the fact that in calculating both the specific heat and the total scattering cross section for neutrons, one integrates over the entire frequency spectrum so that the calculated results do not depend sensitively on the exact shape of the spectrum.

Recently a lot of experimental work on the measurement of angular and energy distributions of neutrons scattered by a single crystal has been done (Brockhouse and Stewart 1955, 1958, Carter *et al.* 1957, Brockhouse and Iyengar 1958, Pelah *et al.* 1957) and from these measurements the dispersion relations for the lattice vibrations have been deduced. As is to be expected, these results differ completely from the Debye approximation. To explain the observed results it is necessary to calculate more precisely the actual shape of the dispersion curve and the frequency distribution function. Squires (1956) has made these calculations for aluminium using the Born von Karman theory of lattice vibrations and the known values of the elastic constants. Neutron scattering surfaces calculated by using his results agree well with experiment (Brockhouse and

† Communicated by the Author.

Stewart 1958, Carter *et al.* 1957). However, for most of the metals an exact knowledge of the dispersion curve and frequency distribution function is lacking and in order to make any reasonable predictions about the results of neutron scattering experiments, it is necessary to improve upon the Debye approximation (in what follows we shall use this term to include both (i) the use of Debye spectrum and (ii) a constant sound velocity).

With the increasing accuracy of total scattering cross section measurements it has again become necessary to refine the theory. Normally one calculates the scattering cross section using (i) the incoherent approximation and (ii) the Debye approximation. The first step in improving the theory is to avoid the incoherent approximation and sum over the reciprocal lattice vectors instead of integrating over them. It is known that this difference between the two results, which gives the correction to the incoherent approximation, depends considerably on the actual form of the dispersion relation (Placzek and van Hove 1955) and use of the Debye approximation only gives an estimate of this correction. For various materials that have been studied (Squires 1952, Kothari and Singwi 1955, 1957, Bhandari 1957) this correction is normally found to be within about 10% of the one-phonon scattering cross section. To be able to calculate this correction better and also to get a better result for the scattering cross section in the incoherent approximation, it becomes necessary to improve upon the Debye model.

In the present paper using a dispersion relation and a frequency distribution function which is more realistic than that used by Debye, we have studied neutron scattering in aluminium. In § 2 the lattice spectrum is discussed and in § 3 we derive the relevant expressions for the scattering cross section. The one great advantage of the Debye approximation is that the calculations are greatly simplified. This advantage is here lost and the calculations become somewhat more involved. The results are discussed in the next section. The last section deals with the scattering surface for long wavelength neutrons. The results agree very well with the more exact calculations of Squires (1956).

§ 2. Lattice Spectrum

We consider an isotropic lattice, so that the dispersion relation is the same in all directions. We assume that this dispersion relation is of the same form as given by the Born von Karman theory for a linear chain of equally spaced mass points, each point carrying the same mass and with interaction confined between nearest neighbours (Blackman 1955). The frequency ν is given, in terms of the wave vector f, by the relation

$$\nu = \nu_0 |\sin \pi f/2f_0|, \quad . \quad . \quad . \quad . \quad . \quad . \quad . \quad . \quad . \quad (1)$$

where f_0 is the maximum allowed value of f and is related to the average particle separation, d by the relation $f_0 = \pi/d$. ν_0 is the highest frequency that can be propagated through the lattice and corresponds to $f = f_0$. One

can show that it is related to c_0, the phase velocity for long wavelength sound waves ($f \to 0$), by the relation

$$\nu_0 = c_0 f_0/\pi^3 = c_0/\pi d, \quad \ldots\ldots\ldots \quad (2)$$

The number of lattice vibrations lying between frequencies ν and $\nu + d\nu$, for each polarization of the sound wave, is (Blackman 1955)

$$dn \equiv Ng'(\nu)d\nu = \begin{cases} \dfrac{24N}{\pi^3\nu_0} \dfrac{\{\sin^{-1}\nu/\nu_0\}^2}{\sqrt{[1-(\nu/\nu_0)^2]}} d\nu & \text{for } \nu \leqslant \nu_0 \\ 0 & \text{for } \nu > \nu_0. \end{cases} \quad \ldots \quad (3)$$

N is the number of atoms in a lattice of volume V, $g'(\nu)$ is the frequency distribution function for any given polarization and is normalized to unity. It should be pointed out that in deriving (3) one makes use of the relation connecting the volume of the unit cell in direct space V/N, and the volume of the cell in reciprocal space B_r, i.e.

$$N/V = B_r = 4\pi/3(2d)^3. \quad \ldots\ldots\ldots \quad (4)$$

From the known value of V/N for a given lattice, one can determine d and hence f_0.

The limiting velocity c_0 for both longitudinal and transverse vibrations is quite different and to take account of this fact we write the distribution function for all the three polarizations as

$$g(\xi)d\xi = \{g'_{\mathrm{L}}(\xi) + 2g'_{\mathrm{T}}(\xi)\}d\xi, \quad \ldots\ldots\ldots \quad (5)$$

where $\xi = h\nu$ is the energy of the phonon and h is Planck's constant; g'_{L} refers to longitudinal and g'_{T} to transverse vibrations. Defining

$$\xi_{0\mathrm{L}} = h\nu_{0\mathrm{L}} = hc_{0\mathrm{L}}/\pi d, \quad \xi_{0\mathrm{T}} = h\nu_{0\mathrm{T}} = hc_{0\mathrm{T}}/\pi d, \quad \ldots\ldots \quad (6)$$

and

$$\xi_{0\mathrm{L}}/\xi_{0\mathrm{T}} = c_{0\mathrm{L}}/c_{0\mathrm{T}} = \alpha$$

we have

$$g'_{\mathrm{L}}(\xi) = \begin{cases} \dfrac{24}{\pi^3\xi_{0\mathrm{L}}} \dfrac{\{\sin^{-1}\xi/\xi_{0\mathrm{L}}\}^2}{\sqrt{[1-(\xi/\xi_{0\mathrm{L}})^2]}} & \text{for } \xi \leqslant \xi_{0\mathrm{L}}, \\ 0 & \text{for } \xi > \xi_{0\mathrm{L}}, \end{cases} \quad \ldots \quad (7a)$$

$$g'_{\mathrm{T}}(\xi) = \begin{cases} \dfrac{24\alpha}{\pi^3\xi_{0\mathrm{L}}} \dfrac{\{\sin^{-1}\alpha\xi/\xi_{0\mathrm{L}}\}^2}{\sqrt{[1-(\alpha\xi/\xi_{0\mathrm{L}})^2]}} & \text{for } \xi \leqslant \xi_{0\mathrm{L}}/\alpha, \\ 0 & \text{for } \xi > \xi_{0\mathrm{L}}/\alpha. \end{cases} \quad \ldots \quad (7b)$$

In the case of aluminium, which we shall consider in some detail, the elastic constants (density $= 2{\cdot}71$ g/cm^3, compressibility $= 1{\cdot}36 \times 10^{-12}$ cm sec^2/g and Poisson's ratio $= 0{\cdot}337$), give

$$c_{0\mathrm{L}} = 6{\cdot}35 \times 10^5 \text{ cm/sec}; \quad c_{0\mathrm{T}} = 3{\cdot}14 \times 10^5 \text{ cm/sec}.$$

However, the values deduced from the slopes of the actual dispersion curve obtained by Brockhouse and Stewart (1958) are somewhat lower and for the present calculations we have taken

$$c_{0\mathrm{L}} = 6{\cdot}0 \times 10^5 \text{ cm/sec}; \quad c_{0\mathrm{T}} = 3{\cdot}0 \times 10^5 \text{ cm/sec}.$$

(These give a Debye temperature of 394°K in comparison to the observed value of 398°K.) The corresponding limiting frequencies are

$$\nu_{0L} = 0{\cdot}929 \times 10^{13}\,\text{sec}^{-1}; \quad \nu_{0T} = 0{\cdot}465 \times 10^{13}\,\text{sec}^{-1}.$$

Similarly knowing the volume of a unit cell of aluminium (it has four atoms per cell) one can deduce d and hence f_0, using eqn. (4)

$$f_0 = 1{\cdot}528 \times 10^{8}\,\text{cm}^{-1}.$$

Fig. 1

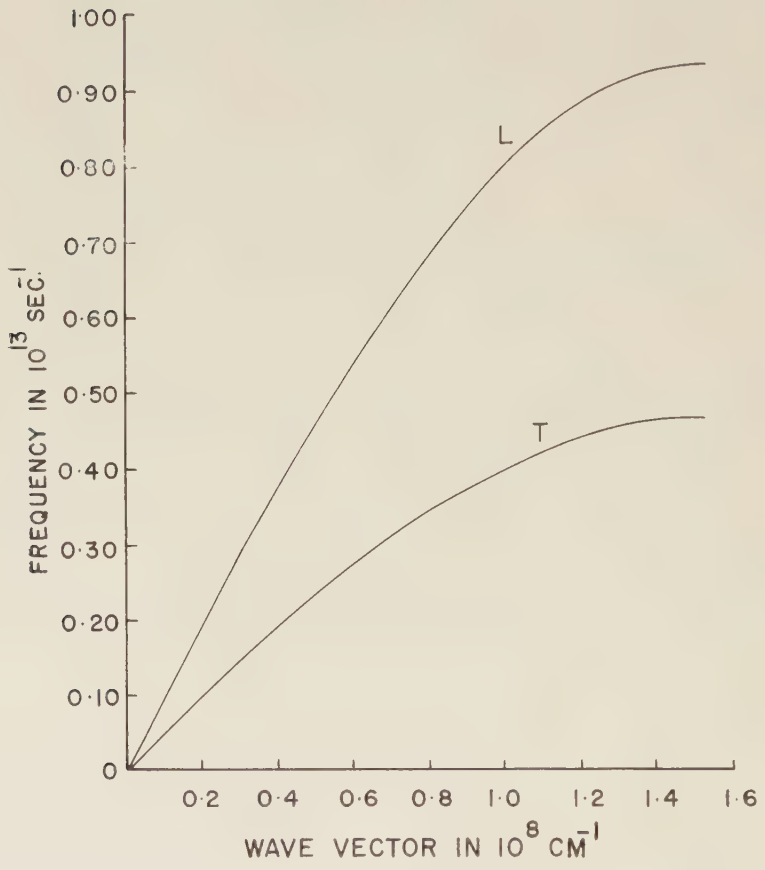

Frequency plotted as a function of the magnitude of the phonon wave vector. Curve L corresponds to longitudinal vibrations and curve T to the transverse vibrations.

The dispersion relations obtained by using these values in (1) are shown in fig. 1. The lower curve corresponds to the transverse vibrations whereas the upper one represents the longitudinal vibrations.

The calculated frequency distribution function $g(\nu)$ (eqns. (5) and (7)) is plotted against ν/ν_{0L} in fig. 2. It shows two sharp peaks. Though the curve at the two limiting frequencies ν_{0L} and ν_{0T} tends to infinity, the area enclosed is finite. It is interesting to compare these results with a similar curve obtained from x-ray data (quoted by Blackman 1955, p. 354) which again shows two sharp peaks, one around $\nu = 0{\cdot}47 \times 10^{13}\,\mathrm{sec}^{-1}$ and another around $\nu = 0{\cdot}93 \times 10^{13}\,\mathrm{sec}^{-1}$, with the first peak much higher than the second. However, agreement with Squires' (1956) calculations is not as good. He obtains one flat maximum around $\nu = 0{\cdot}4$–$0{\cdot}5 \times 10^{13}\,\mathrm{sec}^{-1}$ and another sharper maximum at $\nu \approx 0{\cdot}8 \times 10^{13}\,\mathrm{sec}^{-1}$.

Fig. 2

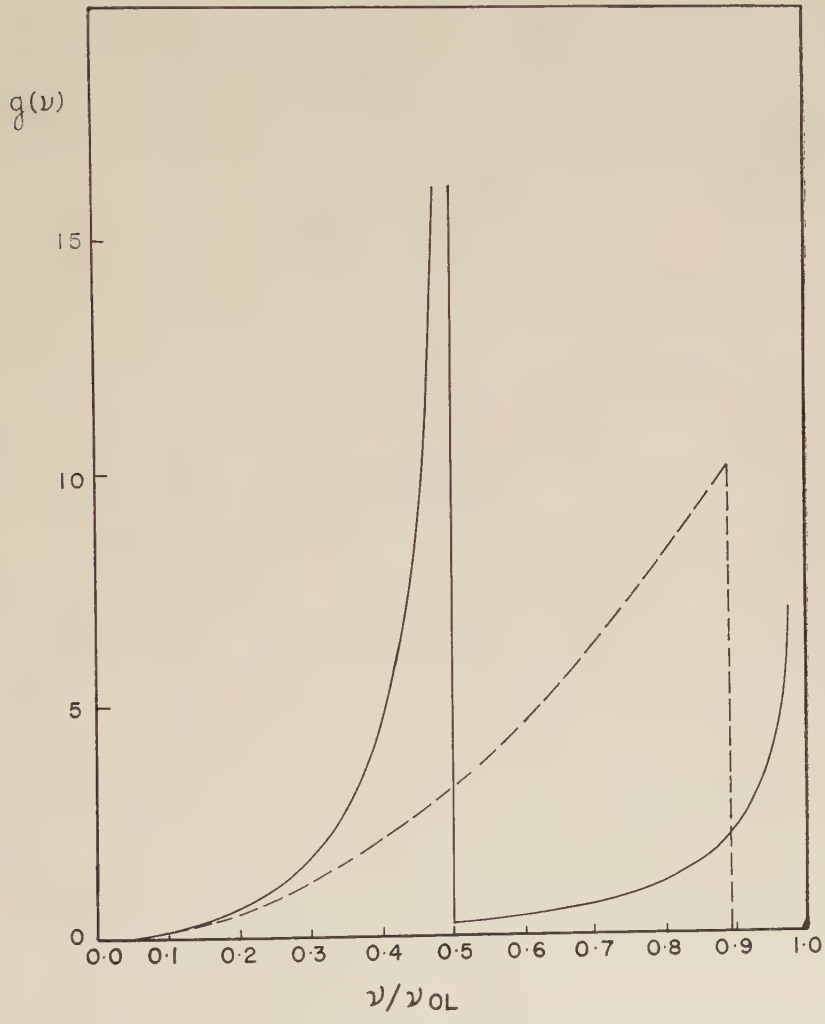

Frequency distribution function plotted against ν/ν_{0L}. Broken curve gives Debye spectrum ($\Theta_D = 398°K$).

§ 3. Inelastic Scattering Cross Section

3.1. *Coherent Scattering*

The total one-phonon coherent scattering cross section for a neutron of energy E_1 and wave vector k_1 being scattered by a polycrystalline sample was first calculated by Weinstock (1944). For the case in which the velocity of phonons in the medium is dependent upon their wave vector f, Weinstock's result for the phonon absorption cross section becomes

$$\sigma_1(E_1)=\frac{Sh(F_\tau^2/n)}{48\pi m k_1^2}\int_0^{f_0}\sum_\tau\int_{\lambda_1}^{\lambda_2}\frac{M^\tau}{\tau}\frac{(2\pi\tau+\lambda f)^2}{(\exp[hfc(f)/k_0T]-1)}$$
$$\times\exp(-2W^\tau)\,\frac{f\,df\,d\lambda}{c(f)} \quad . \quad . \quad . \quad . \quad . \quad . \quad . \quad (8)$$

where S is the coherent scattering cross section for a bound atom of mass m, τ is a reciprocal lattice vector with multiplicity M^τ, F_τ^2 is the structure factor for the unit cell containing n atoms, $\hbar$ is Planck's constant divided by 2π, k_0 is Boltzmann's constant and T is the temperature of the scatterer. λ is a variable of integration with limits λ_1 and λ_2 given by

$$\left.\begin{aligned}\lambda_1&=\max\left(-1,\frac{|k_2-k_1|-2\pi\tau}{f}\right)\\ \lambda_2&=\min\left(+1,\frac{|k_2+k_1|-2\pi\tau}{f}\right)\end{aligned}\right\} \quad . \quad . \quad . \quad . \quad . \quad (9)$$

where

$$k_2^2=k_1^2+\frac{2m_0}{\hbar}fc(f)=k_1^2+\frac{2m_0}{\hbar^2}\xi(f), \quad . \quad . \quad . \quad . \quad (10)$$

k_2 being the wave vector of the neutron after scattering and ξ being the energy of the phonon f. Exp $(-2W^\tau)$ in (8) is the Debye–Waller factor, where W^τ is given by

$$W^\tau=\frac{3F}{M}\frac{\hbar^2}{2m_0\xi_{0L}}(2\pi\tau+\lambda f)^2. \quad . \quad . \quad . \quad . \quad . \quad (11)$$

In eqn. (11) $M=m/m_0$, m_0 being the mass of the neutron, and F is given by the expression

$$F=\frac{\xi_{0L}}{18}\int\xi^{-1}g(\xi)\coth(\xi/2k_0T)\,d\xi, \quad . \quad . \quad . \quad . \quad . \quad (12)$$

where $g(\xi)$ is defined by eqns. (5) and (7). In terms of the integral

$$I(b)=\frac{4}{\pi^3}\int_0^1\frac{(\sin^{-1}x)^2}{\sqrt{(1-x^2)}}\coth\frac{x}{(2b)}\frac{dx}{x}, \quad . \quad . \quad . \quad . \quad . \quad (13)$$

F can be written as

$$F\left(\frac{k_0T}{\xi_{0L}}\right)=\frac{1}{3}\left[I\left(\frac{k_0T}{\xi_{0L}}\right)+2\alpha I\left(\frac{\alpha k_0T}{\xi_{0L}}\right)\right], \quad . \quad . \quad . \quad . \quad (14)$$

where $\alpha=\xi_{0L}/\xi_{0T}$. For $b<1$, the integral defining $I(b)$ in (13) has to be evaluated numerically whereas for $b\geqslant 1$, one can expand the coth function

in a power series and the integration carried out term by term. It gives

$$I(b)=2\pi b\left\{\ln 2+\frac{1}{18}\left(\frac{\pi}{2}\right)^2\frac{1}{(2b)^2}-\frac{1}{360}\left(1+\frac{\pi^2}{6}\right)\frac{1}{(2b)^4}+\ldots\right\}, \quad . \quad . \quad . \quad . \quad (15)$$

which is a rapidly convergent series for $b\geqslant 1$. Values of the function $I(b)/b$ for various b are given in table 1. In table 2 are given the values of F for aluminium calculated using the constants given in § 2. For comparison, in column 3 of this table we also give the values obtained on the Debye approximation.

Table 1. Values of the Function $I(b)/b$

b	$I(b)/b$	b	$I(b)/b$	b	$I(b)/b$
0·1	2·0416	0·8	0·6044	2·50	0·5680
0·2	1·1011	0·9	0·5956	3·00	0·5649
0·3	0·8331	1·0	0·5899	4·00	0·4635
0·4	0·7226	1·25	0·5794	5·00	0·5629
0·5	0·6675	1·50	0·5742	6·00	0·5626
0·6	0·6364	1·75	0·5707	8·00	0·5622
0·7	0·6171	2·00	0·5688	10·00	0·5621

For aluminium, which is a face-centred cubic lattice, $F_\tau^2/n=0$ for all reciprocal lattice vectors, except for those whose indices are either all even or all odd. In this later case $F_\tau^2/n=1$. Hence in summing (8) over τ, we need take only those reciprocal lattice vectors which have indices either all even or all odd and forget about the term F_τ^2/n.

Table 2. Values of the Function $F(T)$

T in units of ξ_{0L}/k_0	$F(T)$	$F_{\text{Debye}}(T)$
0·5	0·5041	0·5429
0·75	0·7269	0·7791
1·00	0·9548	1·0220
1·50	1·4169	1·5145
2·00	1·8820	2·0112

Integrating (8) over λ we obtain,

$$\sigma_1(E_1)=\frac{S\hbar}{96\pi mk_1^2\gamma^3}\int_0^{f_0}\sum_\tau\frac{M^\tau}{\tau}\left[p\exp(-p^2)-q\exp(-q^2)+\int_0^q\exp(-z^2)dz-\int_0^p\exp(-z^2)dz\right]\frac{df}{c[\exp(\hbar cf/k_0T)-1]}, \quad (16)$$

where

$$p=\gamma(2\pi\tau+\lambda_1 f);\quad q=\gamma(2\pi\tau+\lambda_2 f);\quad \gamma=\left(\frac{3F\hbar^2}{m\xi_{0L}}\right)^{1/2}. \quad (17)$$

Taking a fixed value of f, we sum over all allowed values of τ and then the integral over f if evaluated graphically over both the branches of the dispersion relation, the transverse branch being weighted by a factor 2. The results obtained are discussed in a later section.

3.2. *Incoherent Approximation*

In the incoherent approximation, the total one-phonon scattering cross section for a neutron of energy E_1 being scattered by a cubic lattice is given by the expression (Kothari and Singwi 1959)

$$\sigma_1(E_1)=\frac{(S+s)h^2}{24\pi m k_1}\int\int k_2\xi^{-1}g(\xi)(\mathbf{k}_1-\mathbf{k}_2)^2\exp(-2W)[\exp(\xi/k_0T)-1]^{-1}d\xi\,d\Omega \quad . \quad . \quad . \quad (18)$$

where, now

$$2W=\gamma(\mathbf{k}_1-\mathbf{k}_2)^2. \quad . \quad . \quad . \quad . \quad . \quad . \quad . \quad . \quad . \quad (19)$$

We expand the Debye–Waller factor in a power series and integrate over the solid angle. If only the first term of the expansion is retained, the expression gives the first term of the Placzek (1954) expansion, $\sigma^1(E_1)$. This takes account of the multiphonon processes also.

3.2.1. *Placzek expansion*

Substituting for $g(\xi)$ from (5) and (7) and putting $a=E_1/\xi_{0L}$ and $b=k_0T/\xi_{0L}$, one can show after a little simplification that

$$\sigma^1(E_1)=\frac{4(S+s)}{\pi^3 M\sqrt{a}}\Big[I_{3/2}(a,b)+aI_{1/2}(a,b)+\frac{2}{\alpha^{1/2}}\Big(I_{3/2}(\alpha a,\alpha b)+\alpha a I_{1/2}(\alpha a,\alpha b)\Big)\Big], \quad . \quad . \quad (20)$$

where

$$I_{n/2}(a,b)=\int_{-a}^{1}(a+x)^{n/2}\Big\{\coth\Big(\frac{x}{2b}\Big)-1\Big\}\frac{(\sin^{-1}x)^2}{\sqrt{(1-x^2)}}\,\frac{dx}{x}. \quad . \quad (21)$$

Except in some limiting cases, the integral in (21) has to be evaluated numerically. However, in the case of cold neutron scattering from a sample at $T\geqslant\xi_{0L}/k_0$, which corresponds to $a=E_1/\xi_{0L}\ll 1$ and $b=k_0T/\xi_{0L}\geqslant 1$, the integral can be solved into power series.

In the other limiting case of $E_1/\xi_{0L}\gg 1$, and $k_0T/\xi_{0L}\gg 1$, it is much easier to evaluate the cross section and one finds (taking $\alpha=2$)

$$\sigma^1(E_1)=\frac{4(S+s)m_0k_0TE_1}{m}\Big[\frac{72\ln 2}{\pi^2\xi_{0L}^2}+\Big(\frac{1}{8E_1^2}-\frac{1}{2E_1k_0T}+\frac{1}{12k_0^2T^2}\Big)\Big]. \quad (22)$$

This may be compared with the result in the Debye approximation

$$\sigma^1{}_{\text{Debye}}(E_1)=\frac{4(S+s)m_0k_0TE_1}{m}\Big[\frac{3}{(k_0\Theta_D)^2}+\Big(\frac{1}{8E_1^2}-\frac{1}{2E_1k_0T}+\frac{1}{12k_0^2T^2}\Big)\Big]. \quad . \quad . \quad . \quad (23)$$

The results of this analysis appear in fig. 3 which will be discussed later.

3.2.2. *One-phonon cross section*

In order to find the correction to the incoherent approximation, which arises because of the replacing of the sum over reciprocal lattice vectors by an integral, one must calculate the one-phonon scattering cross section $\sigma_1(E_1)$ on the new model of lattice vibrations. In general, one will have to integrate eqn. (18) numerically over ξ to get $\sigma_1(E_1)$. However, in the limit $a = E_1/\xi_{0L} \ll 1$ and $b = k_0 T/\xi_{0L} \geqslant 1$, one can carry out the integration analytically as in the case of $\sigma^1(E_1)$, though the calculations become a little more involved. The final result is

$$\begin{aligned}\sigma_1(E_1) = \frac{4(S+s)}{\pi^3 M\sqrt{a}}\Bigg[& I_{3/2}(a,b) + aI_{1/2}(a,b) \\ & + \frac{2}{\alpha^{1/2}}\left(I_{3/2}(\alpha a, \alpha b) + \alpha a I_{1/2}(\alpha a, \alpha b)\right) \\ & - \frac{6F}{M}\Bigg\{ I_{5/2}(a,b) + \frac{10}{3} aI_{3/2}(a,b) + a^2 I_{1/2}(a,b) \\ & + \frac{2}{\alpha^{3/2}}\left(I_{5/2}(\alpha a, \alpha b) + \frac{10}{3}\alpha a I_{3/2}(\alpha a, \alpha b)\right. \\ & \left. + \alpha^2 a^2 I_{1/2}(\alpha a, \alpha b)\right)\Bigg\} \\ & + \frac{18F^2}{M^2}\Bigg\{ I_{7/2}(a,b) + 7aI_{5/2}(a,b) + 7a^2 I_{3/2}(a,b) \\ & + a^3 I_{1/2}(a,b) \\ & + \frac{2}{\alpha^{5/2}}\left(I_{7/2}(\alpha a, \alpha b) + 7\alpha a I_{5/2}(a,b)\right. \\ & \left. + 7\alpha^2 a^2 I_{3/2}(\alpha a, \alpha b) + \alpha^3 a^3 I_{1/2}(\alpha a, \alpha b)\right)\Bigg\} \\ & + \ldots .\Bigg] \qquad \ldots\ldots\ldots\ldots \quad (24)\end{aligned}$$

where the various quantities have already been defined.

§ 4. Results and Discussion

We now consider in some detail the scattering of cold neutrons (wavelength larger than the Bragg cut-off wavelength) from a polycrystalline sample of aluminium. For 8 Å neutrons Zimmerman and Palevsky (1955) had observed that the experimental scattering cross section particularly at high temperatures was higher than that calculated on the Debye approximation (Kothari and Singwi 1955). This discrepancy was explained by Kothari and Singwi (1957) by assuming Θ_D to decrease with temperature, as postulated by Owen and Williams (1947) to explain their x-ray scattering data. This approach was phenomenological and to that extent unsatisfactory. We find that the present model of lattice vibrations

explains the higher cross section more satisfactorily. It should also be able to explain the x-ray scattering data, without having to take recourse to the indirect approach of varying the Debye temperature.

Fig. 3

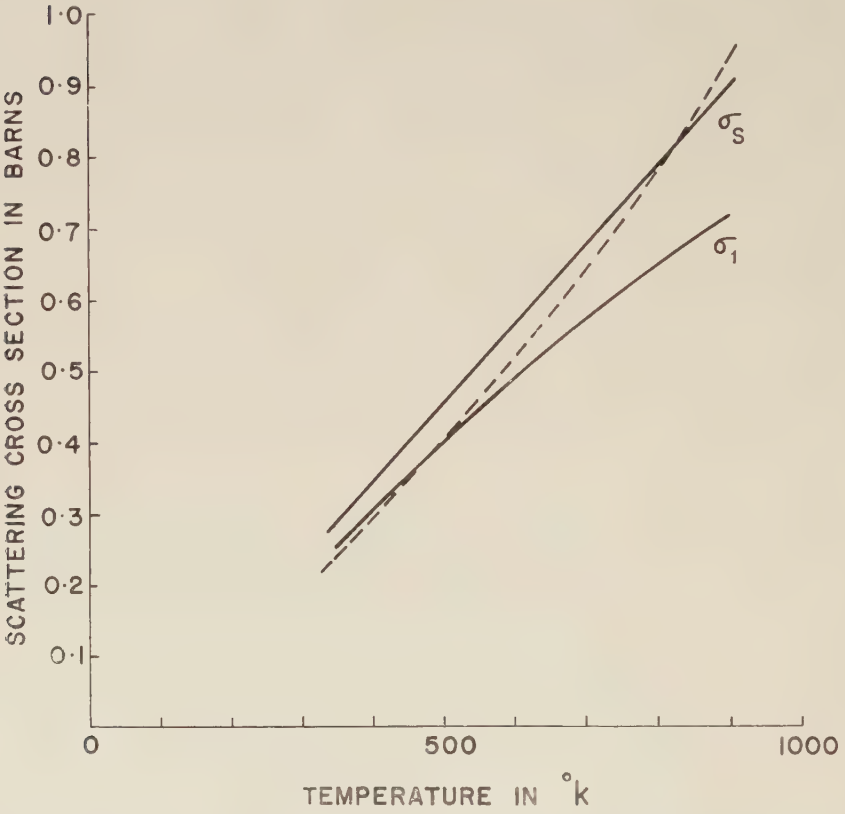

Total scattering cross section for 8 Å neutrons as a function of aluminium temperature. σ_s, total cross section. σ_1, cross section when multi-phonon contribution is neglected. Dashed line represents earlier calculations of Kothari and Singwi (1957).

The total inelastic scattering cross section $\sigma^1(E_1) = \sigma_s$ has been calculated using eqns. (20) and (21) and the results are shown as σ_s in fig. 3. The one-phonon cross section in the incoherent approximation has been calculated using eqns. (24) and (21). The results are plotted as σ_1 in the figure. For comparison we also give the earlier result of Kothari and Singwi (1957) as a dashed curve. It represents the total inelastic scattering cross section calculated on the Debye approximation when allowance is made for the variation of Θ_D with temperature. Correction to the incoherent approximation has also been included in this curve.

Besides giving a higher value for the total scattering cross section $\sigma_s(E_1)$, the new model gives an energy dependence of $d\sigma(E_1, \nu)$ which is quite

different from what one gets on the Debye model. In figure 4 we have plotted $d\sigma(\nu)$ as a function of ν/ν_{0L} for $E_1/\xi_{0L}=0{\cdot}05$ and $k_0T/\xi_{0L}=2$. The curve shows two sharp peaks. The broken curve represents calculations based on the Debye model.

Fig. 4

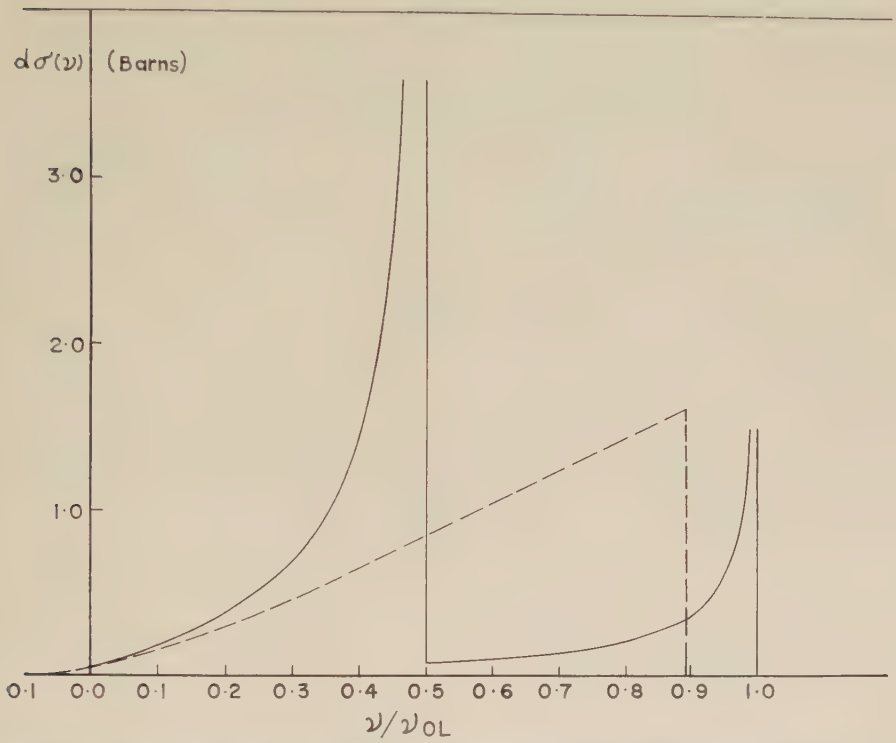

Inelastic scattering cross section $d\sigma(\nu)$ as a function of ν/ν_{0L} for $E_1/\xi_{0L}=0{\cdot}05$ and $k_0T/\xi_{0L}=2$. Broken curve represents calculations on the Debye approximation.

The one-phonon scattering cross section was also evaluated by summing over the reciprocal lattice vectors, using equations (16) and (17) for two temperatures given by $k_0T=1{\cdot}5\xi_{0L}$ and $2\ \xi_{0L}$. In table 3 these results are compared with those obtained on the incoherent approximation. It will be observed that the correction to the incoherent approximation is

Table 3. One-phonon Scattering Cross Section for 8 A Neutrons

T in units of ξ_{0L}/k_0	σ_1 coherent	σ_1 incoherent approximation	Correction to incoherent approximation
1·5	0·540	0·538	+0·37%
2	0·701	0·713	−1·71%

very small (less than 2%). Because of some inherent sources of error in the calculations (e.g. graphical integration) this small correction cannot be given much significance and it has not been included in curve σ_s of fig. 3. The corresponding correction in the Debye approximation was found to be + 4% (Kothari and Singwi 1957).

The experimental value (Hughes and Schwartz 1958) of σ_s for 8 A neutrons at $T = 800°$K is 0·83 barns ($\sigma_{\text{total}} = 1{\cdot}85$ barns, $\sigma_{\text{abs}} = 1{\cdot}02$ barns). This compares rather well with the theoretical value. Similarly at $T = 300°$K; $\sigma_s = 0{\cdot}26$ barn which is again in agreement with theory.

For higher neutron energies, $E_1/\xi_{0L} > 1$ and high scatterer temperatures for which $k_0 T/\xi_{0L} > 1$, one finds from eqns. (22) and (23) that the inelastic scattering cross section on the present model is about 35% higher than that calculated on the Debye model.

§ 5. Scattering Surface

The advantage of taking the dispersion relation of the form given by (1) becomes quite evident when we consider the scattering surface for neutrons. In the case of aluminium, Squires (1956) has calculated the dispersion relations from known elastic constants and Walker's (1956) x-ray scattering data. Using these he obtains the scattering surfaces in a few cases. Experimentally, these results have been verified by Brockhouse and Stewart (1958) and also Carter *et al.* (1957).

Fig 5

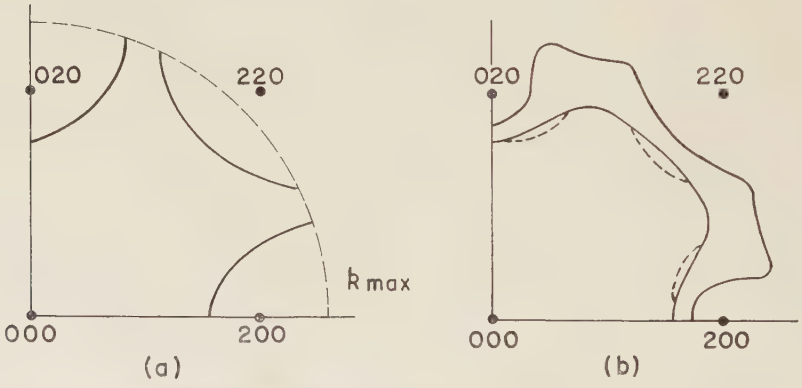

(*a*) Neutron scattering surface for $k_1 = 0$, on the Debye approximation; (*b*) neutron scattering surface for $k_1 = 0$, based on Squires' (1956) calculations.

For infinite wavelength incident neutrons the scattering surface in the plane containing the reciprocal lattice points $hk0$, as calculated using the Debye approximation, is shown in fig. 5 (*a*). The exact calculations of Squires give the two curves shown in fig. 5 (*b*). The inner curve corresponds to the transverse branch and the outer one to the longitudinal branch of the dispersion relation. It is obvious that the Debye approximation gives results which are very much different from the actual curves.

Fig. 6

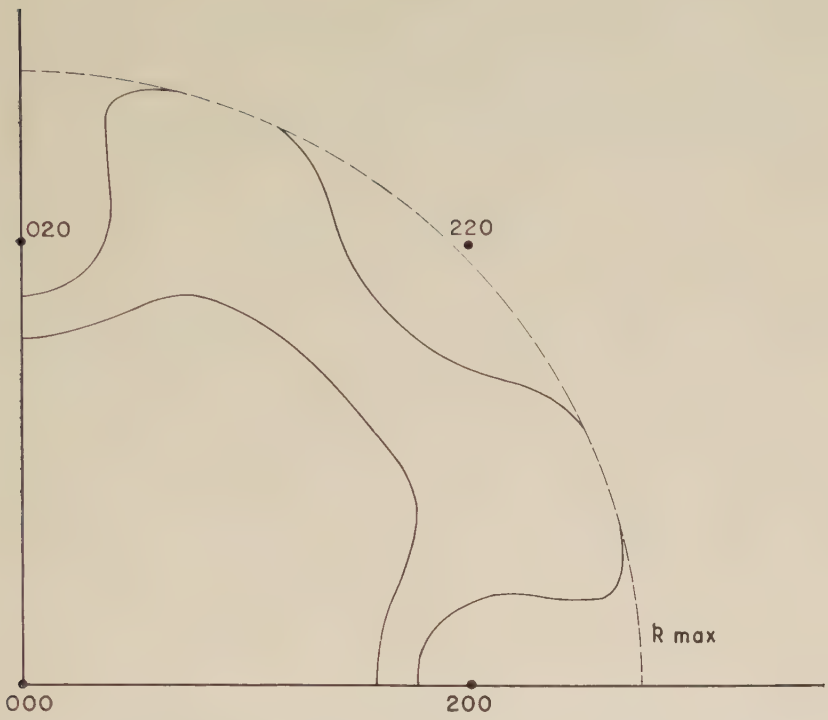

Neutron scattering surface for $k_1=0$ as obtained from the present theory.

In fig. 6 are shown the scattering curves calculated on the basis of the present model of lattice vibrations. The similarity between these and the curves obtained by Squires (fig. 5 (*b*)) is very close. It should be pointed out that the curve for the longitudinal branch (outer curve) in fig. 6 is not continuous. This arises because we have assumed a spherically symmetric Brillouin zone whereas for the cubic crystal of aluminium this will not be so.

References

Bhandari, R. C., 1957, *J. nucl. Energy*, **6**, 104.
Blackman, M., 1955, *Encycl. Phys.*, VII, Part 1, 354.
Brockhouse, B. N., and Iyengar, P. K., 1958, *Phys. Rev.*, **111**, 747.
Brockhouse, B. N., and Stewart, A. T., 1955, *Phys. Rev.*, **100**, 756; 1958, *Rev. mod. Phys.*, **30**, 236.
Carter, R. S., Palevsky, H., and Hughes, D. J., 1957, *Phys. Rev.*, **106**, 1168.
Hughes, D. J., and Schwartz, R. B., 1958, *USAEC Report* No. BNL-325 (Second Edition).
Kothari, L. S., and Singwi, K. S., 1955, *Proc. roy. Soc.* A, **231**, 293; 1957, *Phil. Mag.*, **2**, 694; 1959, *Solid State Physics*, VIII, 109.
Owen, E. A., and Williams, R. W., 1947, *Proc. roy. Soc.* A, **188**, 509.
Pelah, I., Eisenhauer, C. M., Hughes, D. J., and Palevsky, H., 1957, *Phys. Rev.*, **108**, 1091.

Placzek, G., 1954, *Phys. Rev.*, **93,** 895.
Placzek, G., and van Hove, L., 1955, *Nuovo Cim.*, **1,** 233.
Squires, G. L., 1952, *Proc. roy. Soc.* A, **212,** 192; 1956, *Phys. Rev.*, **103,** 304.
Walker, C. B., 1956, *Phys. Rev.*, **103,** 547.
Weinstock, R., 1944, *Phys. Rev.*, **65,** 1.
Zimmerman, R. L., and Palevsky, H., 1955, *Phys. Rev.*, **98,** 1162.

The Growth of Precipitates†

By R. G. Baker, D. G. Brandon and J. Nutting
Department of Metallurgy, Cambridge University

[Received August 17, 1959]

Abstract

During the growth of coherent precipitates stresses are generated because the lattice dimensions of the precipitate differ from those of the matrix. When the strain energy is large enough it will be relieved by the precipitate losing continuity with the matrix, i.e. becoming non-coherent. It is suggested that this will occur by the formation or annihilation of close-packed planes of atoms by the aggregation of either interstitials or vacancies. This leads to the formation of dislocations at the interface. The exact nature of the process in a given precipitate will depend upon both the shear stresses and hydrostatic stresses acting on the close-packed planes and upon the stacking-fault energy of the precipitate. The problem is given a general treatment for the case of precipitation in a f.c.c. matrix.

§ 1. Introduction

The decomposition of supersaturated solid solutions occurs by a mechanism involving nucleation and growth. As the precipitating particles grow, changes take place in the nature of the interface between the particles and the matrix. In the early stages there may be complete lattice continuity across the interface, which is then said to be coherent, and at this stage any misfit between the two lattices is taken up by elastic strain. Further growth results in a progressive loss of coherency by the introduction of surface dislocations and vacancies until ultimately the interface resembles a large angle boundary. At this stage the precipitate is said to be non-coherent.

The modes of formation and growth of the precipitate under any given conditions will be those which result in the greatest rate of fall in free energy of the system. After nucleation the precipitates will grow much faster in the directions in which the lattice misfit is least. The number of possible relationships between precipitate and matrix is thus limited by the requirements for low volume strain energy and low surface energy. In any given system, therefore, the precipitate habit and morphology will depend upon the lattice structures of the precipitated phase and matrix and the relative atomic sizes of the elements of which they are composed. This paper discusses some of the possible mechanisms by which loss of coherency can take place. Only precipitation in a f.c.c.

† Communicated by the Authors.

matrix will be considered but the principles involved are of general application.

§ 2. Coherent Precipitates

The first stage in the precipitation process is the formation of segregates of solute atoms or small zones of short-range order. These regions could be formed at the temperature of solution treatment or possibly during quenching. As precipitation proceeds, these regions grow and may undergo further ordering to form coherent precipitates.

The precipitates will grow in a form which gives the minimum rate of increase in the strain energy of the precipitate and matrix. Shear strains can be minimized if the precipitates grow as thin plates or needles (Nabarro 1940).

For a plate-like precipitate, the maximum misfit may be expected to occur in a direction perpendicular to the plate, while the habit plane of the precipitate should be relatively undistorted since it will be a plane across which the two lattices match well. In this simple case the precipitate may be regarded as being in a state of uniaxial compression or tension, depending on whether the lattice dimensions of the precipitate in a direction perpendicular to the habit planes are greater or less than those of the matrix.

As the precipitate platelets thicken and grow, the strain energy will increase until eventually it may be large enough to inhibit further growth. However, the strain in the system may be relieved, so allowing growth to continue, by introducing or removing one or more planes of atoms parallel to the habit plane of the precipitate. When this occurs there will be a dislocation loop around the periphery of the precipitate. This process constitutes the first stage in the formation of a simple dislocation network at the interface and one form which this network could ultimately take is that of a van der Merwe cross-grid of edge dislocations (van der Merwe 1950).

§ 3. Role of Vacancies and Interstitials

The relaxation of volume strain within the precipitate can also be discussed in terms of the mass transfer of vacancies or interstitials. If the precipitate is in a state of hydrostatic tension, interstitial atoms within the precipitate will have a relatively lower energy than when the precipitate is unstressed, since some of the work necessary to expand the lattice to accommodate an interstitial atom will be done by the stress already present. Thus it follows that the precipitate can act as a sink for interstitials. Similarly, if the precipitate is in a state of compression, it can act as a sink for vacancies.

The relief of volume strain energy afforded by the presence of vacancies or interstitials will be greatest if they form in clusters on the close-packed planes of the lattice as they may then condense and give rise either to extra or missing planes of atoms in the precipitate. The formation of

dislocation loops from quenched-in vacancies has been observed in aluminium. The loops are glissile and are thought to occur when a vacancy cluster collapses and the stacking fault so formed is annihilated by a Shockley partial dislocation. It seems likely that in this case the collapse and shear are not separate operations but take place simultaneously (Hirsch *et al.* 1958). Kuhlman Wilsdorf (1958) has discussed the crystallography of vacancy condensation in the case of both cubic and hexagonal lattices and has given a number of reasons for expecting the clustering and condensation of vacancies to occur on the close-packed planes. By analogy similar arguments may be expected to apply for interstitials.

When the close-packed planes are not the habit planes of the precipitate, it is necessary to take into account both the resolved shear stress and the resolved normal stress on the close-packed planes when considering what dislocation reactions are energetically favourable following the introduction or removal of an extra atom plane.

§ 4. Formation and Annihilation of Stacking Faults

The stacking sequence of close packed-planes in the f.c.c. system is

A B C A B C A B C . . .

A fault may be introduced into the stacking system in two ways (Read 1953):

(*a*) By putting in an extra plane of atoms to give a stacking sequence :

A B C A B C B A B C A B C.

This is an ' extrinsic ' stacking fault and would be formed if clusters of interstitials condensed to form an extra plane of atoms.

(*b*) By removing a plane of atoms to give a stacking sequence:

A B C A B C A C A B C A B C.

This is an ' intrinsic ' stacking fault and would be formed by the collapse of vacancy clusters.

If the fault is confined to the precipitate it will be surrounded at the interface by a dislocation of the sessile $\langle 111 \rangle$ type.

In the absence of any shear stress on the atoms in the faulted plane it may be expected that the stability of the faulted region will depend on the stacking-fault energy of the precipitate. If this is low, the stacking fault will be relatively stable and will be surrounded by a $\langle 111 \rangle$ Frank-sessile dislocation. If it is high, the nucleation of a loop of partial dislocation of burgers vector $\frac{1}{6}a\langle 112 \rangle$ will be energetically favourable. This will annihilate the stacking fault and interact with the sessile dislocation to give a glissile loop of dislocation capable of prismatic slip on two $\{111\}$ planes

$$\text{e.g. } \tfrac{1}{3}a[111]+\tfrac{1}{6}a[11\bar{2}]=\tfrac{1}{2}a[110].$$

§ 5. Influence of a Superimposed Hydrostatic Stress

If the habit plane of the precipitate is a close-packed plane, then the introduction of a stacking fault surrounded by a Frank-sessile dislocation

can relieve all the hydrostatic stress which has arisen during growth of the coherent precipitate.

The energy changes within the system which occur as a result of this process may be summarized as follows. The system will gain energy due to the creation of the stacking fault and the dislocation loop while at the same time energy will be lost as a result of the relaxation of volume strain.

When precipitation results in the generation of compressive stresses, the condensation and collapse of vacancy clusters will not only relieve the volume strain energy but will also reduce the supersaturation of vacancies produced in the system by quenching from the solution treatment temperature. Where tensile stresses are involved it seems unlikely that the interstitials required to produce the extra planes of atoms will diffuse into the precipitate from the matrix since the concentration of interstitials after quenching will be insufficient. Instead it seems more feasible that interstitials are created within the precipitate whilst at the same time vacancies are given to the matrix. During this process the system will gain energy equivalent to that required to form the necessary number of vacancies. Hence it is seen that in the case of precipitation requiring interstitial condensation, the volume strain energy which can be tolerated by the system before the precipitate loses coherency will be very much greater than that which can be tolerated when the system loses coherency by vacancy condensation.

The total energy change in the system, ΔE, will be given by :

$$\Delta E = E_{\text{dislocation}} + E_{\text{stacking fault}} - E_{\text{volume strain}} - E_{\text{vacancy formation}}$$

for compressive strain; and

$$\Delta E = E_{\text{dislocation}} + E_{\text{stacking fault}} - E_{\text{volume strain}} + E_{\text{vacancy formation}}$$

for tensile strain.

If there is no component of the stress parallel to the close-packed plane the annihilation of the stacking fault is not expected to be greatly influenced by the hydrostatic stress. In this case, therefore, the main factor which will determine whether or not annihilation takes place will be the stacking fault energy.

If, however, the habit planes are the cube planes, as is in fact frequently observed in practice (Barrett 1953), then the close-packed planes will experience a strong shear stress. For example, a stacking fault on the (111) plane would normally be expected to annihilate by any one of the three reactions:

$$\tfrac{1}{3}a[\bar{1}\bar{1}1] + \tfrac{1}{6}a[\bar{1}\bar{1}2] = \tfrac{1}{2}a[\bar{1}\bar{1}0] \quad . \quad . \quad . \quad . \quad . \quad . \quad (1)$$

$$\tfrac{1}{3}a[\bar{1}\bar{1}1] + \tfrac{1}{6}a[2\bar{1}1] = \tfrac{1}{2}a[0\bar{1}1] \quad . \quad . \quad . \quad . \quad . \quad . \quad (2)$$

$$\tfrac{1}{3}a[\bar{1}\bar{1}1] + \tfrac{1}{6}a[\bar{1}21] = \tfrac{1}{2}a[\bar{1}01]. \quad . \quad . \quad . \quad . \quad . \quad . \quad (3)$$

If the habit plane of the precipitate is (001) reaction (1) is unlikely to occur, since the dislocation $\frac{1}{2}a[110]$ has no component of its burgers vector

in the direction of the hydrostatic stress and cannot therefore relieve any of the volume strain. Reactions (2) and (3) both relieve some of the volume strain since both the dislocation $\frac{1}{2}a[011]$ and the dislocation $\frac{1}{2}a[101]$ have a component of their burgers vector perpendicular to the habit plane and equal to $\frac{1}{2}a[001]$.

There is another possibility, however, and that is that shear may occur in the [112] direction. This will initially produce a fault of opposite sign to that obtaining before (i.e. replacing an extrinsic fault with an intrinsic one or vice versa) and leave it surrounded by a dislocation of type $\frac{1}{6}a\langle 114\rangle$, i.e.

$$\tfrac{1}{3}a[\bar{1}\bar{1}1]+\tfrac{1}{6}a[112]=\tfrac{1}{6}a[\bar{1}\bar{1}4]. \quad . \ . \ . \ . \ . \ (4)$$

The $\langle 114\rangle$ dislocation has been discussed by Read (1953). A further shear in the same direction will now annihilate the stacking fault to give a $\langle 100\rangle$ dislocation:

$$\tfrac{1}{6}a[\bar{1}\bar{1}4]+\tfrac{1}{6}a[112]=a[001]. \quad . \ . \ . \ . \ . \ . \ (5)$$

The final dislocation can relieve twice as much volume strain as a $\langle 110\rangle$ dislocation without introducing any shear strain in the habit plane of the precipitate. The $\langle 001\rangle$ dislocation loop can then expand and climb out of the close-packed plane by migration of vacancies and interstitials until it surrounds the precipitate.

Frank (1955) has discussed the formation of $\langle 100\rangle$ dislocations in an f.c.c. lattice by reactions such as:

$$\tfrac{1}{2}a[011]+\tfrac{1}{2}a[0\bar{1}1]=a[001] \quad . \ . \ . \ . \ . \ . \ (6)$$

and has concluded that the reaction may be energetically favourable since a reduction in core energy is expected.

If the volume strain is relieved by the formation of $\langle 100\rangle$ dislocations by reaction (6) the expected sequence of events would be:

$$\begin{cases} \tfrac{1}{3}a[111]+\tfrac{1}{6}a[2\bar{1}1]=\tfrac{1}{2}a[0\bar{1}1] \text{ on the } (1\bar{1}\bar{1}) \text{ plane} \\ \tfrac{1}{3}a[\bar{1}11]+\tfrac{1}{6}a[211]=\tfrac{1}{2}a[011] \text{ on the } (\bar{1}11) \text{ plane} \end{cases} \quad . \ . \ . \ (7)$$

followed by climb of the two dislocation loops into the (001) plane and subsequent combination by reaction (6). Whether the [001] dislocation is formed directly by a double shear or whether it forms indirectly by a reaction between two $\langle 110\rangle$ dislocations will depend on the ease with which dislocation loops can nucleate. In the case of vacancies, which are known to form dislocation loops without the aid of any applied stress (Hirsch *et al.* 1958), the [001] dislocation will probably be formed indirectly before the lattice misfit becomes very great. However, it is possible that the formation of dislocation loops from interstitial atoms may occur only when the lattice misfit is of the order of a burgers vector because of the high energy of formation of interstitial atoms. In this case the [001] dislocation may well form directly.

§ 6. Theoretical Predictions from the Simple Model

Loss of coherency need not take place in distinct processes involving first collapse and then shear. It seems more likely that the two processes will occur simultaneously as soon as a sufficiently large cluster of interstitials or vacancies has accumulated on a close-packed plane. Kuhlman-Wilsdorf (1958) has estimated that the smallest stable dislocation loop formed by the condensation of vacancies in aluminium will be about 10 Å in diameter. Hence for a {100} precipitate in a f.c.c. matrix it might be expected that the proposed model would be valid provided that the precipitate remained coherent with the matrix to thicknesses greater than about 10 Å. If we assume that loss of coherency occurs when the lattice misfit perpendicular to the habit plane is of the same order of magnitude as the interplanar spacing in this direction then the model should hold for lattice misfits less than about 25%.

For misfits greater than this, coherency will be lost when the precipitate is only one or two unit cells thick. In this case segregation of vacancies (or interstitials) followed by collapse and shear will be unlikely to occur as distinct and separate processes. Instead, as the precipitate size is less than the minimum stable loop size the dislocation will probably be nucleated directly around the precipitate and it is unnecessary to consider a separate process of nucleation within the precipitate. The process of nucleation around the precipitate is probably complex and it is not proposed to deal with it here.

Some differences in the behaviour of precipitates might be expected depending on whether loss of coherency occurs by the formation of clusters of vacancies or of interstitials. In general, as an interstitial atom has a high energy of formation, it might be expected that the strain field which can occur around a precipitate which is experiencing a hydrostatic tension will be greater than that around one which is experiencing a hydrostatic compression As a corollary it might be expected that a greater increase in growth rate would accompany the formation of an extra plane of atoms, since the growth will have been inhibited to a greater degree. In both types of precipitate, the rate of growth will decrease rapidly as the volume strain increases, since the strain field around the precipitates will interact with the strain fields around the diffusing solute atoms causing a repulsion.

Acknowledgments

The authors would like to thank Professor A. H. Cottrell, F.R.S., and Dr. P. B. Hirsch for many helpful discussions.

We would also like to thank Tube Investments Ltd. for the award of a research fellowship (R.G.B.) and the Department of Scientific and Industrial Research for a maintenance allowance (D.G.B.) during the tenure of which this research was carried out.

References

Barrett, C. S., 1953, *Structure of Metals* (McGraw-Hill), p. 548.
Frank, F. C., 1955, *Rep. Conf. on Defects in Solids* (London : The Physical Society), p. 159.
Hirsch, P. B., Silcox, J., Smallman, R. E., and Westmacott, K. H., 1958, *Phil. Mag.*, **3**, 897.
Kuhlman-Wilsdorf, D., 1958, *Phil. Mag.*, **3**, 125.
van der Merwe, J. H., 1950, *Proc. phys. Soc. Lond.* A, **63**, 616.
Nabarro, F. R. N., 1940, *Proc. roy. Soc.* A, **175**, 519.
Read, W. T., 1953, *Dislocations in Crystals* (McGraw-Hill), p. 107.

The Thickness of the Saturated Helium Film above and below the λ-point†

By L. G. Grimes‡ and L. C. Jackson§
H. H. Wills Physical Laboratory, University of Bristol

[Received June 16, 1959]

Abstract

Measurements of the thickness of the helium film covering a vertical polished metal surface are reported for the height range 1 cm to 7 cm. At 2·04°K the film thickness at a height of 1 cm is $3{\cdot}20 \times 10^{-6}$ cm and agrees within 2% of that determined by Ham and Jackson (1957). The thickness of the helium II film increases slightly with temperature. The results indicate that the thickness of the helium I film is essentially the same as that of the helium II film and confirms the theories of the film which are based primarily on van der Waals' forces of attraction. Under the experimental conditions the thickness of the helium I film was independent of temperature and practically independent of the position of the liquid level.

§ 1. Introduction

The experimental results for the thickness of the saturated helium II film are usually analysed in terms of the theoretical equation for the profile

$$d = \frac{k}{H^{1/z}} \qquad . \qquad . \qquad . \qquad . \qquad . \qquad . \qquad . \qquad . \qquad . \qquad (1)$$

where d is the thickness at a height H and k and z are constants. Examination of the literature shows a large disparity in the results of various authors for k and n. A complete summary of these results has been given by Ham and Jackson (1957) and a more detailed account is given in the review article by Jackson and Grimes (1958). Atkins (1957) has pointed out that the ideal theoretical conditions for the surface on which the film is formed, viz. a perfectly smooth, clean surface in an isothermal enclosure, are very unlikely to be obtained in an experiment. The various degrees of approximation to these ideal conditions in the experimental arrangements is possibly one of the reasons for the general lack of agreement in the results.

The degree of purity of the helium vapour used in an experiment is very important if unambiguous results are to be obtained. Bowers and Mendelssohn (1950) correlated the very high transfer rates obtained by some authors with the presence of solid impurities on the surface over which

† Communicated by the Authors.
‡ Now at the Physics Department, University of Pennsylvania, Philadelphia 4.
§ Now at the Royal Military College of Canada, Kingston, Ontario.

the film flowed. Ham and Jackson (1957) have shown that solid impurity on a surface increases the film thickness (in their case by a factor of about three) at temperatures below the λ-point; above the λ-point the thickness is unaffected. Smith and Boorse (1955) have suggested that the random error in their transfer rates was probably a result of not having the same surface conditions for each experiment. The latter is out of the control of the experimenter but impurity in the helium vapour leading to solid impurities on the surfaces on which the film is formed may be avoided.

The other important factor, which may be controlled, is the temperature distribution on the surface on which the film forms. This is not so critical at temperatures below the λ-point but excessive temperature gradients may give rise to ambiguous results, see for example, Ham and Jackson (1957). Above the λ-point the film will not be observed if insufficient care is taken to reduce temperature gradients on the mirror to a minimum. Since in all the methods that have been employed to measure the film thickness there is some energy influx into the surface on which the film is formed, ideal isothermal conditions are impossible.

The purpose of the present work was to extend the thickness measurements of the helium film to a height of 7 cm above the liquid surface. Impurity content and temperature distribution are carefully controlled and the accuracy of the method increased.

§ 2. Method of Observation and Apparatus

The determinations of film thickness were made by the method of Burge and Jackson (1951) as modified by Ham and Jackson (1957). The apparatus was as described in the latter paper apart from the following changes. A longer mirror tube (fig. 1, Ham and Jackson 1957) was constructed to hold the new mirror, 8 cm long and 1 cm wide, and the reservoir R was increased in volume. The cryostat was now filled with liquid helium from a storage vessel in place of the small Joule–Thomson liquefier previously used and the liquid helium was protected by a Dewar vessel containing liquid nitrogen instead of two Dewar vessels containing liquid hydrogen and liquid nitrogen respectively. A new phase retardation plate with a retardation of 78° 36′ for sodium yellow light replaced that previously used. In view of these changes the calibration of the nicol rotation in terms of helium film thickness was repeated for the new mirror and the corrections for the residual birefringence of the Dewar vessels and for the change of birefringence with pressure for the mirror tube were determined. The final calibration curve did not differ appreciably from that of Ham and Jackson (1957), fig. 3. Detailed accounts of these calculations have been given by Ham (1954) and Grimes (1958).

§ 3. Experimental Procedure

The pressure in the mirror tube was maintained at about 10^{-6} mm Hg for several days before each experiment and during the filling of the cryostat. Usually $\frac{1}{2}$ to $\frac{3}{4}$ litre of liquid helium was sufficient for an experiment and

after temperature equilibrium had been attained, a number of readings of the position of the nicol prism for matching of intensity across the 1–3 boundary were taken. These readings represented the zero position of the nicol and the mean of them was corrected for birefringent effects caused by the pressure difference across the glass of the mirror tube. The corrected zero position was reproducible to $\pm 3'$ of arc. Helium gas, which had been collected from over the surface of liquid helium, was then passed from reservoir R through charcoal cooled in liquid nitrogen into

Fig. 1

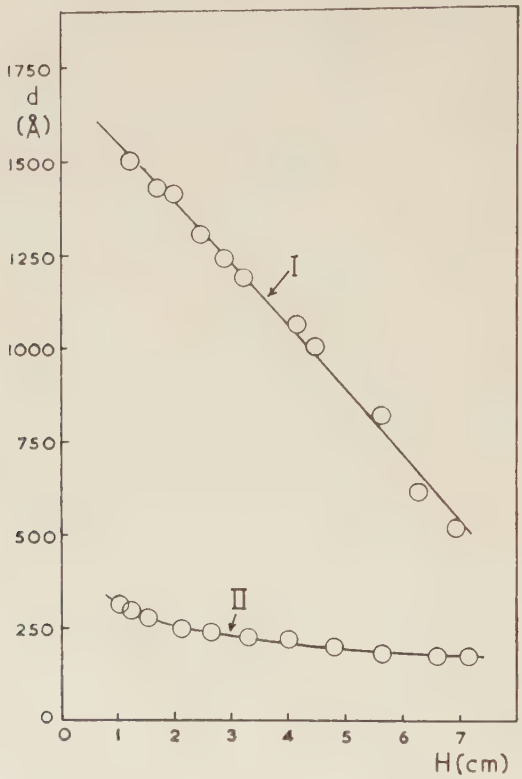

Film thickness as functions of height at 1·86°K.

1. Contaminated surface.
2. ' Clean ' surface.

the mirror tube until the required quantity had condensed. The nicol position was read when temperature equilibrium had again been attained. This was usually about 10 min for temperatures below the λ-point but much longer above the λ-point. Further condensations allowed the measurement of the thickness of the film as a function of the height of the point of observation above the liquid surface. Generally only one temperature

was studied during each experiment and once the series of experiments were commenced the optical components and the Dewar vessels were not moved.

§ 4. The Film below the λ-point

The observation of Ham and Jackson (1957) that an anomalously thick, stepped film could appear when a Taconis resonance was set up in the inlet of the mirror tube, was confirmed and again it was found that opening Tap T_1 (fig. 1, Ham and Jackson 1957) prevented the oscillations and gave the normal film profile.

The present work also confirmed the observation of Ham and Jackson (1957) that solid impurity deposited on the substrate leads to a considerable increase in thickness of the film below the λ-point. In a set of observations with impure helium containing about 1% of air, the zero position of the nicol prism had changed by 3° at the end of the experiment as a result of the deposition of a layer of solid air upon the mirror. To correct for the gradual increase in thickness of the air deposit with each condensation it has been assumed, although not strictly correct, that the nicol shift arising from the air deposit increases linearly with the number of condensations. The resulting nicol shifts after allowing for this drift of the zero have been converted into helium film thicknesses using the new calibration curve. Although this is not a strictly correct procedure, as the optical properties of the substrate vary, it enabled an estimate to be made of the helium II film thickness under 'dirty' conditions. The results for 1·86°K are shown in fig. 1, curve 1, while curve 2 is the corresponding one for the helium film on an uncontaminated surface. The impurity deposit on the mirror remained transparent and colourless throughout the experiment.

Measurements of film thickness have been made under satisfactory conditions for the height range 1–7 cm at 2·04, 1·83 and 1·63°K. The helium gas condensed in the mirror tube for these observations was obtained by filling reservoir R (fig. 1, Ham and Jackson 1957) with gas drawn from above the surface of liquid helium at 4·2°K and then passing this gas through a charcoal purifier cooled with liquid nitrogen. The film thicknesses so obtained were reproducible from run to run within the accuracy of the observations. In some further experiments the charcoal purifier was cooled with liquid hydrogen but no evidence was obtained of any significant improvement in the purity of the helium.

Smooth curves were drawn through the observations for these temperatures. The film thicknesses observed by Ham and Jackson (1957) at 2·05°K, 1·81°K and 1·55°K, corrected approximately to 1·63°K, at heights less than 1 cm fall on the smooth prolongation of these curves. At greater heights (1–1·6 cm) the observations of Ham and Jackson (1957) are some 3 to 5% lower than the newer values. At 1 cm height the two series agree within 2%. Figure 2 shows the smooth curve for 1·83°K drawn through the combined observations. Film thicknesses read from the curves are given in the table.

Fig. 2

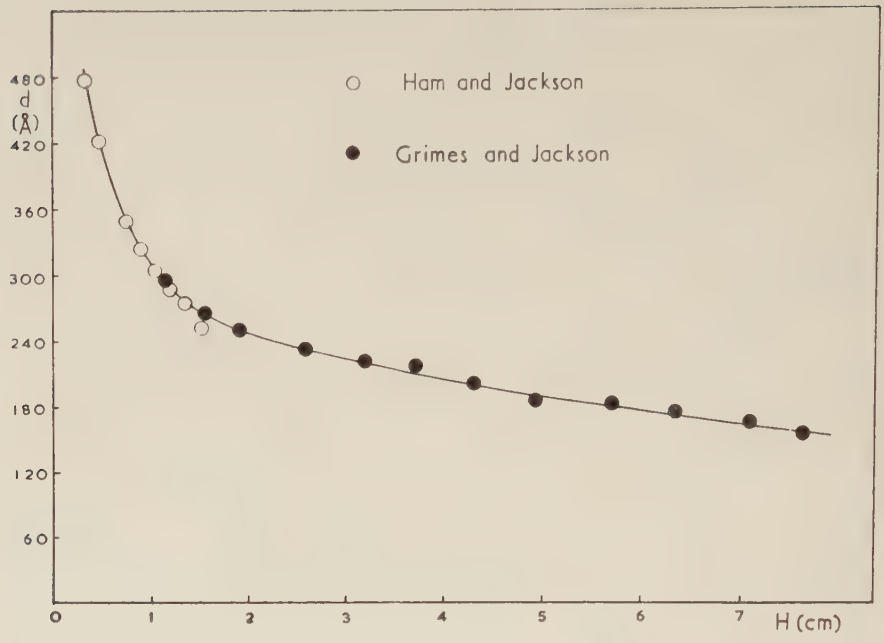

Film thickness as function of height for the range 0·4 to 7·0 cm at 1·83°K.

Smoothed Values of Film Thickness

$T=2{\cdot}05$°K		$T=1{\cdot}83$°K		$T=1{\cdot}63$°K	
H (cm)	d (Å)	H (cm)	d (Å)	H (cm)	d (Å)
0·4	450	0·4	440	0·4	414
0·6	391	0·6	379	0·6	365
0·8	350	0·8	339	0·8	333
1·0	322	1·0	310	1·0	308
1·2	302	1·2	287	1·2	288
1·4	286	1·4	273	1·4	272
1·6	274	1·6	262	1·6	259
1·8	264	1·8	253	1·8	249
2·0	256	2·0	246	2·0	240
2·5	240	2·5	233	2·5	224
3·0	228	3·0	222	3·0	213
4·0	208	4·0	205	4·0	195
5·0	193	5·0	189	5·0	180
6·0	181	6·0	176	6·0	168
7·0	170	7·0	165	7·0	157

The data of this table are compared with various theoretically derived expressions in a later section of this paper.

§ 5. The Film above the λ-point

Observations have also been made in the temperature range 2·47°K to 3·56°K to repeat and extend the work of Ham and Jackson (1957) above the λ-point. As the observed thickness of the film depended greatly on the method of formation and time of observation, many experiments were carried out to determine the conditions necessary for the observation of stable equilibrium values of the film thickness.

The observations at 2·47°K may be quoted as typical. Helium gas was condensed into the mirror tube until the liquid was in contact with the mirror. After the temperature had been held constant for 40 min a further $\frac{1}{2}$ litre of gas was condensed. A thick, uniform film formed immediately to a thickness much greater than that of the helium II film. After about 1 min the uniform film broke up into one of very uneven thickness which drained down steadily and became thinner. After 36 min the film thickness at the point of observation (7·31 cm above the liquid surface) had fallen to 117 Å and continued at this value for a further 24 min, showing that an equilibrium thickness had been reached appropriate to the conditions of observation. The thickness of the helium II film just below the λ-point is 150 Å at the same height.

Fig. 3

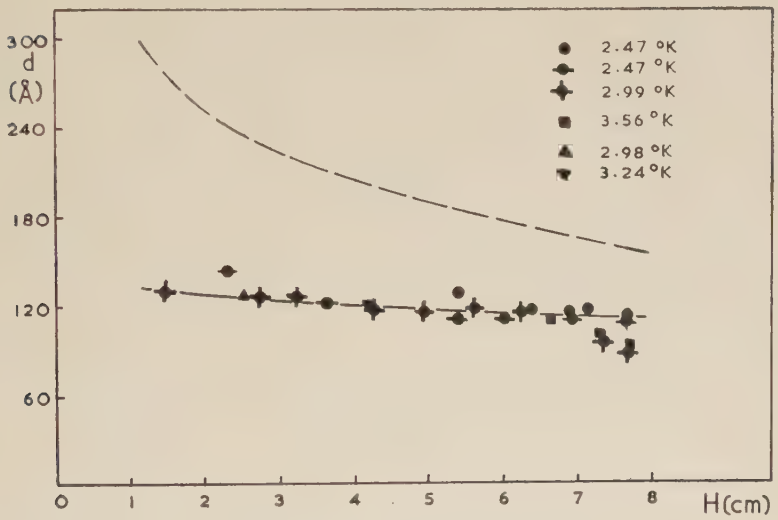

Film thickness above the λ-point.

The film was then evaporated by bringing a 6 W lamp close to the cryostat and a reading of the nicol prism was made immediately after switching off the lamp. The nicol reading was very close to the zero film thickness position. A film built up rapidly in the first minute. From 15 min onwards. the observations agreed well with the equilibrium thickness mentioned above. The film thickness at other heights at 2·47°K are shown

in fig. 3. The observations at higher temperatures were all similar to those at 2·47°K except that the condensed film was initially always very uneven in thickness. The stable values of thickness, at the higher temperatures, of the film reformed after evaporation and observed not less than 15 min after the evaporation are also shown in fig. 3.

These equilibrium values of film thickness above the λ-point all fall close to a single curve of thickness against height which exhibits a much smaller variation of d with H than is observed below the λ-point. At the greater heights the ratio of thickness above to that just below the λ-point is of the order of 0·8. The reason for the difference between the d-H curves above and below the λ-point is discussed in a later section of this paper.

§ 6. Discussion

The data of the table for the thickness of the helium II film cannot be reproduced within the accuracy claimed for the observations (about 2%) by either the formula of Schiff (1941) and Frenkel (1940)

$$d = k/H^{1/3}$$

with k = constant (independent of temperature) or of Franchetti (1957)

$$H = \frac{A}{d^3} + \frac{B(T)}{d^2}$$

with A = constant, $B(T)$ = function of temperature.

An examination of the data showed, however, that they can be reproduced by the Schiff–Frenkel formula with $k = 3{\cdot}24 \times 10^{-6}$ at $T = 2{\cdot}05$°K, $3{\cdot}14 \times 10^{-6}$ at 1·83°K and $3{\cdot}04 \times 10^{-6}$ at 1·63°K plus a small term in which Δd is an oscillatory function of H as shown in fig. 4 (*a*) (H and d in centimetres). The maximum amplitude of Δd is 2% of the observed thickness for $T = 2{\cdot}05$°K, 5% for 1·83°K and 2% for 1·63°K, and so the correcting term is hardly outside the magnitude of the experimental error.

In view of this result a similar attempt was made to reproduce the data by means of the Franchetti formula plus a small residual term. A fit could be obtained with

Temperature (°K)	$A \times 10^{17}$	$B(T) \times 10^{12}$
2·05	2·65	0·69
1·83	2·65	1·90
1·63	2·65	2·88

and residual terms Δd shown as functions of H in fig. 4 (*b*) (H and d in centimetres). The maximum amplitude of Δd now corresponds to 4% of d (2·05°K), 4·5% (1·83°K) and 2% (1·63°K).

The oscillatory nature of the residual term may be caused by the presence of a very small and otherwise undetected Taconis oscillation in the gas column connected to the mirror tube (Ham and Jackson 1957) or to some other heat input which produces a very small disturbance of the temperature uniformity over the film.

This analysis of the data is presented to show how difficult it is to make a completely satisfactory analysis of data on film thickness as a function of height. Apart from the experimental difficulties so clearly summarized by Atkins (1957), the thickness would have to be known to appreciably better than 1% in order to distinguish clearly between the two expressions quoted above and to obtain a reliable value for the temperature dependent term in the Franchetti expression.

Fig. 4

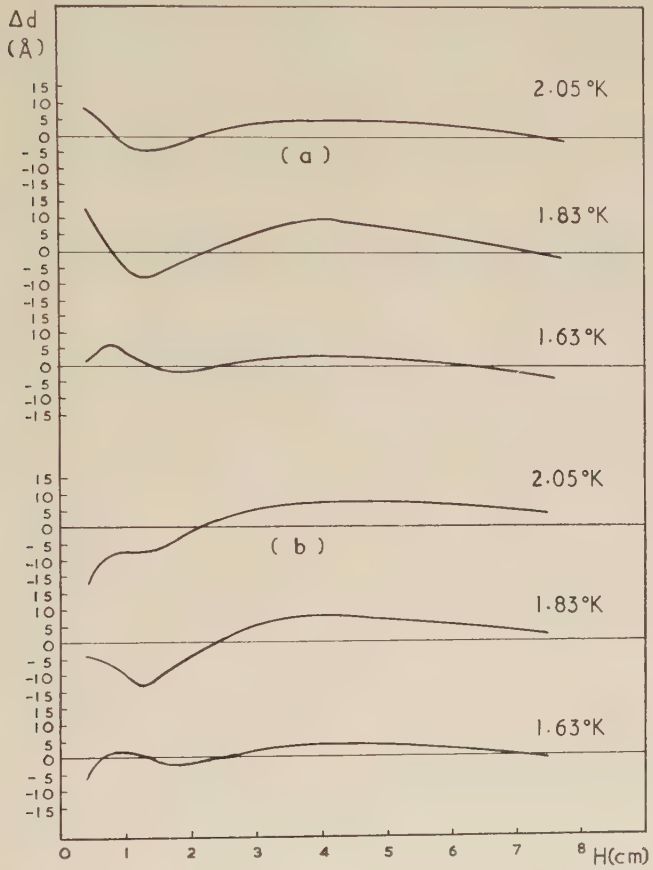

Differences Δd between calculated and observed film thickness as function of height for:

(*a*) $d=k/H^{1/3}$ at 2·05, 1·83, 1·63°K.

(*b*) $H=A/d^3+B/d^2$ at 2·05, 1·83, 1·63°K.

As 1% of the film thickness corresponds to one-half to one atomic layer in the height range now under consideration, it is unlikely that the necessary precision will be attained.

It is believed that the difference between the curves of thickness against height for helium II and for helium I is due to the surface of the mirror at the point of observation not having exactly the same temperature as the bulk liquid in the case of liquid helium I. The temperature is higher by an amount ΔT due to the absorption of that part of the incident sodium light which is not reflected by the mirror. It is estimated that this energy input is of the order of 10^{-5} cal/sec. Ham and Jackson (1957) have shown, on the basis of the work of Atkins (1954) and Meyer (1955), that the thickness of the film at height H and a temperature $(T+\Delta T)$ corresponds to that at a height $H+(RT/mg)\,(1/V)\,(dV/dT)\Delta T$ and temperature T. The effect of various values of ΔT on the profile of the film is shown in fig. 3, Grimes and Jackson (1959). In particular for a value of ΔT of 10^{-4} deg. the thickness of the film is practically independent of the height of the point of observation above the liquid level and the expected thickness agrees closely with that observed in the experiments on liquid helium I. A calculation showed that the temperature rise of 10^{-4} deg. is reasonable with the estimated energy input if the energy is dissipated through the gas phase. Dissipation by conduction through the metal of the mirror to the bulk liquid below would demand a much larger temperature rise, of the order of 10^{-2} deg.

It is not anticipated that this effect will be of importance in an adequately shielded substrate in contact with liquid helium II as any temporary temperature difference will produce a superfluid flow by the fountain effect, replenishing any evaporated helium in the film and reducing the temperature difference below 10^{-6} deg. A rough calculation of the superfluid flow, which will result from the absorption of 10^{-5} cal/sec by the mirror, suggests that the superfluid may be moving at a velocity up to 20 cm/sec. This raises the question of the possible effect of this movement on the thickness of what would otherwise have been regarded as a static film.

A formula giving the thickness of a moving helium II film has been derived by Kontorovich (1956) and by Arkipov (1957). This indicates that the moving film is a few per cent thinner than the stationary film at the same height and temperature. Franchetti (1958) has also treated the problem and has deduced a formula which gives an effect of the movement on the thickness identical with that of Kontorovich in magnitude but opposite in sign. Franchetti emphasizes that when the film movement is that of gravity-induced transfer from a beaker, the chemical potential of the moving film must be derived by differentiation of the Gibbs function at constant pressure, constant temperature and *constant flow* and that this last condition necessarily leads to an *increase* of the moving film over that of the stationary film. The only available experimental evidence directly applicable to a test of the theory is the work of Grimes and Jackson (1958). In these preliminary experiments a *decrease* in thickness of a few per cent was observed on a beaker emptying by gravity-induced film transfer. As the mechanism of the possible movement of the helium II film on the mirror in the present experiments is definitely not gravity-induced transfer, it is

not yet clear what effect the movement of the film may have on the observed thickness.

Acknowledgment

The authors acknowledge gratefully a grant from the D.S.I.R. in support of the experimental programme and also a maintenance grant to one of us (L. G. G.).

References

Arkipov, R. G., 1957, *J. exp. theor. Phys.*, **33,** 116.
Atkins, K. R., 1954, *Canad. J. Phys.*, **32,** 347; 1957, *Progr. Low Temp. Phys.*, **2,** 105.
Bowers, R., and Mendelssohn, H., 1950, *Proc. phys. Soc. Lond.* A, **63,** 1318.
Burge, E. J., and Jackson, L. C., 1951, *Proc. roy. Soc.* A, **205,** 270.
Franchetti, S., 1957, *Nuovo Cim.*, **5,** 1266 ; 1958, *Ibid.*, **10,** 622.
Frenkel, J., 1940, *J. Phys., Moscow*, **2,** 365.
Grimes, L. G., 1958, Thesis, Bristol.
Grimes, L. G., and Jackson, L. C., 1958, *Low Temp. Conf. Leiden, Physica,* suppl. ; 1959, *Phil. Mag.*, **4,** 756.
Ham, A. C., 1954, Thesis, Bristol.
Ham, A. C., and Jackson, L. C., 1957, *Proc. roy. Soc.* A, **240,** 243.
Jackson, L. C., and Grimes, L. G., 1958, *Advanc. Phys.*, **7,** 435.
Kontorovich, V. M., 1956, *J. exp. theor. Phys.*, **30,** 805.
Meyer, L., 1955, *Phys. Rev.*, **97,** 22.
Schiff, L. I., 1941, *Phys. Rev.*, **59,** 839.
Smith, B., and Boorse, H. A., 1955, *Phys. Rev.*, **99,** 346.

Dislocation Loops in Neutron-irradiated Copper†

By J. Silcox and P. B. Hirsch
Crystallographic Laboratory, Cavendish Laboratory, Cambridge

[Received August 19, 1959]

Abstract

Electron transmission microscope observations have been carried out on copper irradiated with neutrons at temperatures of 35°c and 60°–100°c, and subsequently thinned by electropolishing. Specimens irradiated to a dose of $6{\cdot}7\times10^{17}$ cm^{-2} (at 35°c) contain $\sim3\times10^{15}$ defects c.c.$^{-1}$ in the form of small regions of strain (average diameter ~75 Å), some of which can be resolved as dislocation loops. With increasing dose of irradiation ($5{\cdot}6\times10^{18}$, $1{\cdot}4\times10^{20}$ n cm^{-2}) many more of the defects can be recognized as loops, and their average diameter increases to ~150 Å and ~300 Å respectively. The dislocation density in the form of loops is 10^{10}–10^{11} cm^{-2}.

The stability of the loops and their behaviour on annealing are as expected from prismatic loops. The loops are considered to nucleate as a result of the collapse of discs of vacancies produced by vacancy clustering in the central region of a displacement spike, and to grow by migration of vacancies or of vacancy clusters.

Radiation hardening is interpreted in terms of the large density of dislocations in the form of loops. The hardening anneals out at the same temperature at which the loops are observed to disappear by climb.

§ 1. Introduction

It was first pointed out by Wigner (Seitz 1952) that the passage of an energetic nuclear particle through crystals should cause considerable damage to the crystal structure. Physical properties of a metal which depend on the defects in its crystalline structure, e.g. residual electrical resistivity, mechanical properties, etc., should therefore alter under neutron irradiation. The importance of these effects at the present time need hardly be stressed and a considerable amount of research has been carried out on this topic (for review see Seitz and Koehler 1956, Kinchin and Pease 1955, Glen 1955, Cottrell 1956a, Dienes and Vineyard 1957). The broad physical picture of these effects is complicated since many defects are thought to play a part. These include vacancy/interstitial pairs (Frenkel defects), crowdions (Lomer and Cottrell 1955, Blewitt *et al.* 1956), thermal spikes (Seitz and Koehler 1956), displacement spikes

† Communicated by the Authors.

(Brinkman 1954) and small zones whose density is less than that of the parent lattice (Seeger, unpublished).

For copper, experimental studies of radiation effects have been carried out on the lattice parameter (Simmons and Balluffi 1958), macroscopic length (Vook and Wert 1958), internal friction (Thompson and Holmes 1956, Thompson *et al.* 1957, Barnes *et al.* 1958, Barnes and Hancock 1958), stored energy (Overhauser 1954, Blewitt *et al.* 1956, Blewitt 1958), residual electrical resistivity (including Cooper *et al.* 1954, Corbett *et al.* 1956, Meechan and Brinkman 1956, Blewitt *et al.* 1956, 1957) and work-hardening properties (Jamison and Blewitt 1952, 1953, Redman *et al.* 1953, McReynolds *et al.* 1955, Makin 1958, 1959). The effect of neutron irradiation on the yield stress of copper single crystals, for example, is an increase by a factor of ten for an irradiation of $\sim 10^{18}$ n cm^{-2} (Makin, quoted by Cottrell 1958). The correct dependence of the flow stress on the temperature of measurement and neutron dose can be predicted by theories based on the creation of obstacles (of a not very well defined nature) in the 'spikes' produced in the lattice by neutron irradiation (Seeger, unpublished, Holmes, quoted by Blewitt 1956). Another explanation has been put forward by Cottrell (1956 b, 1958) who interpreted the hardening as being due to large numbers of jogs formed on the dislocation lines by the absorption of point defects produced by the irradiation. It appears difficult by studies of the type outlined above to decide between these theories and also to determine the exact nature of the obstacles (if any are formed). However, the recent experiments by Adams and Higgins (1959), which will be discussed in § 4.5, show that hardening is partly due to obstacles dispersed throughout the volume of the metal, and partly due to source hardening.

Strong similarities are observed between the behaviour of neutron-irradiated and quenched metals (Cottrell 1958) and hardening may be due to similar effects, since point defects in excess of equilibrium concentrations are thought to be produced in each case. Recently, evidence has been obtained by the use of the transmission electron microscope technique for the existence of small dislocation loops in quenched Al (Hirsch *et al.* 1958 a) and quenched Cu (Hirsch and Silcox 1958, Smallman and Westmacott 1959), of small stacking-fault tetrahedra in quenched Au (Silcox and Hirsch 1959) and loops and tetrahedra in quenched Ag (Smallman and Westmacott 1959). These are thought to be formed by the collapse of discs of vacancies. The experiments have been extended to aluminium irradiated by $\sim 10^{18}$ fast neutrons cm^{-2} at -195°C by Smallman and Westmacott (1959). On warming the metal to room temperature, dislocation loops are observed. These observations, however, do not appear to be extensive and the concentration of loops is somewhat low (apparently $\sim 3 \times 10^{13}$ c.c.$^{-1}$). Small angle x-ray scattering experiments have been carried out by Atkinson *et al.* (1959) on neutron-irradiated copper, and, for a dose of $\sim 8 \times 10^{19}$ n cm^{-2}, the observed scattering effects have been interpreted in terms of small disturbed regions of ~ 100 Å in size. Owing to the possible ambiguities in interpretation of the low-angle scattering,

the nature of these regions could not be determined. These experiments, however, lend support to the view that neutron irradiation gives rise to local structural disturbances in the crystal which may be observable directly by the transmission electron microscope technique. Accordingly such observations were carried out on copper, neutron-irradiated in bulk and subsequently thinned. These are reported in this paper.

§ 2. Experimental Techniques

The copper used for this investigation was supplied by Johnson Matthey and Co. Ltd., in the form of foil 0·003 in. and 0·005 in. thick and was of the 'superpure' and 'specpure' qualities. Prior to irradiation, the specimens were vacuum annealed and then sealed off in silica tubes under an argon atmosphere. One set of 'specpure' specimens was given an anneal of $2\frac{1}{2}$ hours at 800°c and subsequently irradiated to an estimated fast neutron (Energies >1 Mev) dose of $6{\cdot}7\times10^{17}$ n cm^{-2} in the Harwell atomic pile BEPO at a temperature of ~35°c. Another set of 'superpure' specimens was annealed for 2 hours at ~900°c and subsequently irradiated to doses of $6{\cdot}7\times10^{17}$ n cm^{-2}, $5{\cdot}6\times10^{18}$ n cm^{-2} (in BEPO at ~35°c), $1{\cdot}4\times10^{20}$ n cm^{-2} and $4{\cdot}1\times10^{20}$ n cm^{-2}. The last two doses were obtained in the Harwell atomic pile DIDO at a pile temperature of $\gtrsim60$°c and certainly <100°c. The dimensions of the foils were governed by the facilities available in the pile and, for BEPO were $\frac{1}{2}$ in. by 1 in. The specimens for DIDO were smaller, being $\frac{1}{12}$ in. by $\frac{3}{4}$ in. Following irradiation the foils were allowed to rest for several weeks to allow the induced radioactivity to decay to a level low enough to permit ease in handling. Some specimens were thinned and examined in this state. Other specimens given the lowest dose ($6{\cdot}7\times10^{17}$ n cm^{-2}) were given various treatments as follows. One was aged for 3 hours at 100°c and others were given 22 min and 6 hour anneals at 350°c. The anneals at 350°c were carried out, under a vacuum of 10^{-2} mm Hg, by placing the specimen in a copper tube immersed in a thermostatically controlled salt bath. Another specimen was deformed $\sim3\%$ in tension using a hand-strainer.

Following treatment, the foils were thinned by standard electropolishing techniques (e.g. Tomlinson 1958) using a bath of 80% methyl alcohol, 20% nitric acid. After washing with methyl alcohol, the specimens were examined in a Siemens Elmiskop I electron microscope operating at 100 kv. Difficulty was experienced in polishing the specimens irradiated to the higher doses. It is not clear at present whether this is simply due to the small size of specimens or due to a change in polishing conditions due to irradiation (Smallman and Westmacott 1959). In all, four microscope specimens of the foil irradiated to $1{\cdot}4\times10^{20}$ n cm^{-2} were examined. While all showed similar effects, good micrographs were obtained from only one specimen. Two microscope specimens of the foil irradiated to $4{\cdot}1\times10^{20}$ n cm^{-2} were examined. These again showed similar effects and good micrographs were obtained from two areas.

§ 3. Observations

3.1. *Low Doses*

Figures 1, 2, 10(*a*), 11, 12(*a*), (*b*),† are micrographs of copper irradiated to a dose of $6{\cdot}7 \times 10^{17}$ n cm^{-2} in BEPO. Contrast effects in the form of spots of diameter between 50 Å and 150 Å are observable in high densities‡.

An example of an area in annealed copper is shown in fig. 3(*a*). This is free from such effects. Sometimes (30–40% of the areas examined) small densities of spots are observed in the annealed specimens (about four or five to an area equivalent to fig. 3(*a*)) and rarely, (~5% of the areas examined) in higher densities, as is shown in fig. 3(*b*). Even in these areas, however, the density is much lower than in the irradiated specimens. The contrast is genuine Bragg diffraction contrast but the origin of it at present is not understood. It may be an impurity effect. That the density of the effects in the irradiated specimens is much greater than in these examples can be seen by a comparison of figs. 1 and 3(*a*) which are of comparable magnifications. Furthermore, the spots were observed in every area of any irradiated specimen which was investigated. It was therefore concluded that the majority of the spots are due to some effect caused by the neutron irradiation. It may be noted that similar effects have been observed in fatigued Cu (Segall and Partridge, private communication) and in quenched Al (Hirsch *et al.* 1958a).

The contrast may be due to surface contamination, etch pits at the surface of the foil, or in fact, due to some defect lying within the foil. Variations in contrast typical of that from dislocations were observed as the specimen was tilted in the stereo-holder. It thus appears that contrast is due to the Bragg diffraction mechanism. This would not be expected from surface contamination. It is also thought unlikely that the effects are due to etch pits since these would give rise in general to contrast effects lighter than the background. The reverse is true in practice. Comparison of the density of the spots at the edge of the foil with that in areas further away from the edge suggests that the density decreases towards the edge of the foil. This would be expected if the spots were distributed over the volume of the foil rather than the surface. The observation is difficult to make since the foils are apparently wedge-like over only a short distance and the contrast is often not very clear. Nevertheless all these considerations lead to the conclusion that most of the effects are due to disturbances of some kind in the crystalline structure of the metal.

At high magnifications and also occasionally at low magnifications, it proves possible to resolve some of the spots as black rings or double lines (see e.g. at L on figs. 1, 2, and also several on fig. 11). These contrast effects are typical of those obtained from prismatic dislocation loops

† All figures, with the exception of fig. 13, are shown as plates.

‡ Somewhat similar spots have been reported recently in neutron irradiated thin films of Au (Noggle 1959). *Note added in proof.*—Recent observations by the present authors show the existence of exactly similar spots (and also dislocation loops) in Au, neutron irradiated in bulk.

formed by vacancy condensation after quenching aluminium (Hirsch *et al.* 1958 a). It is thus concluded that some of these effects are prismatic dislocation loops. The fact that the loops appear to be very stable is taken as confirmatory evidence that the loops are prismatic in character. The nature of the other effects which appear as dots cannot be established with certainty but it is inferred from these results that they may be the nuclei of the loops (possibly three-dimensional clusters if very small) and loops at various stages of growth. In fact similar spots have been observed in quenched Al (Hirsch *et al.* 1958 a). It should be noted that the image of a dislocation loop lies either outside or inside the loop; the width of the dislocation image is ~ 100 Å in a typical case, and the image is displaced from the dislocation core by a similar amount (Hirsch *et al.* 1958 b, 1959). If the diameter of a loop is less than this value, the reduction of the strain field outside the dislocation loop, due to the cancelling effect of the two opposite sides (of opposite sign) of a loop, will result in a narrowing of the dislocation image, should this lie on the outside of the loop. However, if the image lies inside, for loops $< \sim 100$ Å the dislocation images of opposite sides of the loop are expected to merge into one image, the diameter of which will be somewhat smaller than that of the loop. Thus, the very small dots which are observed could represent small loops, although of course they could also be due to regions of rather less well defined strain.

In order to give figures of density of loops it is necessary to know the foil thickness, which may be obtained, for example, from a slip trace caused by the movement of a dislocation on a (111) plane, together with the knowledge of the crystal orientation obtained by selected area diffraction. However, in these foils very little slip was observed. Consequently a foil thickness of 1000 Å will be assumed and, for two different specimens irradiated separately to a dose of $6{\cdot}7 \times 10^{18}$ n cm^{-2}, counts of several plates gave $2{\cdot}6 \times 10^{15}$ c.c^{-1} and 3×10^{15} c.c^{-1} respectively. The difference is not thought to be significant. It is also difficult to give a figure for the average diameter of the loops (assuming that all the effects are due to dislocation loops), since the size of the defects is of the order of the width of the dislocation image. The largest loops observed are ~ 150 Å and the average size is estimated as 75 Å. These figures lead to a dislocation density in loops of $\sim 10^{10}$ cm^{-2}. The density of dislocations not in loops is similar to that in the annealed specimens, being estimated as 5×10^{7}–5×10^{8} cm^{-2}.

3.2. *Higher Doses*

With foils irradiated to $5{\cdot}6 \times 10^{18}$ n cm^{-2} exactly similar effects are observed and are shown at low and high magnification in figs. 4 and 5, which are of comparable magnifications to those shown for the low dose in figs. 1 and 2. The density of spots is increased to $6{\cdot}5 \times 10^{15}$ c.c.$^{-1}$, and, as can readily be seen from the larger proportion of spots resolved as rings, the average diameter of the loops has also increased. The largest loops

that can be resolved as such are ~ 300 Å in diameter. An average value for the loop radius is estimated as ~ 150 Å. The contrast from these loops behaves in the same manner when the stereoholder is tilted as the phenomena described in §3.1. The density of dislocations in loops is now $\sim 4 \times 10^{10}\,\mathrm{cm}^{-2}$.

The effect of an even higher dose of $1{\cdot}4 \times 10^{20}\,\mathrm{n\,cm}^{-2}$ (in DIDO) is shown in figs. 6, 7 and 8. All show, quite clearly, the presence of completely resolved loops. (The magnification of fig. 6 is intermediate between those of figs. 1 and 2. Some loops showing 'double image' contrast effects are shown at M in fig. 7 and are similar to those observed in quenched Al (Hirsch *et al.* 1959). The density of loops is now apparently slightly lower, being $\sim 1{\cdot}4 \times 10^{15}\,\mathrm{c.c.}^{-1}$, but the average loop diameter has increased to about 300 Å. It should be noted however that no account has been taken in these figures of the very small and rather faint spots which can also be observed in the background; the quality of the photographs is not sufficiently good to decide if these are of the same nature as those observed in specimens irradiated to the lower doses. Sometimes complicated networks are also seen (fig. 8). The density of dislocations in the network shown in fig. 8 is $\sim 3 \times 10^{10}\,\mathrm{cm}^{-2}$ and may be compared with the dislocation density in loops in other areas $\sim 2 \times 10^{10}\,\mathrm{cm}^{-2}$.

In the specimen irradiated to $4{\cdot}1 \times 10^{20}\,\mathrm{n\,cm}^{-2}$, dislocations in loops and networks were observed, similar to those in the specimen irradiated to $1{\cdot}4 \times 10^{20}\,\mathrm{n\,cm}^{-2}$.

The observations outlined above show that one of the effects of neutron-irradiation of copper is the creation of new dislocation lines. At low doses, these are in the form of small prismatic dislocation loops. As the dose is increased, the density of loops increases and some of those already in the crystal grow. Eventually, the loops may intersect to form a dislocation network in some areas at very high doses. A decrease in density of the loops is also apparently observed at high doses together with a slight decrease in dislocation density. This may be due to differences in foil thicknesses between these specimens and those irradiated to lower doses. It should also be noted that in these cases the presence of a high density of small loops or regions of strain cannot be ruled out. Further, it must be pointed out that the very high doses were obtained in DIDO which operates at a higher temperature and a greater neutron flux than BEPO (in which the lower dose specimens were irradiated). The significance of altering these variables is not clear at present.

3.3. *Annealing Experiments*

The results of some preliminary annealing experiments on the foils irradiated to $6{\cdot}7 \times 10^{17}\,\mathrm{n\,cm}^{-2}$ are reported in this section. These were carried out both on bulk specimens which were subsequently thinned by electropolishing, and on microscope specimens, using a high temperature object stage in the electron microscope.

3.3.1. *Annealing of bulk specimens*

No significant difference was observed between foils aged at 100°C for 3 hours after irradiation and those not aged. Two other specimens were annealed for 22 min and 6 hours at 350°C. The effect of the 22 min anneal was to reduce the loop density by a factor of four to 8×10^{14} c.c.$^{-1}$. A typical area is shown in fig. 9 (*a*). (The magnification is intermediate between that of fig. 1 and fig. 2.) No marked changes in the distribution of loop sizes (e.g. the occurrence of large loops) was noted. The density of spots in the specimen given a 6 hour anneal was reduced still further to $\sim 10^{14}$ c.c.$^{-1}$ in some areas (see fig. 9 (*b*)) while other areas were observed to be completely free from spots.

3.3.2. *Heating stage experiments*

The high temperature stage used for this work and the calibration procedure was described by Whelan (1958) (see also Silcox and Whelan 1959). After two to three minutes at 360–370°C, the spots disappear. The larger spots are observed to shrink before disappearing. Figures 10 (*a*) and (*b*) show typical, but not identical areas of a specimen before, (10 (*a*)), and after, (10 (*b*)), annealing. In a similar experiment, the effects observed in the foils irradiated to $5{\cdot}6 \times 10^{18}$ n cm^{-2} also disappeared in times of the order of two to three minutes at ~ 370°C. If it is assumed that the loops in the thin microscope specimen are disappearing by a vacancy emission process controlled by the line tension and curvature of the loop, then the lifetime τ of a loop of initial radius r_0 is approximately given as (Silcox and Whelan 1959)

$$\tau = \frac{{r_0}^2}{\alpha z \nu \mathbf{b}^2} \exp \frac{E_D}{kT} \quad . \quad . \quad . \quad . \quad . \quad . \quad . \quad . \quad (1)$$

where z is the atomic coordination number (~ 11), ν is an atomic frequency ($\sim 10^{13}$ sec^{-1}), $\mathbf{b}$ is the Burgers vector of the dislocation ring ($= 2{\cdot}55$ A), $E_D = E_f + E_m$ where E_f and E_m are respectively the activation energies for formation and movement of vacancies and kT is the usual Boltzmann factor. The constant α is dependent on the rigidity modulus G, Poisson's ratio ν and the temperature T but is independent of the radius of the loop. Taking $G = 3{\cdot}95 \times 10^{11}$ dynes cm^{-2} at 350°C and $\nu = 0{\cdot}35$, then $\alpha = 56$ for copper at 350°C (cf. Silcox and Whelan 1959). The activation energy E_D is then given by eqn. (1), and taking $r_0 = 15b$, $\tau = 120$ sec and $T = 373$° C, $E_D \sim 2$ ev. The variation in α due to a variation of temperature from 350°C to 373°C, is small and, since E_D depends logarithmically on α, the resultant error in E_D is small. This value for E_D will be discussed later (§ 4.6) but it should be noted that irradiation effects in copper anneal out at temperatures between 300°C and 400°C (Redman *et al.* 1953, McReynolds *et al.* 1955). This confirms that the observed effects are due to neutron irradiation.

3.4. *Other observations*

The density of spots in the specimens irradiated to $6{\cdot}7 \times 10^{17}$ cm^{-2} is fairly uniform all over the specimens. Figure 11 is a micrograph showing

the density of spots close to a grain boundary. A marked denuded zone such as occurs in quenched aluminium (Hirsch *et al.* 1958 a) is not observed. If there is any variation in density with distance from the grain boundary it is at most $\sim 30\%$ within about $\frac{1}{4}\mu$ of the boundary†. The grain boundary therefore exerts much less influence on the formation of loops, than in the case of loops formed by quenching.

Dislocations other than those in loops are shown in fig. (10 *a*) (neutron dose $\sim 6{\cdot}7 \times 10^{17}\,\mathrm{cm}^{-2}$). These are usually irregular in shape, e.g. at X; this suggests strongly that climb has taken place as a result of irradiation.

After irradiation to $6{\cdot}7 \times 10^{17}\,\mathrm{n\,cm}^{-2}$, one foil was given 3% extension. Figure 12 (*a*) shows some of the dislocations observed in this foil. At points such as Z, the cusp-like nature of the dislocation lines suggests that the lines are pinned at these points. However, it has not yet proved possible to decide whether the dislocations are pinned at loops. The effectiveness of the pinning was shown by a sequence in which a short section of the dislocation line XY (fig. 12 (*a*)) bowed out until it met the surface. The process occurred too rapidly for intermediate stages to be photographed but fig. 12 (*b*) shows clearly the points C, D where the bowed out section has met the foil surface, and the pinning points A, B.

§ 4. Interpretation

4.1. *General*

The observations outlined in § 3 leave little doubt that one of the effects of neutron irradiation of copper is the production of new dislocation lines. The nature of the contrast, the annealing behaviour, and the variation of the dislocation structure with dose all support this view. For small doses the observations show the existence of a few loops and a high density of small regions of strain. The latter are thought to be either the nuclei of loops or loops at various stages of growth. As irradiation proceeds, more and bigger loops are observed. Eventually the density of loops appears to reach a maximum, while the radii of the loops continue to increase. Thus at $\sim 10^{20}\,\mathrm{n\,cm}^{-2}$, nearly all the observed defects are either fairly large loops or dislocations in networks. (However, the presence of large numbers of small defects cannot be ruled out in this case.) The dislocation densities in the specimens are high, being $\sim 10^{10}$–$10^{11}\,\mathrm{cm}^{-2}$. The stability and annealing behaviour of the loops suggests that they are prismatic in character. Evidence has been obtained for the climb and pinning of dislocations.

Since exactly similar loops are observed in quenched metals, it might be thought that the loops are formed by *vacancy* condensation. It must be pointed out, however, that interstitial clusters may also form and there seems no reason why an interstitial platelet should not undergo a reaction exactly analogous to that pointed out by Kuhlmann-Wilsdorf (1958), which turns a vacancy platelet into a prismatic dislocation loop. The

† *Note added in proof.*—Further observations have confirmed the existence of a slight denuded region.

formation of interstitial platelets has in fact been proposed as an explanation of radiation hardening by Kunz and Holden (1954). It is also possible that the small regions of strain are some form of three-dimensional clusters of interstitials although this seems unlikely. Since interstitial clusters may disappear by vacancy absorption, these clusters may anneal out at about the same temperature as that at which vacancy loops or clusters anneal out. There thus seems to be no way at present of distinguishing between the two types of loops, or clusters, and, in fact, the preliminary annealing experiments reported above (§ 3.3) have not shown any difference in behaviour between any of the loops. On the basis of these observations, no decision can therefore be taken as to whether the loops arise by vacancy or interstitial agglomeration or both. A picture consistent with other data will however, be developed below.

4.2. *Previous Models*

The passage of fast neutrons (~ 2 Mev) through a metal like copper results primarily in the creation of a number of high energy 'primary knock-ons'. These are atoms which have been torn from their lattice sites and are passing through the metal with a high energy ($\sim 10^5$ ev). 'Primary knock-ons' may lose energy by ionizing the crystal or through Rutherford and hard-sphere types of collision with atoms in the crystal. In the case of copper, almost all the energy is expended in hard-sphere collisions (see e.g. Seitz and Koehler 1956). In these circumstances a cascade process occurs in which more and more atoms get struck from their lattice sites while the average energy per displaced atom decreases. Eventually the energy of the displaced atoms decreases to a level where they are no longer capable of displacing others and the cascade ends at this point. The energy actually stored as point defects at the end of such a process is a very small fraction of the total available energy of the primary knock-on. The remainder is dissipated in the form of lattice vibrations and the physical effects of this process have been interpreted in a number of different ways. Seitz and Koehler (1956) have suggested that the lattice vibrations may be excited at localized points along the paths of the knock-ons at which the interaction with the lattice is sufficient to transfer energy without displacing atoms. The result of this is to raise small local regions around the paths of the knock-ons to very high temperatures (~ 1000°C) for short periods of time ($\sim 10^{-11}$ sec). These phenomena are termed thermal spikes. Brinkman (1954), on the other hand, argues that the mean free path of the knock-ons between collisions is of the same order of magnitude as the interatomic separation. Accordingly, it is meaningless to refer to individually separated points at which displacements occur. Instead, he suggests that a region of crystal around the path of the primary knock-on melts and re-solidifies quickly, generally with the same orientation as the parent lattice. A few Frenkel pairs may survive this process together with, perhaps, one or two dislocation loops and small crystals of a different orientation to that of the parent lattice. In a later development of this

concept, Brinkman (1956) proposed the transient formation of a hole (or multiple vacancy) surrounded by a shell of vacancy/interstitial pairs surrounded in turn by a shell of interstitial atoms. In the later stages of the spike, the hole will collapse under the pressure of the shell of interstitial atoms and, under the influence of the thermal vibrations, the material will recrystallize with the original orientation. Based on these ideas, Seeger (unpublished) has put forward a model in which the collapse gives rise to zones of density 20–30% less than that of the parent crystal. Some of the interstitials are thought to be shot away from the spike as dynamic crowdions. The view point adopted by Cottrell (1956a) lies somewhat between the displacement and thermal spike concepts. His model consists of a pear-shaped cluster of Frenkel defects in which, due to the high thermal energies available, most of the pairs will anneal out. He suggests that only those defects at the edge of cluster survive the thermal spike.

While Brinkman (1954, 1956) suggested that isolated dislocation loops might be formed within a displacement spike, the nature of these loops was not specified. Seitz and Koehler (1956) have also pointed out that the compressive stresses associated with the thermal expansion of a displacement spike may cause the nucleation of dislocation loops on slip planes, which, on cooling, should contract. However, if several loops intersect, a stable interlocking network might be formed. The observations of isolated dislocation loops after low dose irradiations show that this latter mechanism does not seem to be important in neutron irradiated copper. The observed formation of stable prismatic dislocation loops does appear to be consistent however with any displacement spike model (e.g. Brinkman 1954, 1956, Cottrell 1956a, Seeger, unpublished) in which local concentrations of vacancies or of interstitials are produced. The absence of any zone *markedly* denuded of loops near a grain boundary suggests that the loops are *nucleated* within the spike, and not primarily by migration and condensation of isolated vacancies (see fig. 11). In the following section the previous displacement spike models will be elaborated a little to include specifically the formation of loops.

4.3. *The Model*

We suppose that some of the interstitials are shot away from the site of the spike as dynamic crowdions. This leaves the centre of the spike with an excess concentration of vacancies, surrounded by a shell of vacancy/interstitial pairs (fig. 13 (*a*)). We may assume that in a typical case, 100 interstitials at the surface of the spike might survive (Cottrell 1956a). If we assume that these are shot away as crowdions, then an excess concentration of 100 vacancies will be left in the centre of the spikes. The spike itself is estimated by Cottrell to contain perhaps $\sim 60\,000$ atoms. The local concentration of vacancies is therefore $\sim 2 \times 10^{-3}$ which is extremely large and is in fact considerably larger than is usually encountered in quenching experiments. The effective chemical stress

aiding nucleation of a loop due to a supersaturation of vacancies is given as $(kT/\mathbf{b}^3)\log c/c_0$ where c is the actual concentration and c_0 the equilibrium concentration of vacancies. Under the conditions of irradiation (i.e. $T \sim 35$–100°C), this is found to be $\sim G/7$. While these numbers are not to be

Fig. 13

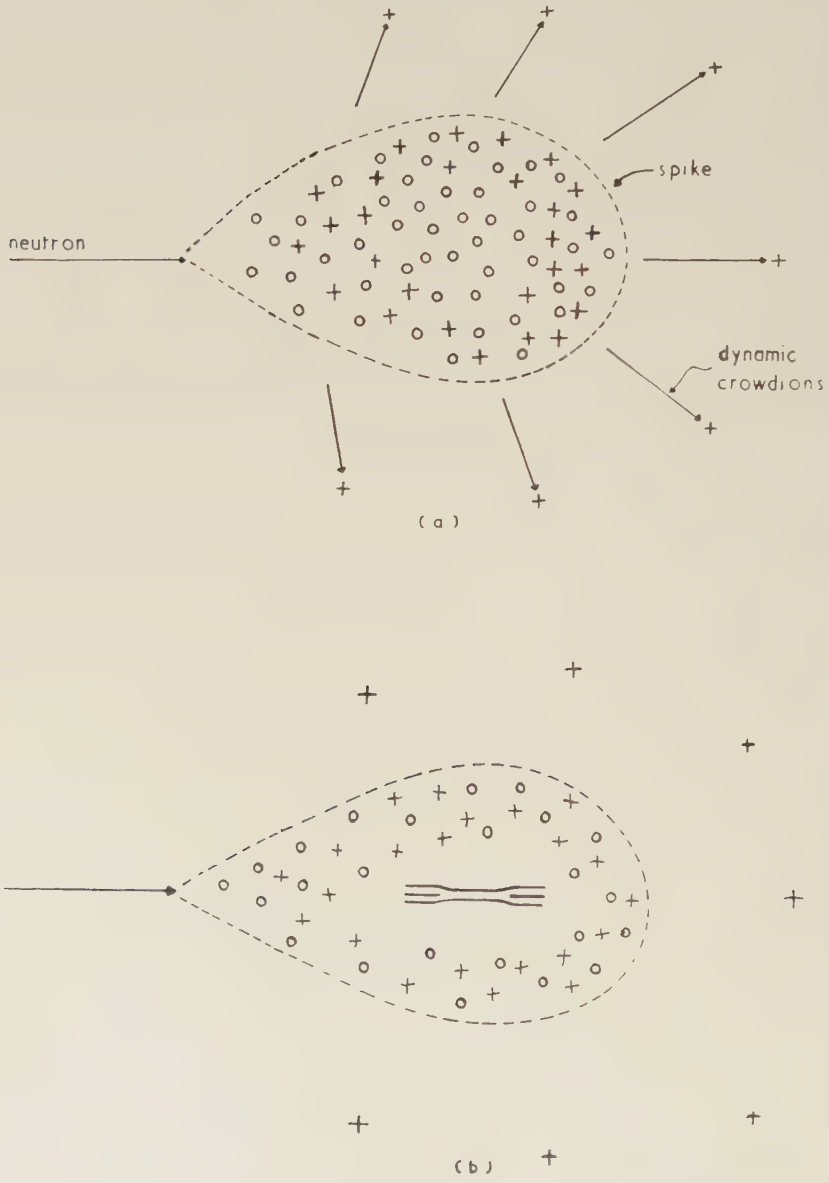

(*a*) A transient stage in the formation of dislocation loops in a displacement spike. O vacancy ; + interstitial atoms.
(*b*) Prismatic dislocation loops formed at the end of the displacement spike.

regarded as accurate quantitative estimates they are expected to represent the relevant orders of magnitude. Such large concentrations of vacancies would be expected to precipitate into discs, which subsequently collapse to form dislocation loops (as in fig. 13 (*b*)), if the temperature is high enough for vacancy migration to take place. At present, there is still some discussion about the temperature at which this occurs, but the most recent electrical resistivity experiments on quenched Cu (Airoldi *et al.* 1959) suggests that the activation energy for vacancy migration is $\sim 1{\cdot}3$ ev; if this value is correct no appreciable single vacancy movement could have taken place during these experiments. But even if the average temperature is not so high, during the formation of the spike the effective local temperature is expected to be very high (say ~ 1000°c) for a very short time (say $\sim 10^{-11}$ sec) and during this time several atomic jumps may take place, sufficient for the small discs of vacancies to be formed. If the local concentration of vacancies is very high the activation energies of movement may also be lowered below that for single vacancy migration (e.g. if di- or multi-vacancies are formed). Formation of vacancy discs and dislocation loops would also be aided by the compressive stresses due to the shell of Frenkel pairs and interstitials surrounding the central region of the spike. All these arguments suggest that loops may form or nucleate at temperatures below that at which vacancy migration takes place. In fact, the present experiments show that precipitation and collapse of vacancy discs takes place at temperatures as low as ~ 35°c. Furthermore, assuming the effect of deuteron irradiation to be similar, the experiments of Simmons and Balluffi (1958) and Vook and Wert (1958) on length changes in deuteron irradiated Cu indicate that most of the increase in length after irradiation disappears below room temperature, so that the vacancy rich regions must have collapsed below this temperature. Another argument suggesting that collapse takes place during the formation of the spike is the fact that there is virtually no annealing or change of the increase in flow stress after irradiation at 20°k up to about 300–400°c. (It will be shown below that the increase in flow stress can be explained in terms of dislocation loops.)

The above section may be summarized as follows:

(1) Under the conditions of large vacancy concentration believed to occur in displacement spikes, loops are expected to be formed at a temperature at which vacancy migration occurs.

(2) It is known that prismatic loops are formed during irradiation at ~ 35°c which is thought to be lower than the temperature for vacancy migration.

(3) It is probable that loops are formed at even lower specimen temperatures during the formation of the spike.

With regard to the surrounding shell of Frenkel defects, these are expected to annihilate at a temperature at which sufficient activation energy is available. Seeger suggests that in low temperature (20°k) neutron-irradiated Cu, these defects anneal out in stages I, II and III

corresponding to temperature ranges of 20–50°K, 50–240°K and 240–300°K. While these processes affect the electrical resistivity, X-ray lattice parameter and length changes, they have little effect on the mechanical properties. Under the present conditions of irradiation the Frenkel defects have therefore probably annihilated.

The crowdions which are originally ejected from the spike are thought to be absorbed at other dislocation loops, by vacancies, at the original dislocations, at grain boundaries or at the surface. The occurrence of the last three absorption processes allows the dislocation density in the form of loops to increase. However, when the loops are sufficiently numerous and large enough to interact to form a network, further absorption of interstitials or vacancies will cause the network to move but not to change significantly in density. Prior to this saturation effect however, the increase in dislocation density in the form of loops is entirely due to the small increase in the number of vacancies due to the disappearance of some interstitials at other sinks. (The formation of interstitial platelets as postulated by Kunz and Holden (1954) is thought to be rather more unlikely, since the concentration of interstitials at any time or place will be low.) The nature of the increase in dislocation density with continued irradiation will be discussed in the following section.

Pile	BEPO	BEPO	DIDO
Total neutron flux	$6{\cdot}7\times10^{17}$ cm^{-2}	$5{\cdot}6\times10^{18}$ cm^{-2}	$1{\cdot}4\times10^{20}$ cm^{-2}
Density of defects	3×10^{15} c.c.$^{-1}$	$6{\cdot}5\times10^{15}$ c.c.$^{-1}$	$1{\cdot}4\times10^{15}$ c.c.$^{-1}$
Density of neutron collisions	10^{17} c.c.$^{-1}$	10^{18} c.c.$^{-1}$	$2{\cdot}5\times10^{19}$ c.c.$^{-1}$
Loop size (diameter)	75 Å	150 Å	300 Å
Number of vacancies per loop	800	3100	12400
Total number of vacancies	$2{\cdot}4\times10^{18}$ c.c.$^{-1}$	2×10^{19} c.c.$^{-1}$	$1{\cdot}7\times10^{19}$ c.c.$^{-1}$
Vacancies per neutron collision	24	20	0·6
Distance between collisions	215 Å	100 Å	35 Å
Distance between loops	700 Å	535 Å	900 Å
Dislocation densities (in loops)	10^{10} cm^{-2}	4×10^{10} cm^{-2}	$1{\cdot}7\times10^{10}$ cm^{-2}

4.4. *Concentration of Defects*

The values of some of the quantities relevant to the present discussion are shown in the table. It should be emphasized that the values deduced from the micrographs are of a preliminary nature. The density of neutron

collisions, and hence the number of primary knock-ons and the number of spikes are given by the product of the total neutron flux, the density of atoms in the metal and the neutron cross section for elastic scattering of copper. The cross section was taken as 2×10^{-24} cm^2 (Hughes and Harvey 1955). From the size and density of the loops, the concentration of vacancies surviving in loops can be evaluated. From this and the density of neutron collisions, the average number of vacancies surviving in a spike can be found. For the lower doses, in BEPO, this is about 20 per spike. Theory predicts that the number of Frenkel pairs produced is ~ 1000 (e.g. Cottrell 1956a) and consequently only a small fraction ($\sim 2\%$) of the created defects survive in the spike. When the dislocation loops are so large and numerous that they form a dislocation network, saturation occurs and the number of surviving defects per spike is expected to decrease. This may possibly account for the rather low value for the third dose ($1{\cdot}4 \times 10^{20}$ n cm^{-2}). However, it should be pointed out that the micrographs do not rule out the presence of small loops or regions of strain. Further, the temperature and flux (n cm^{-2} sec^{-1}) in the case of the third dose were greater than for the other two specimens. The influence of these variables is not understood at present.

It will be noted that the number of loops is smaller than the number of spikes calculated from the number of neutron collisions; furthermore each loop contains more vacancies than the average number expected to survive at the spike. This could be due to the fact that if a dislocation line lies in a displacement spike then it will act as a site for the absorption of vacancies. Thus, if a previously formed loop lies within a displacement spike, the vacancies may combine with it causing it to grow, rather than forming a new loop. However, the diameter of the spikes is expected to be ~ 75–100 Å (Brinkman 1954, Cottrell 1956a), and while this is of the order of the inter-collision distance, it is rather lower than the interloop distance (see table). Thus, while spikes are expected to overlap, it appears that a loop would not necessarily lie in a spike unless the latter are about 500 Å in diameter, which seems unreasonably large. However, the large number of vacancies per loop, and the growth of the loops under continued irradiation can be explained if some vacancy migration is assumed. Thus, it is possible that some of the smaller loops formed initially during irradiation disperse as vacancy clusters as a result of interstitial absorption; these small vacancy clusters might migrate (at relatively low temperatures) to other loops causing these to grow. This migration of vacancies or of vacancy clusters could also be accelerated by the local temperature rise in the spike. We suggest therefore that the loops are *nucleated* in the spikes, but that further *growth* takes place as a result of vacancy or of vacancy cluster migration.

4.5. *Irradiation Hardening*

Irradiation hardening is similar in nature to quench and fatigue hardening (Cottrell 1956b, 1958, Broom and Ham 1959). All three types of hardening

are characterized by a high yield point, sometimes accompanied by a subsequent yield drop, but always followed by a stage in the stress strain curve in which the rate of work-hardening is small; furthermore, the temperature dependence of the yield stress is greater for irradiated or fatigued than for cold-worked crystals. This type of hardening has been attributed to the presence of point defects (Cottrell 1958, Broom and Ham 1959), but there has been some doubt as to the precise mechanism of hardening. Recent transmission electron microscope experiments on quenched Al and Cu (Hirsch *et al.* 1958 a, Hirsch and Silcox 1958, Smallman and Westmacott 1959) and fatigued Al (Wilson and Forsyth 1959, Segall and Partridge 1959). and Cu (Segall and Partridge unpublished), together with the present results on irradiated Cu and those of Smallman and Westmacott (1959) on irradiated Al, all show the presence of dislocation loops. It is considered therefore that the general level of the stress strain curve after initial yielding in all three cases is due to the large density of dislocations in the form of loops. More specifically the flow stress is determined by the stress required for a dislocation to cut through the 'forest' of loops. On this model, the temperature dependent part of the flow stress, τ_s, is due to the stress required to make the jog, while the temperature independent (after correction for the shear modulus) part τ_g, is due to the long-range elastic strain field of the loop. While τ_s will be the same as that for a work-hardened metal with similar dislocation density, τ_g will be smaller for loops because the elastic strain field decreases more rapidly with distance from a small loop than from a long straight dislocation. Consequently τ_s/τ_g is expected to be larger for crystals containing small loops than for crystals containing networks. Thus the relatively larger temperature dependence of the flow stress in irradiated, or fatigued metals can be explained, at least qualitatively, in terms of the observed dislocation loops.

With regard to the absolute magnitude of the yield stress, on the theory of forest hardening from dislocation networks (Hirsch 1958, Thornton 1959, Basinski 1959), τ_g is expected to be $\sim(G\mathbf{b}/2\pi l)$ where l is the average distance between loops intersecting the slip plane. If n is the number of loops per unit volume, L their average diameter, it is easy to show that $l=[(\pi/2)nL]^{-1/2}=[\rho/2]^{-1.2}$, where ρ is the dislocation density, assuming that the loops are randomly orientated. Using the data given in the table, τ_g is found to be 0·96, 2·01, 1·315 kg/mm^2 for the three doses. The values of τ_g for the two lower doses are of the same order of magnitude as those observed experimentally (Makin reported by Cottrell 1958, Blewitt and Coltman 1951, Greenfield and Wilsdorf 1959). Blewitt (1956) reports that the flow stress varies as (dose)$^{1/3}$. The present determinations of dislocation density are however too inaccurate to allow this law to be tested on the present model. It is clear however from the electron microscope observations that there may not be a simple interpretation of the (dose)$^{1.3}$ law, as both the number and size of the loops vary with increasing dose. The important parameter, however, is the dislocation density.

While the general level of the stress strain curve after the initial yielding can be accounted for in terms of dislocation loops, the initial yield point,

sometimes followed by a yield drop, is likely to be influenced by pinning of dislocations by point defects, as suggested by Cottrell (1956 b, 1958). The electron microscope observations in fact suggest the presence of 'joggy' dislocations, confirming the occurrence of this process (see fig. 12 (*a*)). The initial yield point may also be determined by the criterion that a dislocation loop must act as a source, as suggested by Kuhlmann-Wilsdorf (1958). Thus, essentially there are two types of hardening present: 'source' hardening, and 'dispersion' hardening due to loops; these have been measured separately for irradiated Cu by Adams and Higgins (1959), by determining the variation of yield stress with grain size. Both types of hardening increase with increasing dose, but the temperature dependence of the yield stress is determined by the dispersion hardening component, which we identify with loops.

While the above considerations are still mainly qualitative and of a preliminary nature, they do suggest that the main features of the hardening mechanism in irradiated, quenched and fatigued metals can be explained in terms of (1) forest hardening due to dislocation loops and (2) source hardening due to either initial locking of the dislocations other than loops by the formation of many jogs, or to the fact that the loops themselves may act as sources. There seems to be no need to postulate a hardening mechanism specific to irradiated metals, as suggested by Seeger (unpublished) in which the defects are zones of ~ 10 Å diameter, of density less than that of the perfect crystal. While such zones are probably too small to be observed in the electron microscope, the occurrence of loops in specimens irradiated at ~ 35°C suggests that collapse takes place at least at that temperature. Furthermore, the results of the annealing of length changes (Vook and Wert 1958, Simmons and Balluffi 1958) indicate that nearly all the collapse takes place even somewhat below this temperature. Thus for irradiation at room temperature and above only dislocation loops are thought to contribute to the dispersion hardening. Although we believe that this is also true at lower temperatures, this cannot be proved at present.

4.6. *Annealing*

Preliminary annealing experiments described in § 3.3 show that the loops disappear in the range of temperature (300–400°C) in which radiation hardening anneals out, and from the heating stage experiments a preliminary value for the activation energy of the process was found to be ~ 2 ev. This may be compared with the values of 2·2 ev and 2 ev found by Redman *et al.* (1953) and by McReynolds *et al.* (1955) respectively for the same annealing range. These values are close to the value of 2·05 ev found for the energy of self-diffusion by Kuper *et al.* (1954), although recent preliminary electrical resistivity measurements on quenched copper by Airoldi *et al.* (1959) indicate a higher value of 2·3 ev for the sum of the activation energies of formation and migration of vacancies. In the absence of a more complete investigation, however, we may conclude that

the annealing is consistent with that found by other workers and is governed by the activation energy of self-diffusion. Accordingly the time taken for a loop of diameter 75 Å to anneal out at 350°C is ~ 10 min (using formula 1) and thus the observed decrease in density of loops by a factor of four in the foil annealed for 22 min at 350°C is to be expected. A complete anneal is not expected as this would correspond to the lifetime of a loop of larger than average radius (as pointed out by Silcox and Whelan 1959).

The various stages of the annealing of the resistivity due to irradiation at very low temperatures have been discussed by several authors (Koehler *et al.* 1956, Blewitt *et al.* 1956, Seeger unpublished), and they will not be considered here.

§ 5. Conclusions

The results of this paper may be summarized as follows:

(1) Dislocation loops are formed in Cu irradiated with neutrons at a temperature a little above room temperature.

(2) For small doses (10^{18} n cm $^{-2}$) many of the defects observed can only be resolved as small regions of strain; the diameter of those defects which can be recognized as loops is 100 Å or less.

(3) With increasing dose of irradiation the average diameter of the loops increases, and a large proportion of the defects can be recognized as loops.

(4) For large doses of irradiation (10^{20} n cm^{-2}) dense dislocation networks are observed in some areas.

(5) The stability of the small defects and loops, and their behaviour on annealing is that expected from prismatic loops.

(6) The loops are thought to nucleate in the centre of a displacement spike by the collapse of disc-shaped cavities formed in a region containing a very high supersaturation of vacancies, and to grow as a result of migration of vacancies or of vacancy clusters.

(7) Radiation hardening is interpreted in terms of a forest of dislocation loops. The density of dislocations in loops exceeds $\sim 10^{10}$ cm^{-2}.

(8) Radiation hardening anneals out at a temperature at which the loops disappear by climb.

These results are only of a preliminary nature, and further systematic investigations are in progress on irradiated Cu and other metals.

Acknowledgments

Our thanks are due to Professor N. F. Mott and Dr. W. H. Taylor for their interest, encouragement and helpful discussion during the course of this work; to Dr. N. H. Hancock and Mr. W. Wynd of A.E.R.E., Harwell, for irradiating the specimens; to Mr. G. Rickards for maintenance of the electron microscope and for help in the heating stage experiments, and to our colleagues in the Metal Physics group for advice and discussion. One of us (J.S.) is indebted to the A.E.R.E. for a maintenance grant.

References

Adams, M. A., and Higgins, P. R. B., 1959, *Phil. Mag.*, **4**, 777.

Airoldi, G., Bacchella, G. L., and Germagnoli, E., 1959, *Phys. Rev. Letters*, **2**, 145.

Atkinson, H. H., Smallman, R. E., and Westmacott, K. H., 1959, *J. appl. Phys.*, **30**, 646.

Barnes, R. S., and Hancock, N. H., 1958, *Phil. Mag.*, **3**, 527.

Barnes, R. S., Hancock, N. H., and Silk, E. C. H., 1958, *Phil. Mag.*, **3**, 519.

Basinski, Z. S., 1959, *Phil. Mag.*, **4**, 393.

Blewitt, T. H., 1956, *Dislocations and Mechanical Properties of Crystals* (New York : Wiley), p. 573 ; 1958, *Institute of Metals Monograph and Report Series*, No. 23, p. 213.

Blewitt, T. H., and Coltman, R. R., 1951, *Phys. Rev.*, **82**, 769.

Blewitt, T. H., Coltman, R. R., Holmes, D. K., and Noggle, T. S., 1956, *Dislocations and Mechanical Properties of Crystals* (New York : Wiley), p. 603 ; 1957, *Creep and Recovery of Metals*, **84** (Cleveland : American Society for Metals).

Brinkman, J. A., 1954, *J. appl. Phys.*, **25**, 961 ; 1956, *Amer. J. Phys.*, **24**, 246.

Broom, T., and Ham, R. K., 1959, *Proc. roy. Soc.*, **251**, 186.

Cottrell, A. H., 1956 a, *Met. Rev.*, **1**, 479 ; 1956 b, *Dislocations and Mechanical Properties of Crystals* (New York : Wiley) p. 577 ; 1958, *Institute of Metals Monograph and Report Series*, No. 23, p. 1.

Cooper, H. G., Koehler, J. S., and Marx, J. W., 1954, *Phys. Rev.*, **94**, 496.

Corbett, J. W., Denney, J. M., Fiske, M. D., and Walker, R. M., 1956, *Phys. Rev.*, **104**, 851.

Dienes, G. J., and Vineyard, G. H., 1957, *Radiation Effects in Solids* (New York : Interscience).

Glen, J. W., 1955, *Advanc. Phys.*, **4**, 381.

Greenfield, I. G., and Wilsdorf, H. G. F., 1959, *Bull. Amer. phys. Soc.*, **4**, 136.

Hirsch, P. B., 1958, *General Motors Symposium* (to be published).

Hirsch, P. B., Silcox, J., Smallman, R. E., and Westmacott, K. H., 1958 a, *Phil. Mag.*, **3**, 897.

Hirsch, P. B., Howie, A., and Whelan, M. J., 1958 b, *Proceedings of the IVth International Electron Microscopy Conference, Berlin* (to be published) ; 1959, *Phil. trans. roy. Soc.* (in the press).

Hirsch, P. B., and Silcox, J., 1958, *Report of the Cooperstown Conference on the Growth and Perfection of Crystals*, Ed. Doremus, Roberts and Turnbull (New York : Wiley), p. 262.

Hughes, D. J., and Harvey, J. A., 1955, *Neutron Cross Sections*, U.S.A.E.C. (New York : McGraw Hill).

Jamison, R. F., and Blewitt, T. H., 1952, *Phys. Rev.*, **86**, 641 ; 1953, *Phys. Rev.*, **91**, 237.

Kinchin, G. H., and Pease, R. S., 1955, *Rep. Progr. Phys.*, **18**, 1.

Koehler, J. S., Henderson, J. W., and Bredt, J. H., 1956, *Dislocations and Mechanical Properties of Crystals* (New York : Wiley), p. 587.

Kuhlmann-Wilsdorf, D., 1958, *Phil. Mag.*, **3**, 125.

Kunz, F. W., and Holden, A. N., 1954, *Acta Met.*, **2**, 816.

Kuper, A., Letaw, H., Slifkin, L., Sonder, E., and Tomizuka, C. T., 1954, *Phys. Rev.*, **96**, 1224.

Lomer, W. M., and Cottrell, A. H., 1955, *Phil. Mag.*, **46**, 711.

Makin, M. J., 1958, *J. Inst. Met.* **86**, 449 ; 1959, *Acta Met.*, **7**, 233.

McReynolds, A. W., Augustyniak, W., McKeown, M., and Rosenblatt, D. B., 1955, *Phys. Rev.*, **98**, 418.

Meechan, C. J., and Brinkman, J. A., 1956, *Phys. Rev.*, **103**, 1193.

Noggle, T. S., 1959, *Bull. Amer. Phys. Soc.*, **4,** 137.
Overhauser, A. W., 1954, *Phys. Rev.*, **94,** 1551.
Redman, J. K., Coltman, R. R., and Blewitt, T. H., 1953, *Phys. Rev.*, **91,** 448.
Segall, R. L., and Partridge, P. G., 1959, *Phil. Mag.*, **4,** 912.
Seitz, F , 1952, *Phys. Today*, **5,** 6.
Seitz, F., and Koehler, J. S., 1956, *Solid State Physics*, **2,** 305 (New York : Academic Press).
Silcox, J., and Hirsch, P. B., 1959, *Phil. Mag.*, **4,** 72.
Silcox, J., and Whelan, M. J., 1960, *Phil. Mag.* (in the press).
Simmons, R. O., and Balluffi, R. W., 1958, *Phys. Rev.*, **109,** 1142.
Smallman, R. E., and Westmacott, K. H., 1959, *J. appl. Phys.*, **30,** 603.
Thompson, D. O., and Holmes, D. K., 1956, *J. appl. Phys.*, **27,** 713.
Thompson, D. O., Blewitt, T. H., and Holmes, D. K., 1957, *J. appl. Phys.*, **28,** 742.
Thornton, P. R., 1959, Ph.D. Dissertation, University of Cambridge.
Tomlinson, H., 1958, *Phil. Mag.*, **3,** 867.
Vook, R., and Wert, C., 1958, *Phys. Rev.*, **109,** 1529.
Whelan, M. J., 1958, *Proceedings of the IVth International Conference on Electron Microscopy, Berlin* (to be published).
Wilson, R. N., and Forsyth, P. J. E., 1959, *J. Inst. Met.*, **10,** 336.

CORRESPONDENCE

Temperature Dependence of the Strength of Zone Hardened Aluminium–Silver Alloys†

By Morris E. Fine

Department of Metallurgy and Materials Science,
The Technological Institute, Northwestern University,
Evanston, Illinois

[Received August 28, 1959]

The critical resolved shear stress of a fully cold hardened Al–6 at % Ag alloy (water quenched from 560°C and aged 8 hrs at 160°C) is 9 Kg/mm² at room temperature and increases 12% on cooling to 77°K (Kelly *et al.* 1959).

In two previous papers, Kelly and Fine (1957) and Kelly (1958), the principal source of the strength of aluminium-rich silver alloys containing Guinier–Preston zones has been attributed to chemical changes associated with shearing of zones during plastic deformation. During shearing of zones the number of Al–Ag bonds increases; the number of Al–Al and Ag–Ag bonds decreases. The following relation of σ_c, the critical resolved shear stress, was obtained:

$$\sigma_c = \frac{f^{1/2}\Delta E(\mathrm{Ag})}{\alpha b^3}. \qquad \ldots\ldots\ldots \quad (1)$$

Here b is the Burger vector, α is a numerical factor, f is the volume fraction of zones, and $\Delta E(\mathrm{Ag})$ is the change in internal energy on removing a silver atom from a zone and putting it into solution. $\Delta E(\mathrm{Ag})$ was considered to be independent of temperature, that is, the change in heat capacity was neglected.

The purpose of the present note is to point out that there is also an increase in entropy resulting from shearing of zones and to discuss the temperature dependence of the flow stress due to the entropy term.

Since the zones contain a relatively small number of atoms, the configurational entropy per atom in a zone is very small and negligible compared to the configurational entropy of an atom in the matrix solid solution. The entropy of mixing of the zones in the matrix solid solution may also be

† This research was sponsored by the United States Air Force through the Air Force Office of Scientific Research of the Air Research and Development Command under Contract No. AF 18(600)–1468.

neglected. The average change in free energy due to removing an atom, silver or aluminium, from a zone and placing it into solution will be

$$\Delta F_T = \Delta E_0 + \int_0^T \Delta C_p dT - T\int_0^T \frac{\Delta C_p}{T} dT - TS_M \cong \Delta E_0 - TS_M. \qquad (2)$$

In eqn. (2), ΔE_0 and ΔC_p refer respectively to the average change per atom in internal energy at 0°K and heat capacity. S_M is the average entropy of mixing per atom in the solid solution. In the second equality the ΔC_p terms which tend to cancel are neglected.

The free energy change may be put on the per atom of silver basis by dividing eqn. (2) by $C_{Ag}(Z)$, the atom fraction of silver in a zone.

$$\Delta F_T(\mathrm{Ag}) = \frac{\Delta F_T}{C_{Ag}(Z)} = \Delta E(\mathrm{Ag}) - \frac{TS_M}{C_{Ag}(Z)}. \qquad . \ . \ . \qquad (3)$$

In eqn. (1) the ΔE(Ag) term should be replaced by ΔF_T(Ag).

According to Gerold (1955) in a 6 at % Ag alloy roughly one-third of the silver atoms are in zones. Assuming the zones to contain 50 at % silver (Kelly, private communication) C_{Ag} of the matrix solid solution is 0·043. The entropy of mixing of a solid solution of this composition, according to the measurements of Hillert *et al.* (1956) is about 0·5 cal/°K mole or $2{\cdot}17 \times 10^{-5}$ ev/°K atom. ΔE of 0·24 ev/atom of silver (Kelly 1958) is computed from the heat of reversion of Köster and Schell (1952).

The table shows values of $\Delta F_T/\Delta F_{273}$ computed as indicated in comparison with the observed values of σ_T/σ_{273}.

T(°K)	σ_T/σ_{273} (observed)	$\Delta F_T/\Delta F_{273}$ (computed)
77	1·11	1·04
155	1·07	1·02
196	1·05	1·01
273	1	1
373	0·97	0·985

In view of the uncertainty in the composition of the zones and the fraction of silver in zones, the computed temperature variation is only qualitative. No account has been taken of the fact that the zones consist of a silver-rich core surrounded by a silver-poor shell. For this reason the 'bond scrambling' and the entropy change due to shearing of zones by one atomic unit would be larger than computed.

It does appear reasonable to suggest, however, that entropy considerations may be important in determining the temperature variation of the flow stress in this alloy.

References

Gerold, V., 1955, *Z. Metallk.*, **46**, 623.
Hillert, M., Averbach, B., and Cohen, M., 1956, *Acta Met.*, **4**, 31.
Kelly, A., 1958, *Phil. Mag.*, **3**, 1472.
Kelly, A., and Fine, M. E., 1957, *Acta Met.*, **5**, 365.
Kelly, A., Lassila, A., and Sato, S., 1959, *Phil. Mag.*, **4**, 1260.
Köster, W., and Schell, H. A., 1952, *Z. Metallk.*, **43**, 454.

On Stress-aided Cross-slip of Dislocations

By C. J. Ball
Department of Physics, Makerere College, Box 262 Kampala, Uganda

[Received November 12, 1959]

Seeger *et al.* (1957) have shown that the reduction in the rate of work hardening in the later stages of deformation of single crystals of face-centred cubic metals (Stage 3) is due to cross-slip of screw dislocations, aided by the large stresses present near the head of piled up groups, and Seeger (1957) and Seeger *et al.* (1959) have estimated the number of dislocations in a piled up group from work hardening curves at very low temperatures. They assume that the stress forcing together the two partials of an extended dislocation at the head of a pile-up is $n\tau$, where τ is the appropriate component of the applied stress and n is the number of dislocations in the pile-up. However, with the possible exception of the first dislocation, the centres of the dislocations are in regions of zero stress. There is a stress forcing together the two partials of an extended dislocation, but this is proportional to the stress gradient at the position of the dislocation and the separation of the partials.

Eshelby *et al.* (1951) have considered the equilibrium of various arrays of dislocations, For the case of screw dislocations piled up under a shear stress τ against an obstacle that exerts only short range forces, the equilibrium positions of the dislocations are given by $G\mathbf{b}u_i/4\pi\tau$, where G is the shear modulus, $\mathbf{b}$ the Burgers vector of the dislocations and u_i one of the roots of the first derivative of the nth Laguerre polynomial, $L_n'(u)$. Further, the appropriate component of the stress gradient at the positions of the dislocations is

$$(8\pi\tau^2/G\mathbf{b})\{(n/u_i)-\tfrac{1}{4}\}.$$

The first dislocation is at the origin, and this expression does not apply. For the next dislocation (at $u=3{\cdot}67/n$) the stress gradient is $\sim(7/G\mathbf{b})(n\tau)^2$.

Applying this to work hardening at very low temperatures, we see that the stresses due to the dislocations of a pile-up are never sufficiently great to force the partials completely together. A stress component normal to the Burgers vector of the total dislocation might do this as it reacts with the edge components of the partials and forces them in opposite directions (Whelan *et al.* 1957), but sufficiently large stresses are unlikely to arise in

a single crystal deforming on primarily one system. Blewitt *et al.* (1955) did not observe Stage 3 in single crystals of copper deformed at 4·2°K. At 78°K Stage 3 was observed when the shear stress was $\sim 7\,\mathrm{kg/mm^2}$. If we suppose that at this temperature cross-slip occurs when the separation of the partials is **b**, we find for the number of dislocations in a pile-up, $n \sim 100$. Seeger's estimate was $n = 25$. He obtained substantially the same estimate from a consideration of the stress near the head of a group, supposing this to be not greater than $G/10$ and equating it to $n\tau$. However, this assumes that no stress relaxation takes place. As the crystal must be deforming on systems other than the primary, in order to form the obstacles on the primary plane, some stress relaxation is presumably taking place.

The stresses acting on the leading dislocation depend rather critically on the exact nature of the obstacle. This is usually assumed to be a Lomer–Cottrell lock. As this consists of three pure edge dislocations it has no long-range interaction with a pile-up of screws. It will, though, react with the partials into which the screw dislocations are split, as these have edge components. If all stacking faults are intrinsic and the pile-up approaches the lock on the side remote from the apex the geometry is such that the nearer partial is repelled, and the further attracted. Thus the stress compressing the partials is greater than $n\tau$. Continuum elasticity theory, neglecting the surface tension effect of the stacking fault, gives it as $4n\tau$, but it will be even greater than this.

The leading partial of a screw dislocation approaching from the other side of the lock will react with the stair rod dislocation at the apex, leaving two glissile dislocations that will present no obstacle to the pile-up.

If the pile-up does not approach on exactly the same plane as one of the stacking faults of the lock (as will probably be the case) it may not be able to react or cross-slip, and then the Lomer–Cottrell lock would be a more effective obstacle. Experimentally it appears that the leading dislocation does not cross-slip much more readily than any of the others—cross-slip traces near the head of a pile-up are not concentrated on a single plane.

It seems, then, that the number of dislocations in a pile-up may be appreciably greater than has been thought.

References

Blewitt, T. H., Coltman, R. R., and Redman, J. K., 1955, *Report of a Conference on Defects in Crystalline Solids* (London: The Physical Society), p. 369.

Eshelby, J. D., Frank, F. C., and Nabarro, F. R. N., 1951, *Phil. Mag.*, **42**, 351.

Seeger, A., 1957, *Dislocations and Mechanical Properties of Crystals* (New York: J. Wiley and Sons Inc.), p. 243.

Seeger, A., Berner, R., and Wolf, H., 1959, *Z. Phys.*, **155**, 247.

Seeger, A., Diehl, J., Mader, S., and Rebstock, R., 1957, *Phil. Mag.*, **2**, 323.

Whelan, M. J., Hirsch, P. B., Horne, R. W., and Bollmann, W., 1957, *Proc. roy. Soc.* A, **240**, 524.

The Dependence of Internal Friction on Frequency

By J. Wilks
Clarendon Laboratory, Oxford

[Received October 12, 1959]

As is well known, the internal friction of annealed pure metals and dilute alloys measured at low amplitudes of oscillation is independent of the strain amplitude. It is often postulated that this friction arises from a viscous-like damping of lengths of dislocation, anchored at each end by some form of pinning point, and vibrating with the applied stress (Koehler 1952, Granato and Lücke 1956). Such a model leads to an expression for the decrement

$$\Delta_I = x \,.\, L^4 \,.\, B \,.\, \omega \quad . \quad . \quad . \quad . \quad . \quad . \quad . \quad . \quad (1)$$

where x is a constant depending on the state of the specimen, L the mean length of the dislocation loops, B the viscous damping coefficient and ω the frequency of the oscillations. In several ways this treatment is quite successful. It gives a friction of roughly the right order of magnitude, and predicts that the modulus defect ΔE and the decrement Δ_I are proportional to the second and fourth powers of the loop length L. Evidence of such characteristic dependence on the loop lengths is given by experiments on the neutron irradiation of copper (Thompson and Holmes 1956) and from observations of the Köster effect discussed by Granato *et al.* (1958).

The model also predicts that the damping should be proportional to the frequency of the oscillations. Such dependence has been reported over small frequency ranges in lead by Hiki (1958), and in aluminium by Hikata and Truell (1957). However, other observations suggest that the dependence on frequency is very weak (Nowick 1950, Takahashi 1956), and indeed the values of the damping reported at megacycle frequencies are usually not much greater than those measured at 1 cycle per second. As several authors have discussed, there are difficulties in obtaining good experimental information over a wide range of frequencies (see, for example, Nowick 1953, Lücke and Granato 1957); nevertheless it seems that in some metals the friction varies much more slowly than the first power of the frequency. In this note we point out that a simple explanation of this behaviour is implied in a recent treatment given by Thompson and Holmes (1959) to account for the temperature dependence of Δ_I at not too high temperatures.

Thompson and Holmes suggest that the friction Δ_I increases with rising temperature because the thermal energy is able to free the dislocations from more pinning points (probably impurity atoms) and thus increase the effective lengths of the loops. These authors measured the friction and

modulus defect of an annealed copper single crystal, and found that between about 100° and 300°K both quantities rose rapidly with temperature and were related so that $(\Delta E/E)^2 \propto \Delta_I$. This last result follows naturally if the main effect of changing the temperature is to vary the loop length, because $\Delta E \propto L^2$ and $\Delta_I \propto L^4$. Such a correlation is difficult to explain otherwise; it could not arise solely from the temperature dependence of the viscous damping coefficient in the equation of motion for a vibrating dislocation, for this does not come into the expression for the modulus defect. (In addition Thompson and Holmes deduce a T^2 temperature dependence for Δ_I which is close to their experimental values, but the exact form of this dependence will depend on the distribution of the pinning points and does not concern us here.)

We now consider how the friction should depend on the frequency of the oscillations. The unpinning of a dislocation from an impurity atom by thermal activation will occur in a mean time

$$\tau = A \exp(Q/kT)$$

where A is a constant and Q an activation energy whose value will depend on the nature of the impurity and the distance to adjacent pinning points. (We assume that the strain amplitudes are so small that the effective value of Q is not changed appreciably by the stress fields acting on the dislocation.) The condition that a dislocation vibrating at a frequency, ω, should be virtually free from such a pinning point may be written

$$1/\omega \gg \tau. \quad . \quad . \quad . \quad . \quad . \quad . \quad . \quad . \quad . \quad (2)$$

At higher frequencies, such that $1/\omega \ll \tau$, the dislocation will remain pinned for virtually all cycles of the applied stress, and thus the effective lengths of the vibrating loops of dislocation are reduced. Hence the term L^4 in eqn. (1) is an inverse function of ω, so that the friction does not vary directly as the frequency but less rapidly.

To get some idea of the magnitude of this effect we use the data of Weertman and Salkovitz (1955) who measured both the amplitude dependent and amplitude independent damping (Δ_H and Δ_I) of dilute lead alloys at room temperature and above. The value of Δ_I increases with temperature so that in a typical specimen the friction at 186°C is 10 times that at 25°C. If Thompson and Holmes' explanation is applicable, this increase comes about because the time, τ, characteristic of unpinning is less at the higher temperatures. An analysis of the amplitude dependent damping (Granato and Lücke 1956) shows that the activation energy for unpinning is about 0·11 ev, so that

$$\frac{\tau_{25}}{\tau_{186}} = \frac{\exp(Q/298k)}{\exp(Q/459k)} \sim 5.$$

Thus changing τ by a factor 5 changes the friction by a factor 10. Now condition (2) implies that, as far as the effect on the unpinning process is

concerned, increasing the frequency is equivalent to increasing τ. Therefore an increase of the frequency by a factor 5 should reduce the effective loop lengths to such an extent that the friction is reduced by a factor 10 on this account alone. Hence, in this particular case, the total dependence of Δ_I on frequency should be quite small; the friction actually decreasing slightly at the higher frequencies.

The magnitude of this frequency effect will depend quite critically on the state of a specimen, particularly on the nature and amount of the impurities, and for a complete discussion one needs measurements of both Δ_I and Δ_H, together with the modulus defect, over a fairly wide range of temperatures. The only measurements of modulus defect are those already mentioned, but Chambers (1957) has given values of Δ_I and Δ_H for aluminium single crystals between room temperature and 300°c which show that Δ_I increases considerably with increasing temperature. If this is due to the loop lengths becoming longer, similar considerations to those given above show that the effect of frequency on the friction will be rather similar to that in copper. The only other relevant measurements are those of Caswell (1958) for Δ_I and Δ_H in copper single crystals below room temperature; these are not inconsistent with our present discussion, although it is not possible to derive a value of the activation energy.

It remains to consider why the friction is sometimes quite accurately proportional to the frequency. The experiments of Hikata and Truell on aluminium were made at frequencies of 5 and 10 Mc/s, and these frequencies are so high that the amount of unpinning will always be small. Hence the term L^4 of eqn. (1) was probably constant, and this leads to the observed dependence of friction on frequency. In Hiki's measurements at 64 and 192 Kc/s the proportionality to frequency was only observed below 220°K, that is in the region where the friction did not vary with temperature. Following Thompson and Holmes, this independence of the friction on temperature implies that the dislocations were always tightly pinned, so the loop lengths were again constant. We also note that Hiki's values obtained at 64 Kc/s begin to rise with increasing temperature above 250°K, and those obtained at 192 Kc/s begin to rise above 220°K. Provided that the friction is independent of the strain amplitude we would expect the rise at the lower frequency to begin at the lower temperature. However, Hiki's data is insufficient to verify that the friction at both frequencies was entirely amplitude independent; more complete experimental data would be of interest.

References

Caswell, H. L., 1958, *J. appl. Phys.*, **29,** 1210.
Chambers, R. H., 1957, Carnegie Inst. Tech. Report AT (30–1)–1193.
Granato, A., and Lücke, K., 1956, *J. appl. Phys.*, **27,** 583, 789.
Granato, A., Hikata, A., and Lücke, K., 1958, *Acta Met.*, **6,** 470.
Hikata, A., and Truell, R., 1957, *J. appl. Phys.*, **28,** 522.
Hiki, J., 1958, *J. Phys. Soc., Japan*, **13,** 1138.
Koehler, J. S., 1952, *Imperfections in Nearly Perfect Crystals* (New York: Wiley), p. 197.

Lücke, K., and Granato, A., 1957, *Dislocations and Mechanical Properties of Crystals* (New York : Wiley), p. 425.
Nowick, A. S., 1950, *Phys. Rev.*, **80**, 249 ; 1953, *Progr. Met. Phys.*, **4**, 1.
Takahashi, 1956, *J. Phys. Soc., Japan*, **11**, 1253.
Thompson, D. O., and Holmes, D. K., 1956, *J. appl. Phys.*, **27**, 713 ; 1959, *J. appl. Phys.*, **30**, 525.
Weertman, J., and Salkovitz, E. I., 1955, *Acta Met.*, **3**, 1.

Detection of Equilibrium Vacancy Concentrations in Aluminium†

By Soji Nenno‡ and J. W. Kauffman
Department of Materials Science,
Northwestern University, Evanston, Illinois, U.S.A.

[Received September 21, 1959]

The objective of this work is to detect and measure equilibrium vacancy concentrations and to estimate the energy of formation of a vacancy in aluminium. For cubic isotropic crystals, if l is the length of a sample and a the lattice parameter at a temperature T while l_0 and a_0 are corresponding values at a standard temperature T_0, the fractional concentration of vacancies, C_v, present at temperature T is expressed as

$$C_v = 3\frac{(l/l_0)-(a/a_0)}{(l/l_0)}$$

provided that T_0 is a low enough temperature that $C_v(T_0)$ is negligible. Therefore, the vacancy concentration is obtained from the difference between these two experimentally measured quantities. The lattice parameter of aluminium was measured at intervals from room temperature up to about 650°C, and was compared to the bulk thermal expansion. In the present work only the x-ray measurements were made.

Comparison of Lattice Thermal Expansion

Author	$(a-a_0)/a_0 \times 10^3$ at					
	200°C	300°C	400°C	550°C	600°C	650°C
Feder and Nowick (1958)	4·85†	7·65†	10·60†	15·40†	17·15	19·00†
Wilson (1942)	4·82	7·57	10·52	—	17·21	19·07
Present work	4·89	7·61	10·53	15·31	17·02	18·80

† These values are obtained from their graph.

Aluminium rods were obtained from Johnson, Mathey with a specified purity of 99·996%. The samples were thin rods annealed and sealed in a quartz capillary under a 2×10^{-7} mm Hg vacuum. Cobalt K radiation was

† This research was partially supported by the United States Office of Naval Research.

‡ Now at Department of Metallurgy, Faculty of Engineering, Osaka University, Osaka, Japan.

used with a Unicam 19 cm diameter powder camera, which was operated under a vacuum of 10^{-5} mm Hg. Around the quartz capillary a length of thin platinum wire was wound which was used as a thermometer. Diffraction patterns of the aluminium sample and platinum were obtained simultaneously at given temperatures. The expansion of the platinum standard was used to determine the temperature. In this way specimen temperature was determined to within 1·5°c. Probable error in lattice parameter measurement of aluminium was 5×10^{-5}.

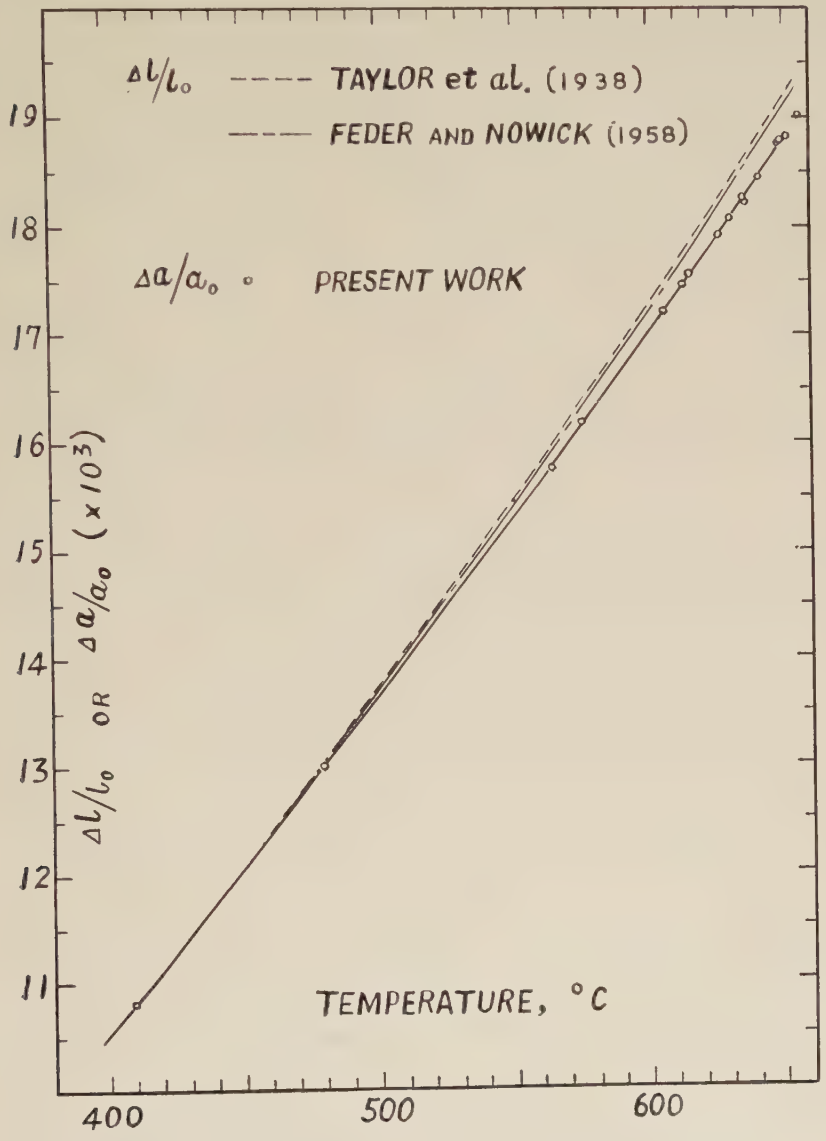

Comparison of lattice and bulk thermal expansion of aluminium.

The result of lattice thermal expansion measurements on the aluminium is expressed as an empirical equation:

$$a_t/a_0 = 1 + 2{\cdot}2724t \times 10^{-5} + 8{\cdot}188t^2 \times 10^{-9} + 2{\cdot}02t^3 \times 10^{-12}.$$

where a_t and a_0 are lattice parameters at t °C and 0°C respectively, the maximum deviation being 8×10^{-5}. A comparison was made between our lattice thermal expansion data and those published by previous investigators (Wilson 1942, and Feder and Nowick 1958), who used aluminium of comparable purity (99·99%), as given in the table. It is noted from the table that they are in good agreement with each other up to about 400°C and are in fair agreement at higher temperatures, i.e. our values are lower than the others at temperatures above about 500°C, for instance, by $0{\cdot}20 \times 10^{-3}$ to $0{\cdot}27 \times 10^{-3}$ at 650°C. It was found experimentally that this slight discrepancy of the lattice thermal expansion at higher temperatures may be explainable in terms of the difference of the degree of vacuum used.

The present data of lattice thermal expansion were compared to the bulk thermal expansion data (Feder and Nowick 1958, and Taylor, Willey, Smith and Edwards 1938) on 99·99% pure aluminium available in the literature. As seen from the figure, they are in good agreement up to about 400°C, while they are not at higher temperatures. The difference between them at higher temperature, which is proportional to the concentration of vacancies, is found to increase exponentially with temperature. The corresponding values of vacancy concentration at the melting point C_v(m.p.) and of the energy of formation, h_v, are: C_v(m.p.) = $(1{\cdot}3 \pm 0{\cdot}1) \times 10^{-3}$, $h_v = (0{\cdot}61 \pm 0{\cdot}07)$ ev, if the bulk expansion data Taylor *et al.* (1938) are used; C_v(m.p.) = $(1{\cdot}0 \pm 0{\cdot}1) \times 10^{-3}$, and $h_v = (0{\cdot}67 \pm 0{\cdot}09)$ ev, if the bulk expansion data of Feder and Nowick (1958) are used. The two sets of these values obtained from two independent data of the bulk thermal expansion are not greatly different. Upon averaging them we have: C_v(m.p.) = $(1{\cdot}1 \pm 0{\cdot}2) \times 10^{-3}$, $h_v = (0{\cdot}64 \pm 0{\cdot}12)$ ev.

The results obtained are in fairly good agreement with quenched-in resistivity experiments in aluminium, using 1·4 micro-ohm-cm/at % vacancies. Desorbo and Turnbull (1959), who used zone refined aluminium find C_v(m.p.) = 10^{-3}, and for the energy of formation, $h_v = 0{\cdot}79 \pm 0{\cdot}04$ ev. Quenching experiments of Bradshaw and Pearson (1957), using 99·99% purity aluminium, give C_v(m.p.) = 7×10^{-4}, and the energy of formation, $h_v = 0{\cdot}75 \pm 0{\cdot}04$ ev.

References

Bradshaw, F. J., and Pearson, S., 1957, *Phil. Mag.*, **2**, 570.

Desorbo, W., and Turnbull, D., 1959, *Acta Met.*, **7**, 83.

Feder, R., and Nowick, A. S., 1958, *Phys. Rev.*, **109**, 1959.

Taylor, C. S., Willey, L. A., Smith, D. W., and Edwards, J. D., 1938, *Metals and Alloys*, **9**, 189.

Wilson, A. J. C., 1942, *Proc. phys. Soc. Lond.*, **54**, 487.

REVIEWS OF BOOKS

Measurement: Definitions and Theories, By C. West Churchman and Philburn Ratoosh (Ed.), (New York : John Wiley and Sons, 1959.) [Pp. 274.] 64*s*.

A collection of papers read to the American Association for the Advancement of Science in 1956. The contributors are: Peter Caws, S. S. Stevens, Paul Kircher, C. West Churchman, Karl Menger, Patrick Suppes, R. Duncan Luce, Henry Margenau, Arthur Pap, John L. McKnight, E. J. Gumbel, Clyde H. Coombs, Donald Davidson and Jacob Marschak.

Those familiar with the basic problems of the philosophy of measurement may gain some profit from a report on work in progress: others will feel that while most of the papers are passable, and one or two quite good, as papers introducing a discussion, they needed to be worked over more if they were to be published: physicists will be chiefly interested in Margenau's suggestion that instead of its being simply the process of measurement that alters the quantum state, we ought rather to distinguish two processes, one of preparation, which can indeed alter the state but may not be provided with a particular system to alter, the other of detection which determines whether there was in fact a system actually in that state. J. R. L.

Masers. By Gordon Troup. (London: Methuen, 1959.) [Pp. 168.] 13*s*. 6*d*.

A year or so ago the author was asked, by the Australian Department of Supply, to prepare a report on the state of developments in the maser field. With no comprehensive reviews available, and with many of the original papers not particularly easy to read, this was no light task. That Dr. Troup's efforts were appreciated is shown by the fact that it was decided to publish the report as a book, and for this all of us who work in the field of masers have reason to thank the Australian authorities.

The book gives a fairly full account of maser developments up till about the end of 1958, and is written for a reader who has no previous knowledge of the subject. A good deal of the first part is devoted to establishing the theory from quite basic ideas, and it is only towards the end that an account is given of the experimental achievements and potentialities. Throughout the emphasis is on the underlying physics, which is perhaps as well, for there are a number of small errors in the formal mathematics, which might otherwise be misleading.

The publication of this volume, the first to be devoted to masers, is most welcome, and it can be recommended as an excellent introduction to the whole field. K. W. H. S.

Atlas of γ-Ray Spectra from Radiative Capture of Thermal Neutrons. By L. V. Groshev, A. M. Demidov, V. N. Lutsenko, and V. I. Pelekhov. Translated from the Russian by J. B. Sykes. (London: Pergamon Press, 1959.) [Pp. 198.] £7.

This is an impressive and useful compilation of the available data up to January 1958 on the γ-ray spectra resulting from the capture of thermal neutrons. It has come at a time when the interest in this field, and the associated field of resonance neutron capture, is expanding.

The book contains a short introduction reviewing the experimental investigations of the subject. This is followed by a table of stable isotopes containing relevant information on the target nuclei employed in these investigations. Such information includes thermal neutron capture cross sections, isotopic abundances, ground state spins and parities, half-lives of resulting isotopes and separation energies of the neutron in the product nucleus.

The main part of the book consists of graphs of γ-ray spectra arranged in order of increasing atomic number. Associated with these graphs are tables presenting the energy and intensity of the observed γ-rays, and in many cases there are γ-transition diagrams for the compound nucleus formed. These have been constructed employing data from other nuclear reactions as well as from the γ-ray work. The ln values found from (d, p) reactions and other inferences concerning shell-model configurations of the levels are also included in the transition diagrams. Two appendices deal with spectra of internal conversion electrons emitted in thermal neutron capture and γ-rays from radioactivity appearing in γ-ray spectra. There is a complete list of references.

The English translation is competent. The tables and diagrams have been reproduced photographically for speed but this has been done a little indiscriminately. It would have been pleasant to have seen the gross distortions on the diagram for Ca removed. Also, occasional parity signs have disappeared. The price is rather disturbing and banishes the book from its rightful place on the research worker's desk to the library reference shelf. J. E. L.

Solid State Physics. Volume 9. By F. Seitz and D. Turnbull (Editors). (New York: Academic Press Inc., 1959.) [Pp. 548.] $14.50.

Students of the physics of solids will by now have a clear idea of the general scope of this series, there is no need here, to solemnly advertise the contents of this volume; readers will already have left a standing order with their bookseller to purchase each volume as it appears. Suffice to say that it is the mixture as before.

And an interesting mixture it is. Where else, for example, would we look for the latest information on the properties of metals in strong magnetic fields, on the phenomena of static electrification, or on the electronic structure of aromatic molecular crystals? Where else can one find such a high standard of authoritative writing on such a wide variety of topics? For the working research man, these review articles, giving compact maps of the numerous bye-ways into which the subject has branches, are invaluable.

Yet there is a general weakness, which only grows more obvious as the volumes continue to appear; the scope of the separate articles is too narrow, and there is no effort to connect them. We are not getting what we were promised in Volume I: " broad elementary surveys that have particular value in orienting the advanced graduate student or investigator having little previous knowledge of the subject ". This has several undesirable results. There is too big a gap left between the elementary books, which try to put all of Solid State Physics into 500 pages, and the articles in these volumes. There is a tendency to omit any lengthy theoretical or mathematical arguments (for fear that they might use up all the pages, and leave no room for references to all the latest papers) so that the students has to go back again to the original papers for the complete proof of even the most elementary and well-agreed formulae. Sometimes there are separate articles on fields that overlap, so that the same general argument is repeated. Sometimes important topics fall between the narrow, hobby horses of two different authors. There is no general consolidation of knowledge, no definition of a corpus of well-established fact and theory to form a basis upon which to build the more speculative, fragmentary ideas which are the raw material of research.

We are offered an impressive list of articles planned for future volumes. Let us hope that the editors will persuade some of these distinguished scholars to put aside their research for a while, turn down requests from other editors for three other review articles on the same subject, and contribute on a more heroic scale. Then we shall see, explicitly, how the subject has really grown since Professor Seitz set it out for us, in his *Modern Theory of Solids*, only 20 years ago.

J. M. Z.

Methods of Experimental Physics. Volume 6, Part A. *Solid State Physics.* Edited by K. Lark-Horovitz and Vivian A. Johnson. (Academic Press, Inc., 1959.) [Pp. 466.] 94*s.* 6*d.*

In the foreword the general editor for this series states his aim to present in these volumes the important methods and general principles needed by experimental physicists together with references for further reading, and to include in the presentation indications of the limits of applicability and accuracy of each method. In this volume, dealing with preparation, structure, mechanical and thermal properties, the editors have largely succeeded in their appointed task. For experienced research workers, teachers and research students, it should provide a readily available source of information basic to the study of solid state physics.

The coverage is comprehensive, including articles on preparation of single crystals, purification, detection of impurities, x-ray, electron and neutron diffraction, deformation and thermal properties, high pressure physics and a discussion of the available methods of observing dislocations. Where space limitations cause a somewhat superficial treatment (e.g. discussion of crystal plasticity is limited to 14 pages), the references are extensive. The writer could find only a few minor omissions, e.g. no mention is made of the Schultz/Berg-Barrett technique for studying crystal perfection.

The volume is well presented with clear diagrams, and the short sections are easily readable and adequately indexed; it should find a place on the shelves of many reference libraries.

P. R. T.

Methods of Experimental Physics. Volume 6, Part B. Edited by K. Lark-Horowitz and Vivian A. Johnson. (Academic Press Inc., 1959.) [Pp. 416.] $11.00.

This is one in an ambitious series of seven volumes, designed to cover all the main fields of research in physics. It is devoted (like Volume 6, Part A) to solid state physics, and contains articles by a large number of different authors on electrical properties, galvanomagnetic and thermomagnetic effects, magnetic properties, optical properties, luminescence and photoelectric phenomena. The aim is to provide a thorough account of the experimental methods available in these areas, with more emphasis on the general principles involved than on mere gadgetry. On the whole this aim is achieved, and the research physicist planning to start work on one of the topics covered would find that to read the appropriate article here would save some days of hunting through the literature. Not all the articles, however, are sufficiently critical to help him much in choosing which is the best method for his purpose, and a few are couched in such general terms as to be almost useless. The book is to be recommended for libraries in research laboratories, but teachers and students of physics are likely to find it less valuable that the Foreword claims.

T. E. F.

BOOK NOTICES

Lectures on the Theory of Elliptic Functions. By HARRIS HANCOCK. (New York. Dover Publications Inc.) [Pp. 498.] Price $2.55. A reprint, in the Dover Edition, of the 1st edition, published in 1958.

International Astronomical Union Symposium, No. 6: Electromagnetic Phenomena in Cosmical Physics. Stockholm, August 1956. By B. LEHNERT. (Cambridge: University Press) [Pp. 544.] Price 50*s*.

Annual Review of Nuclear Science, Vol. 8. Edited by E. SEGRE and others. (New York: Annual Reviews Inc., 1958.) [Pp. 417.] $7.00.

Guide to the Literature of Mathematics and Physics, 2nd edition. By NATHAN GRIER PARKE III. (New York: Dover Publications Inc.) [Pp. 436.] Price £1. A reprint, in the Dover Edition, of the 2nd edition, published in 1958.

Convex Surfaces: Interscience Tracts in Pure and Applied Mathematics, No. 6. By HERBERT BUSEMANN. (New York: Interscience Publishers Inc.) [Pp. 196.] Price 45*s*.

Elasticity, Plasticity and Structure of Matter, 2nd edition. By Dr. R. HOUWINK. (New York: Dover Publications Inc.) [Pp. 368.] Price £1. A reprint, in the Dover Edition, of the 2nd edition, published in 1958.

Nuclear Spectroscopy Tables. By A. H. WAPSTRA, G. J. NIJGH and R. VAN LIESHOUT. (Amsterdam: North-Holland Publishing Co.) [Pp. 135.] Price 60*s*.

The Plasma in a Magnetic Field. A Symposium on Magnetohydrodynamics. Edited by ROLF K. M. LANDSHOFF. (Stanford: University Press. London: Oxford University Press.) [Pp. 130.] Price 36*s*.

Fundamentals of Advanced Missles. By RICHARD B. DOW. (New York: John Wiley & Sons Inc.; London: Chapman & Hall). [Pp. 567.] Price 94*s*.

Colloque National de Magnetisme, Strasbourg July 1957. (Paris: Centre Nationale de la Recherche Scientifique.) [Pp. 336.] Price 4000 fr.

The Design of Physics Research Laboratories. Institute of Physics symposium, London, 27 November 1957. (London: Chapman & Hall.) [Pp. 108.] Price 21*s*.

Proceedings of the International Symposium on Transport Processes in Statistical Mechanics, Brussels, August 1956. Edited by I. PRIGOGINE. (Interscience Publishers, Inc.) [Pp. 436.] Price 75*s*.

Crystal Growth. Discussions of the Faraday Society, No. 5. 1949. (Reprinted by Butterworths Scientific Publications, 1959.) [Pp. 366.] Price 60*s*.

The Fourier Integral. By N. WIENER. (New York: Dover Publications Inc.; London: Constable & Co.) [Pp. xi+201.] Price 12*s*.

A Dictionary of Names Effects and Laws. By D. W. BALLENTYNE and L. E. WALKER. (London: Chapman & Hall.) [Pp. v+205.] Price 30*s*.

[*The Editors do not hold themselves responsible for the views expressed by their correspondents.*]

Fig. 2

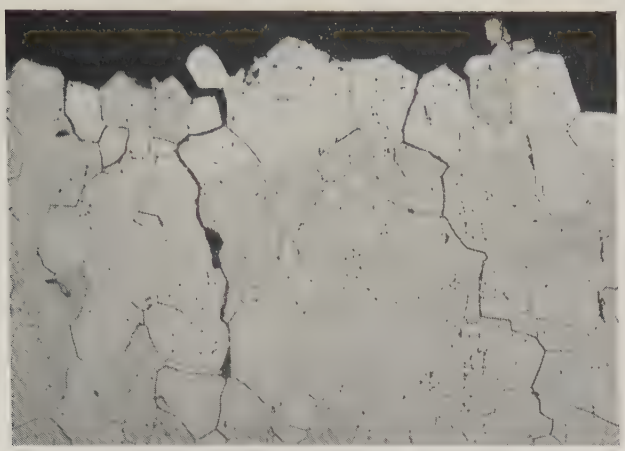

Intercrystalline cracking at fracture surface. Alloy A. Failed 80 000 cycles, ±30 000 p.s.i. ×50.

NOTE—Specimen axis is vertical unless stated otherwise.

Fig. 3

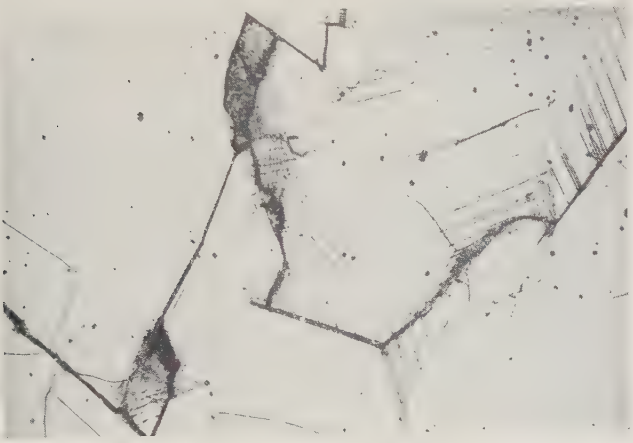

Cracking along crystallographic planes. Alloy C. Failed 112 000 cycles, ±30 000 p.s.i. ×120.

Fig. 4

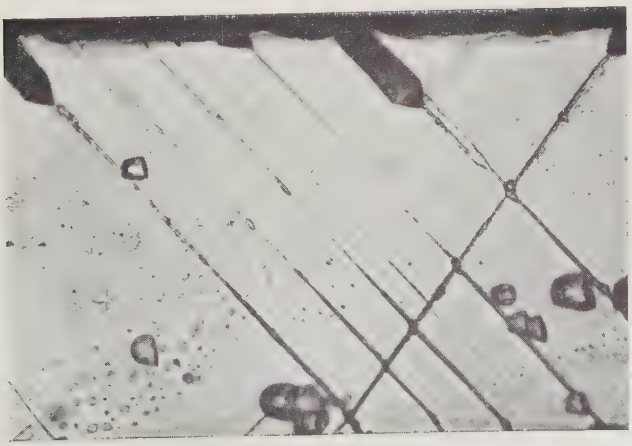

Specimen axis horizontal

Cracks penetrating down slip planes. Alloy D. Failed 898 000 cycles ±25 000 p.s.i. ×500.

Fig. 5

Typical fatigue crack in alloys E, F, and G. $\times 100$.

Fig. 6

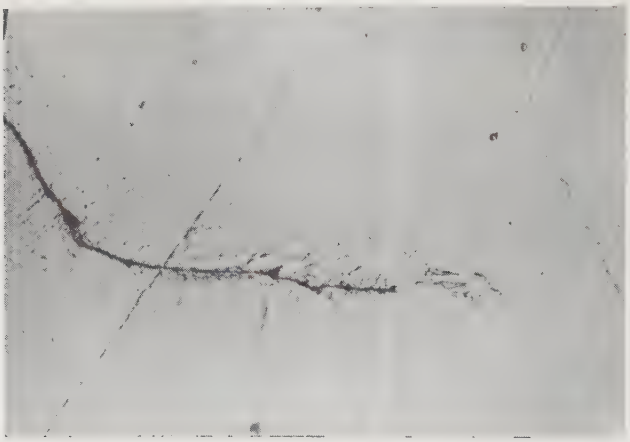

Deformation markings at end of fatigue crack in alloy F. Failed 30×10^6 cycles, $\pm 30\,000$ p.s.i. $\times 500$.

Fig. 7

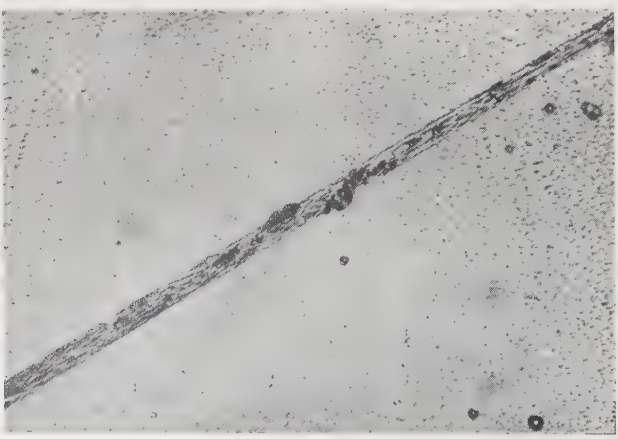

Slip striation containing cubic etch pits alloy J. Failed 347 000 cycles, $\pm 30\,000$ p.s.i. $\times 500$.

Fig. 8(*a*)

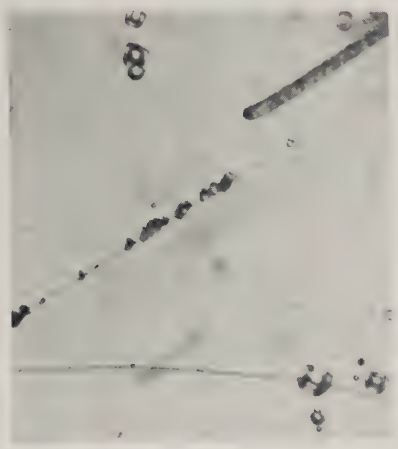

×500.

Fig. 8(*b*)

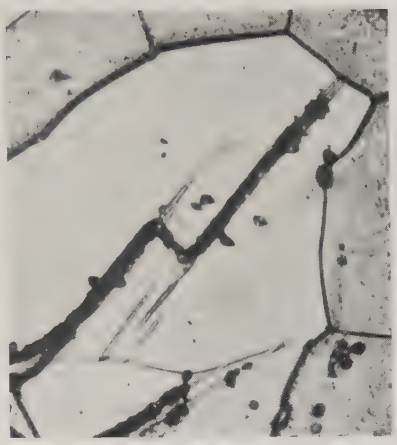

×500.

Possible two stages of crack formation in alloy D. Failed 186 000 cycles, ±30 000 p.s.i.

Fig. 9

Unetched section of alloy J showing cavities at site of slip striation shown in fig. 7. ×500.

Fig. 10

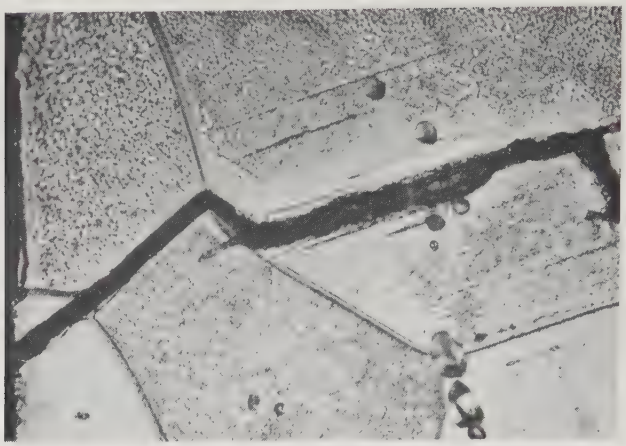

A depleted region associated with a crack. Alloy D. Failed 186 000 cycles, $\pm 30\,000$ p.s.i. $\times 500$.

Fig. 11

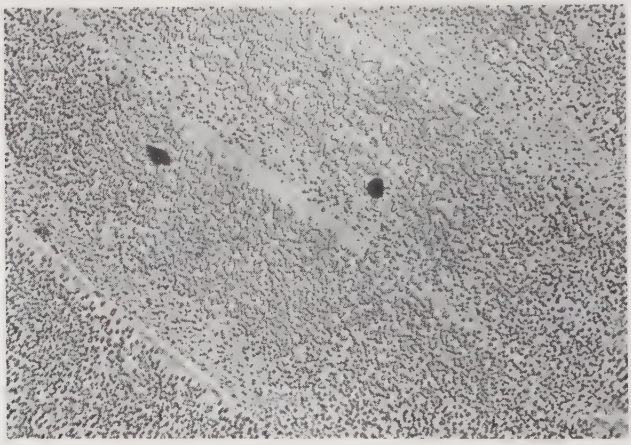

Depletion in slip band regions. Alloy C. Failed 415 000 cycles, $\pm 25\,000$ p.s.i. $\times 500$.

Fig. 12

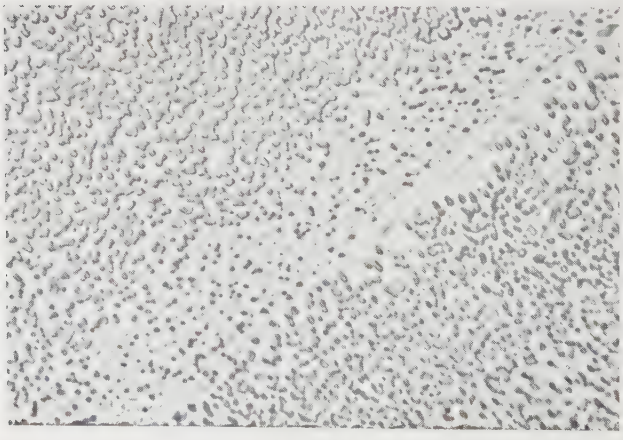

Zones associated with the depleted bands. Enlargement of fig. 11. $\times 1000$.

Fig. 2

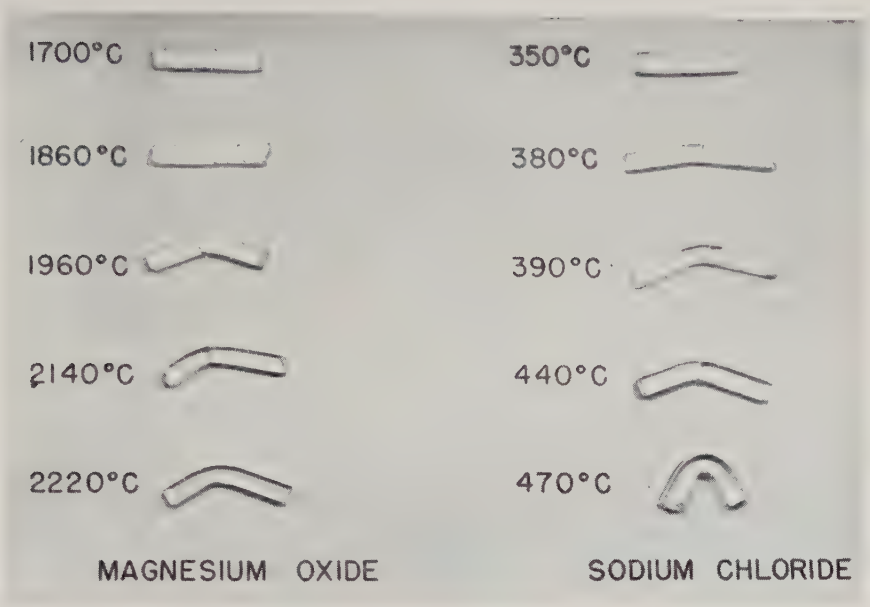

Appearance of sodium chloride and magnesium oxide crystals after impact at the temperatures shown.

Fig. 4

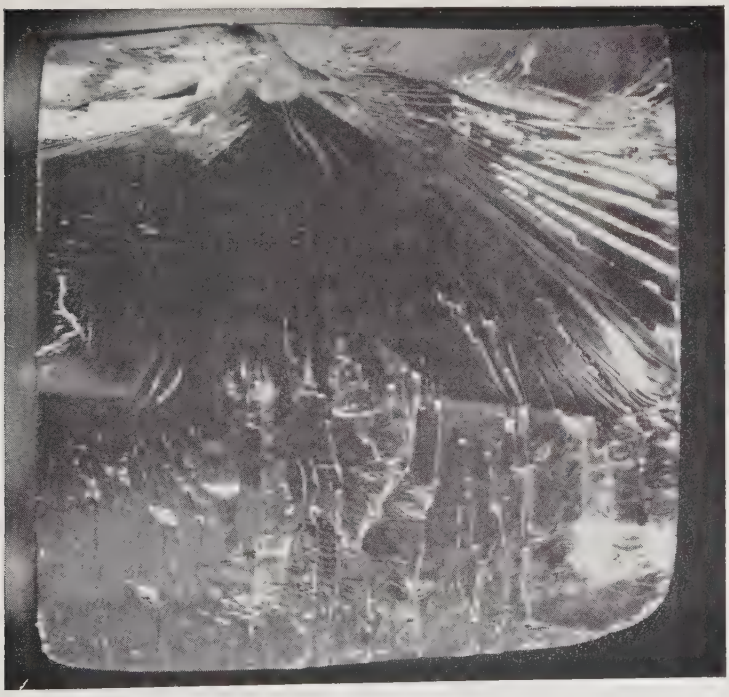

Cleavage surface of a AgCl single crystal having orientation number 1 impacted at liquid nitrogen temperature.

Fig. 5

Fracture surface of a notched AgCl single crystal of orientation number 1 impacted at 65°c. Note the ductile crack region and the lateral contraction at the base of the notch.

Fig. 6

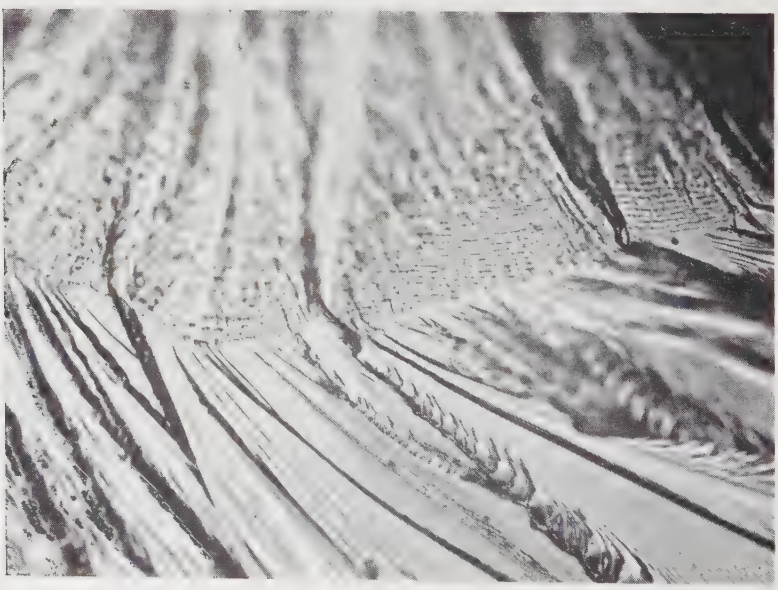

Boundary region between the ductile crack surface and the cleavage surface in a AgCl single crystal impacted at room temperature. (×330.)

Fig. 7

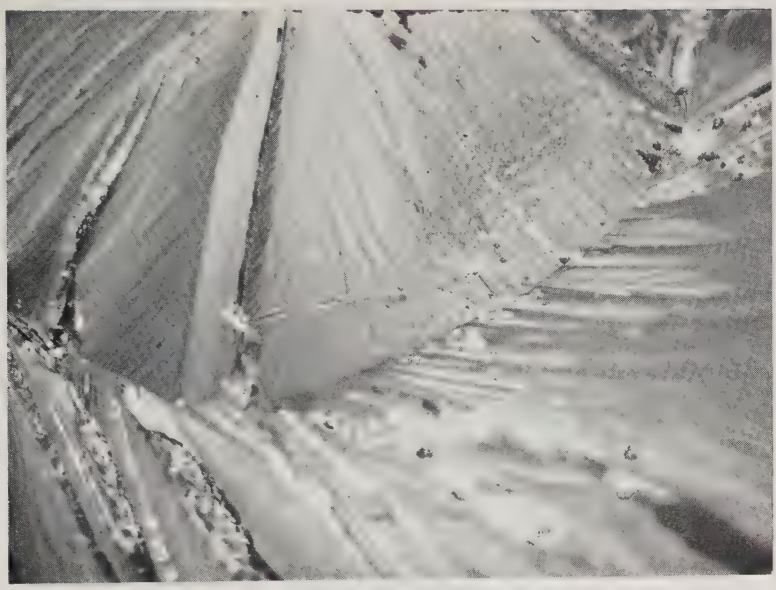

Surface of ductile crack formed in a AgCl crystal impacted at 65°c. (×40.)

Fig. 1

Dislocation loops L and small regions of strain (black spots) in neutron-irradiated copper (low dose) at low magnification. Total flux $\sim 6{\cdot}7 \times 10^{17}$ n cm^{-2}. Mag. $\times 52\,500$.

Fig. 2

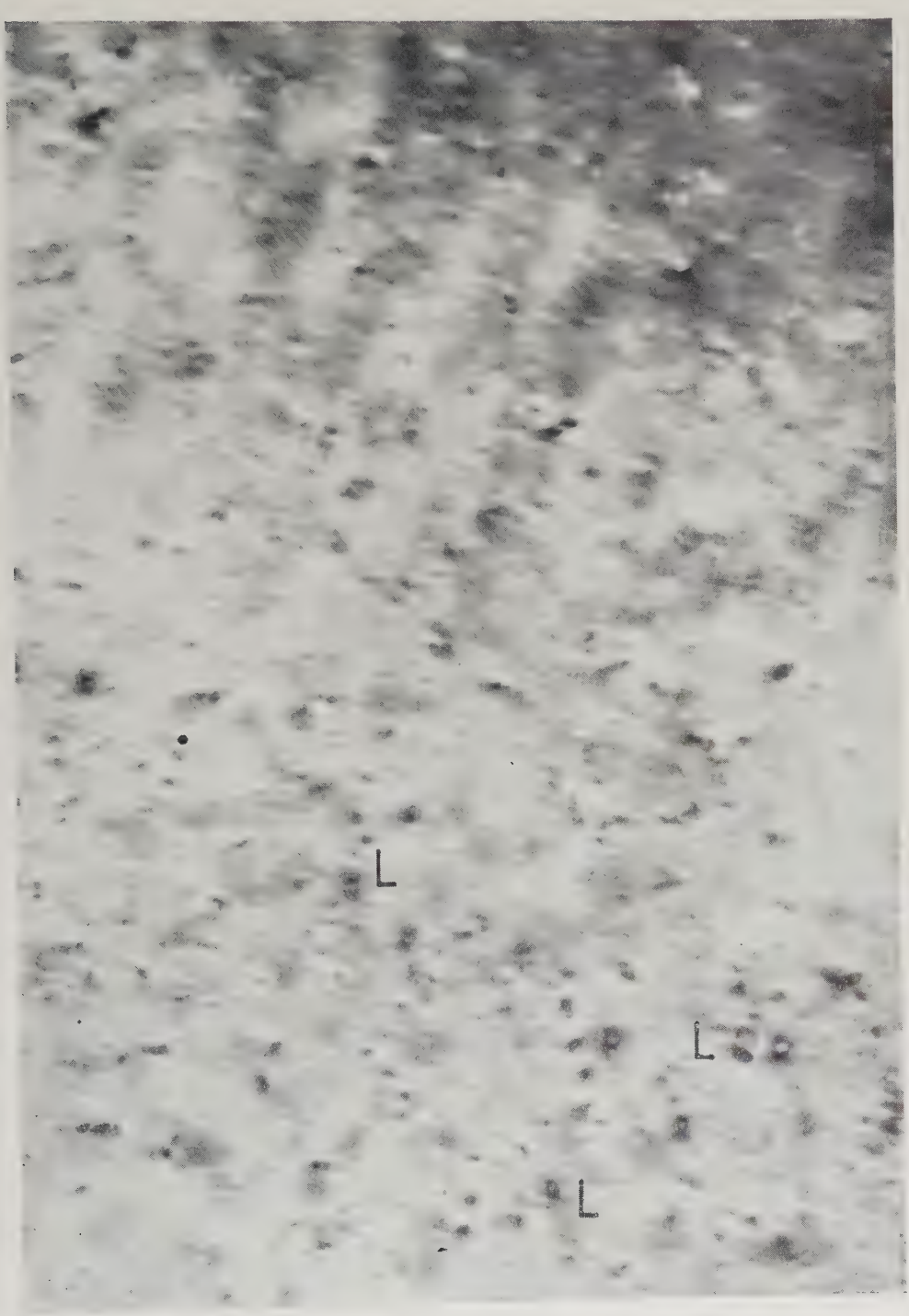

Dislocation loops L and small regions of strain (black spots) in neutron-irradiated copper (low dose) at high magnification. Total flux $\sim 6{\cdot}7 \times 10^{17}$ n cm^{-2}. Mag. $\times 200\,000$.

Fig. 3

0 5μ (*a*)

0 5μ (*b*)

(*a*) Annealed polycrystalline copper showing dislocations. Unirradiated. Mag. $\times 52\,500$

(*b*) Annealed polycrystalline copper showing rare occurrence of spots observed occasionally. Unirradiated. Mag. $\times 52\,500$.

Fig. 4

$0{\cdot}5\,\mu$

Dislocation loops in neutron-irradiated copper (intermediate dose) at low magnification. Note the increase in loop size and density compared with fig. 1. Total flux $\sim 5{\cdot}6 \times 10^{18}$ n cm^{-2}. Mag. $\times 52\,500$.

Fig. 5

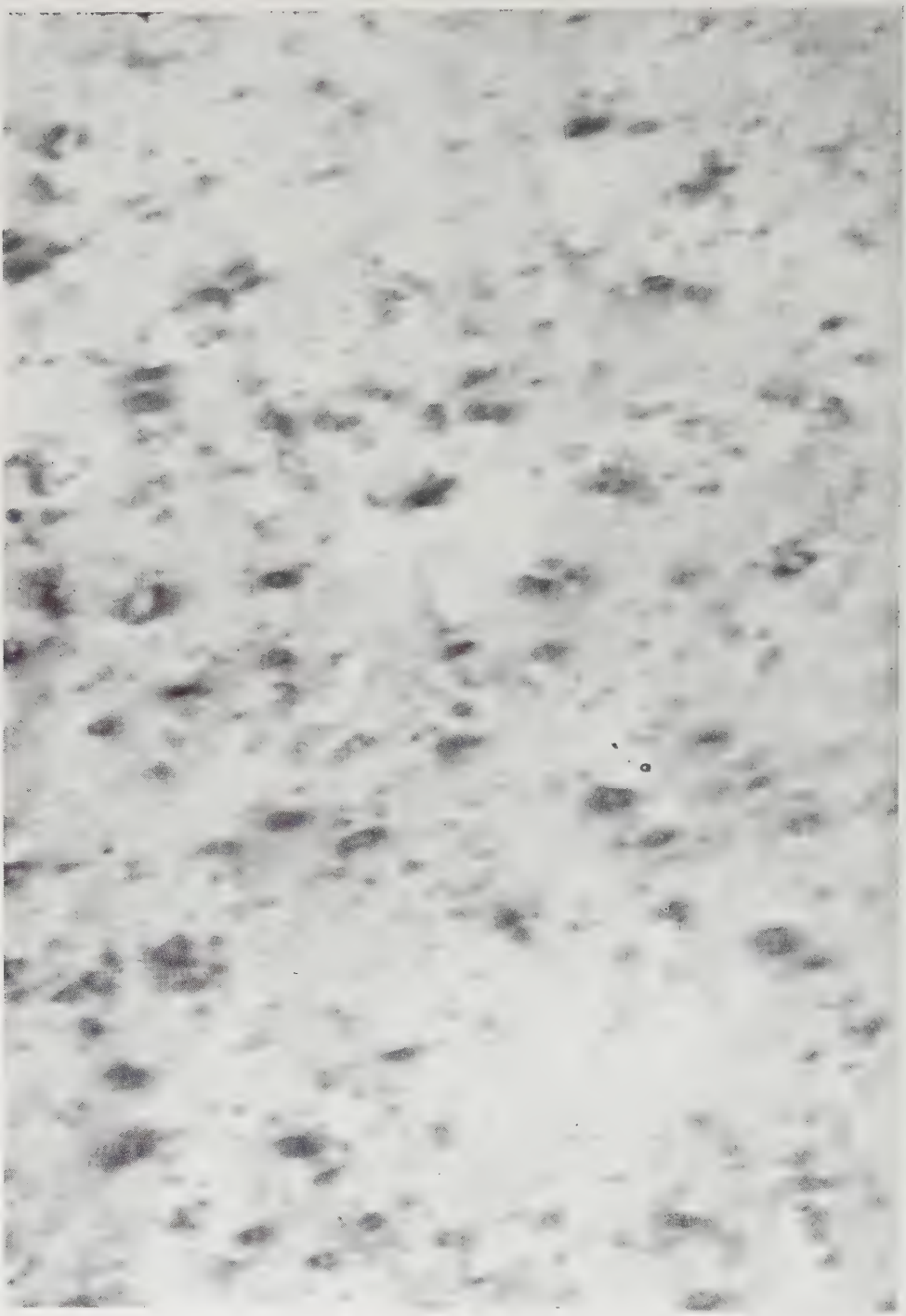

A high magnification micrograph of dislocation loops in neutron-irradiated copper (intermediate dose). Total flux $\sim 5{\cdot}6 \times 10^{18}$ n cm^{-2}. Mag. $\times 200\,000$.

Fig. 6

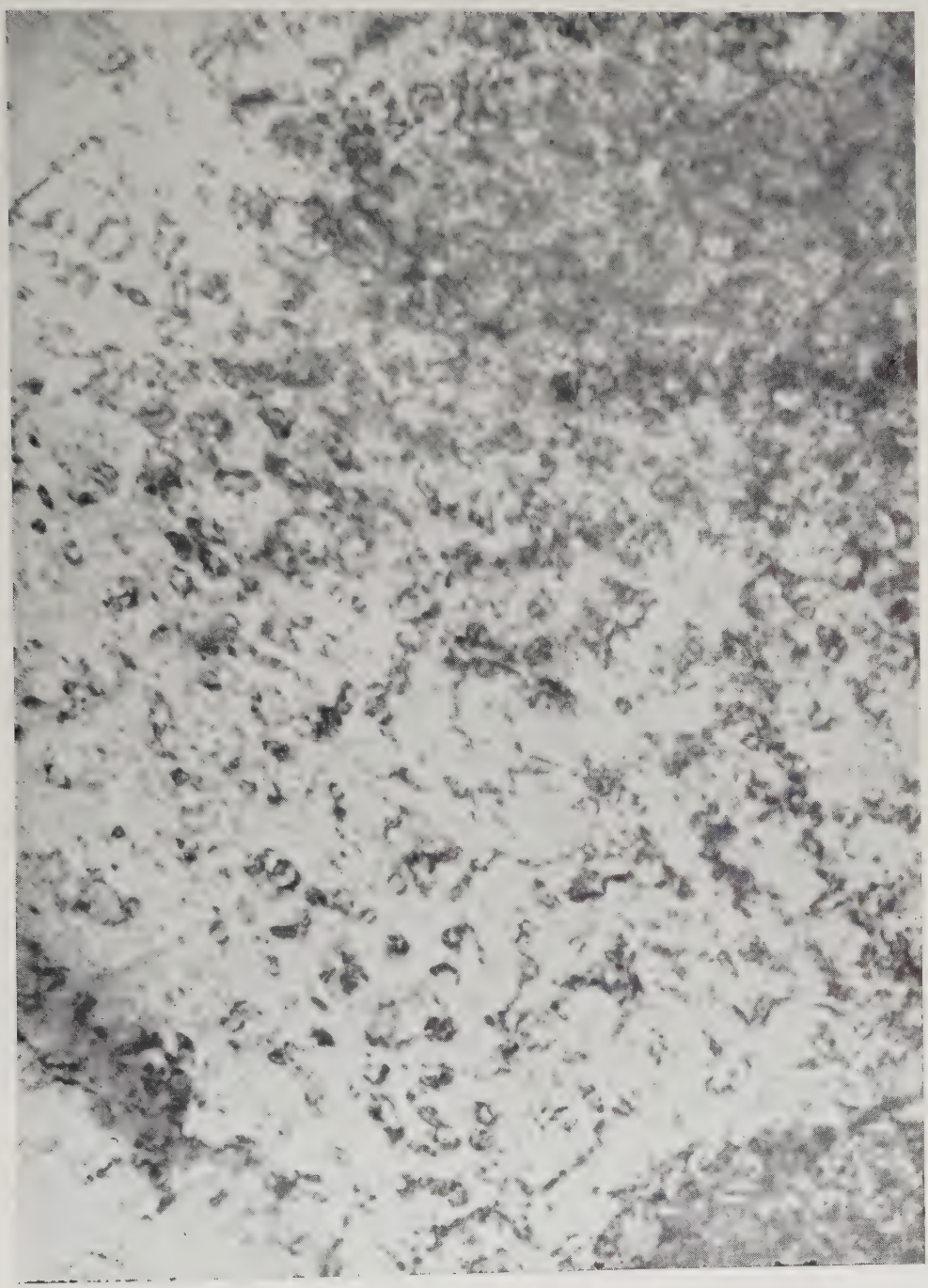

1000 Å

A low magnification micrograph of copper irradiated to a high total flux. Note the large dislocation loops in comparison with fig. 1. Total flux $\sim 1{\cdot}4 \times 10^{20}$ n cm^{-2}. Mag. $\times 90\,000$.

Fig. 7

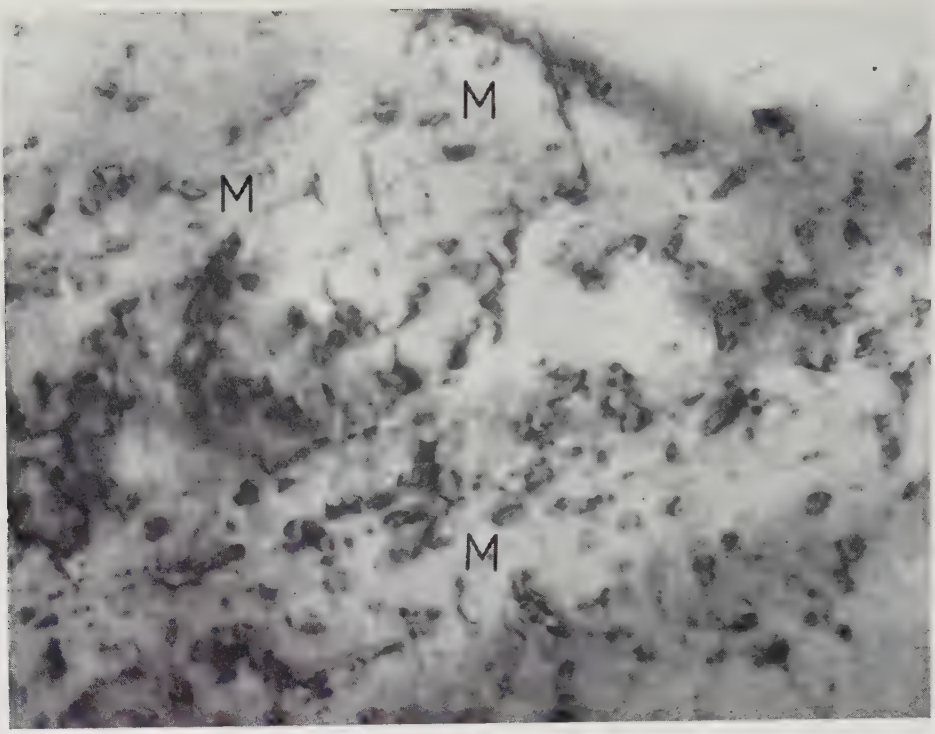

0·25 μ

Copper, neutron irradiated to a high dose. Note the dislocation loops M showing double image contrast effects. Total flux $\sim 1{\cdot}4 \times 10^{20}$ n cm^{-2}. Mag. $\times 84\,000$.

Fig. 8

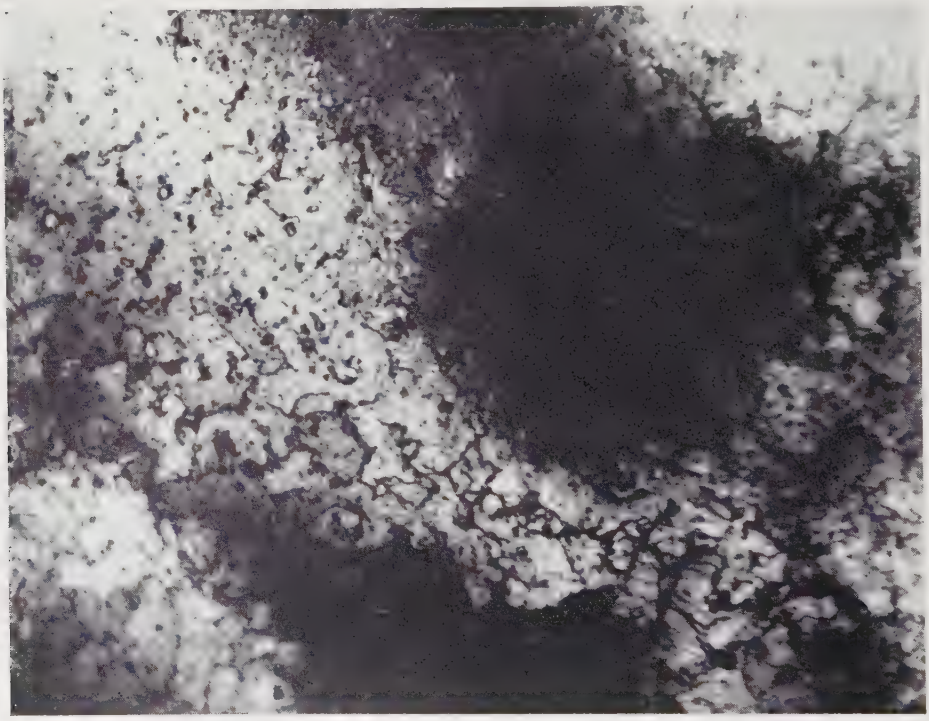

0·5 μ

A dislocation network observed in copper neutron irradiated to a high dose.

Fig. 9

0·25 μ

(*a*)

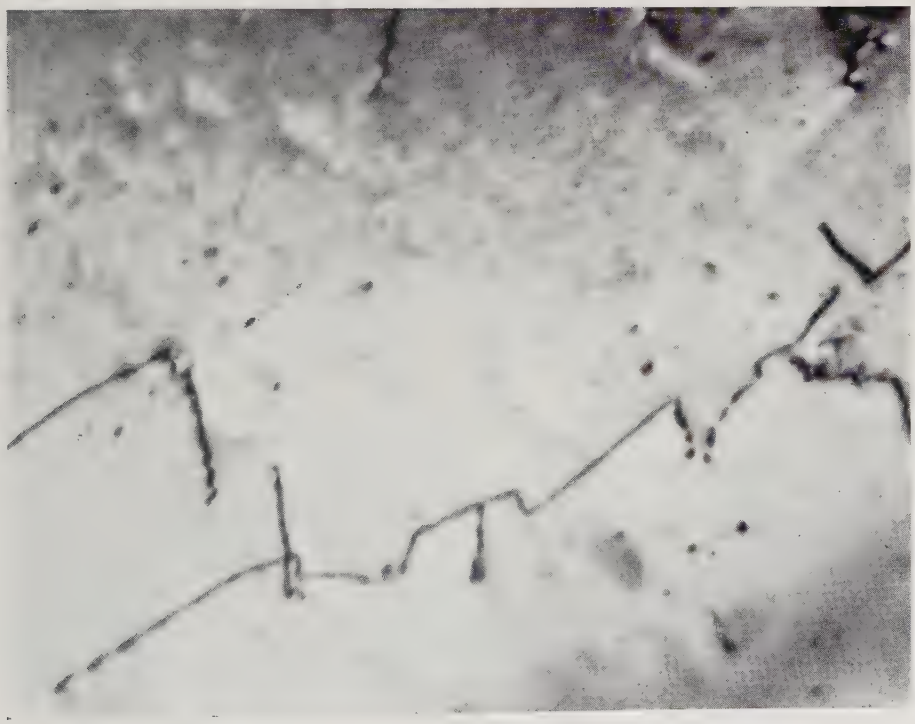

0·25 μ

(*b*)

(*a*) A typical area of a specimen annealed in bulk for 22 min at 350°c after irradiation (low dose). Total flux $\sim 6{\cdot}7 \times 10^{17}$ n cm^{-2}. Mag. $\times 104\,000$.
(*b*) A typical area of a specimen annealed in bulk for 6 hours at 350°c after irradiation (low dose). Total flux $\sim 6{\cdot}7 \times 10^{17}$ n cm^{-2}. Mag. $\times 92\,000$.

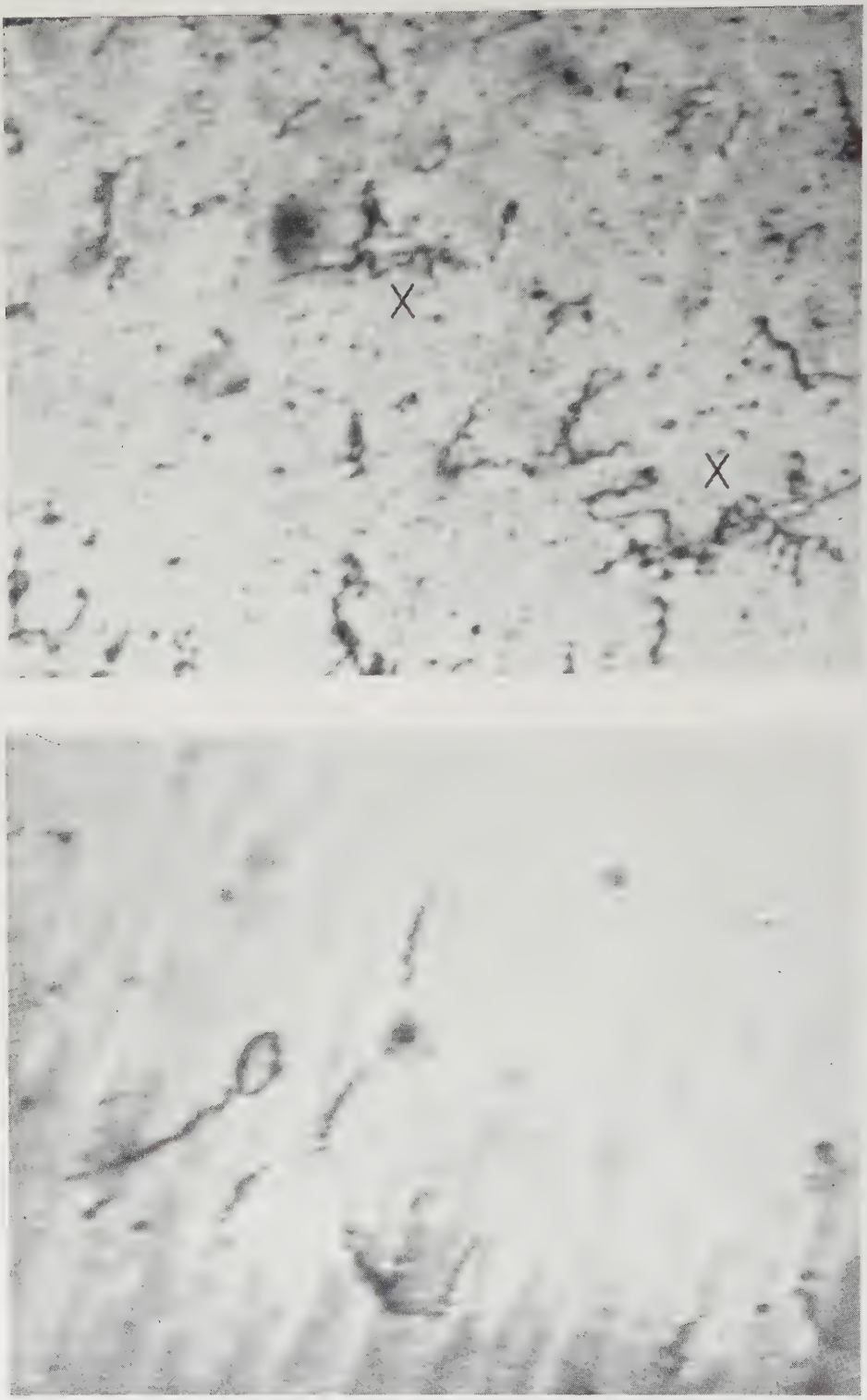

(*a*) An area of an irradiated specimen (low dose) prior to annealing on the high temperature object stage. Total flux $\sim 6{\cdot}7 \times 10^{17}$ n cm^{-2}. Mag. $\times 33\,000$.
(*b*) An area of the same specimen shown in fig. 10 (*a*) after 2 min. at 370°c on the high temperature object stage. Total flux $\sim 6{\cdot}7 \times 10^{17}$ n cm^{-2}. Mag. $\times 33\,000$.

Fig. 11

1000 Å

The distribution of small regions of strain close to a grain boundary. Note the lack of a marked denuded zone. Total flux $\sim 6{\cdot}7 \times 10^{17}$ n cm^{-2}. Mag. $\times 107\,000$.

Fig. 12

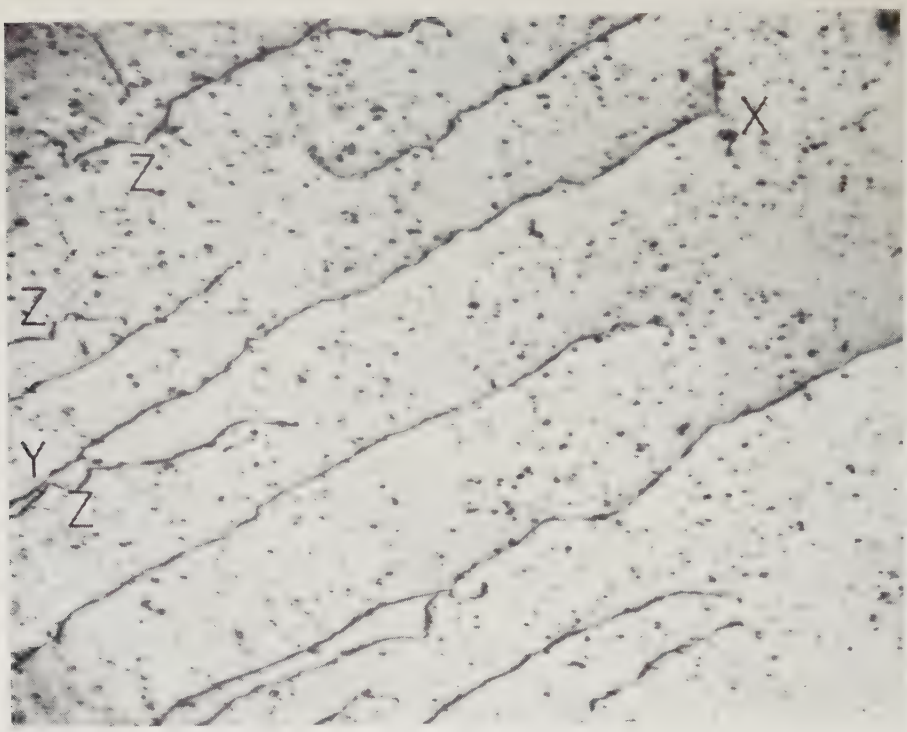

(*a*)

(*a*) Dislocations observed in a specimen pulled ~3% after irradiation. The cusp-like nature of the dislocations at the points Z, suggest strongly that the dislocations are pinned at these points. Total flux $\sim 6{\cdot}7 \times 10^{17}$ n cm^{-2}.

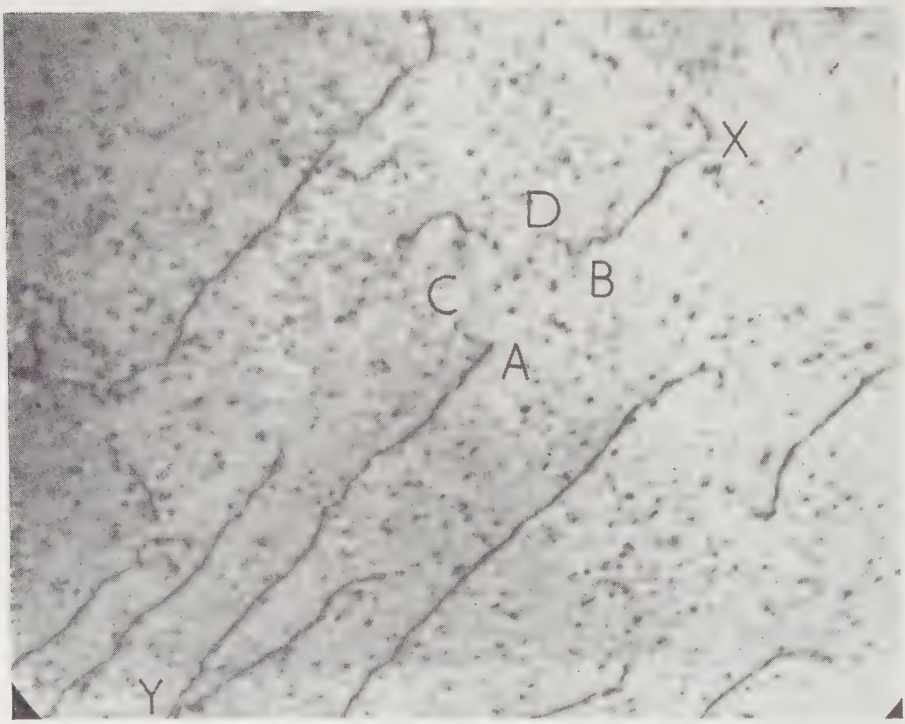

(*b*)

$0{\cdot}5\mu$

(*b*) In the interval between taking this micrograph and the previous one of fig. 12 (*a*), the dislocation XY shown on fig. 12 (*a*) was observed to blow out along a short section of its length until it met the foil surface. The last stage of the sequence is shown in this micrograph and shows the points A, B at which the dislocation is pinned, and the points, C, D, at which it has met the surface. Total flux $\sim 6{\cdot}7 \times 10^{17}$ n cm^{-2}. Mag. $\times 60\,000$.

SUBJECT INDEX

INDEX OF AUTHORS (WITH TITLES)

END OF THE FOURTH VOLUME

Printed by Taylor & Francis, Ltd
Red Lion Court, Fleet Street, London, E.C.4